Buckling Load Optimization of Variable stiffness composite Plate Using FEM and Semi-analytical method

by

Jeegar Vallabhbhai Patel

Thesis

Submitted in partial fulfilment of the requirements
for the degree of Master of Science in Mechanical Engineering at
The University of Texas at Arlington
December, 2021

Arlington, Texas

Supervising Committee:

Dr. Paul Davidson, Supervising Professor
Dr. Seiichi Nomura
Dr. Robert M. Taylor
Dr. Bo. P. Wang

Abstract

Buckling Load Optimization of Variable stiffness composite Plate Using FEM and Semi-analytical method

Jeegar Vallabhbhai Patel, MS.
The University of Texas at Arlington, 2021

Supervising Professor(s) : Dr. Paul Davidson

The advent of new composite manufacturing techniques like Automated Fiber Placement (AFP) offers greater flexibility in structural designs by allowing curvilinear fiber paths. Hence, it is now possible to change laminate stiffness locally, thereby enabling Variable Stiffness (VS) composite structures. Such structures demonstrate superior buckling performance over traditional constant stiffness structures. However, obtaining the optimum fiber paths to improve buckling performance remains an open area of research due to the complexity of determining such fiber paths. This research investigated two approaches for optimizing fiber paths; First, a Finite Element Method (FEM) approach that utilizes linear shape functions to interpolate local fiber angle variation within the plate when given angle values at global manufacturing mesh nodes. Second, a new semi-analytical formulation for calculating in-plane load distribution and stability of a composite laminated plate, with spatial variation in ply-by-ply fiber angles. Double Fourier series approximation is used to achieve variable fiber angle distribution. Ritz method is used to find the approximate solution for the boundary value problem. Using the developed methods, optimization studies were conducted on uniaxially compressed, eight-ply symmetric composite laminate plate, with univariate and bivariate fiber angle distribution. The study used Genetic-Algorithm(GA) and Quasi-Newton method of Broyden, Fletcher, Goldfarb, and Shanno (BFGS) as optimization formulation. The results not only show an 87% and 67% improvement in buckling load for a VS plate using FEM and Semi-analytical method respectively but also provides a better understanding of the influence of fiber angle distribution.

DEDICATION

I would like to dedicate this work to one of the people i admire the most, Dr. Siva Prasad Kowdodi (Dean IIIC at Hyderabad Institute of Technology Management.) who is my mentor and guide. I was never interested in engineering as much before i met him for the projects we did together. I thank him for teaching me two most valuable lesson of life, Never give up and keep trying even if you can not afford the price you pay. I also thank him for sharing his best technical knowledge as a mentor, giving me freedom of thinking, and keep motivating me in time of failures we faced during projects. Consider this is as a small gift from me for being my mentor and giving me an opportunity to actually start my career in the field engineering in a better way and supporting me at the time i needed the most.

ACKNOWLEDGEMENTS

I cannot express enough thanks to the people who helped me to get succeed in the journey and gave me their guidance to keep me on a right path.

I sincerely thank my supervising professor Dr. Paul Davidson, who gave me this excellent opportunity and motivation to embark in the field of composite structures. I thank him for giving his guidance thought the research work and share his best ideas on how to think and approach a problem. I also thank him for providing me all the resources which were necessary for the research work as soon as possible. The journey under him was not only about to improve the technical knowledge in the field but also about self improvement and improvement of presentation and communication skill to share your idea with the scholars and experts efficiently. I really thank him for being patient all the time with me even if i get confused, less focused and lost the track in research work and thank him for the treat we got all the time of presentations.

It is very difficult to put into words but the "LAMMA Lab" is not only filled with members with sharp intelligent mind but with friends and mentors with moral and emotional support who always kept me on right track and helped me to understand and solve the problem together whenever needed.

I also would like to extend my thanks to Dr.S. Nomura for not only teaching me advanced mathematics which paved path for me to succeed in the work i am presenting. As a graduate advisor, he always gave me a right suggestion on the subject i should learn according to my area of interest which can shape my career better. Last but not least, i am really grateful to have him as my thesis dissertation committee member.

Next, I would like to thank Dr. Bo. P. Wang for sharing me his best knowledge about MATLAB and specially FEM which is another foundation for my research work and without this knowledge, it was nearly impossible to achieve my goal in the work. I also thank him for giving his valuable time and being my thesis dissertation committee member.

I can not resit my self to acknowledge the support given by my brother-in-law Mayur and my sister Priyanka who are one of the people who encourage me to graduate and take further step in my career specially Mayur for being there when i were tend to give up, without him i can not even imagine myself being part of the the UTA and the research work i am presenting here.

It would never be enough to say thank you to my parents for being there always for me as a moral,emotional and financial support to get graduated from one of the prestigious university and specially my mother who always keep reminding me to take my dinner on time and never stay hungry.

Contents

List of Figures

List of Tables

Chapter 1

Introduction

1.1 Background

In the aerospace industry, composite material has been superseding metallic material for the last decade due to its high strength to weight ratio and typically constitutes about 50% of an aircraft's weight. Lightweighting with optimum strength is the prime requirement of the aerospace structures such as fuselage and wings, which are thin-walled structures. Since such structures are prone to buckling than the other failure modes, such as a compression or shear failure, it is necessary to design thin structures to have optimum resistance to the buckling under general loading conditions.

One of the distinct advantages of laminated composites over metallic material in structural design is its ability to change the stiffness and strength properties of the laminate by designing the laminate stacking sequence relative to the application of load. Laminate in-plane properties are governed by the number of layers with different fiber orientation angles, and bending properties are governed by the relative positioning of the layers with reference to the mid-plane. Therefore, with the same number of plies in the laminate, one can get entirely different in-plane and bending properties by rearranging the laminate stacking sequence. With the given flexibility to change in-plane and bending properties of the laminate, one can easily design a distinct laminate that offers maximum in-plane or buckling resistance for a given boundary and loading conditions while maintaining the load-carrying capability without failures. Similarly, one can determine the minimum number of layers and their orientation angles to minimize the structure's weight for a specified buckling load factor with given boundary and loading conditions.

Before the emergence of the Automated Fiber Placement (AFP) techniques, designers were left with little choice but to design the composite structure with a conventional straight fiber layup as shown in Figure 1.1 which give constant stiffness distribution thought the structure even if the stress distribution is not uniform(for example a plate with a hole or non-uniform loading condition). Therefore the directional material stiffness offered by advanced composites is not utilized. However, the recent development of the AFP has made it possible to steer the individual fiber tows or tape curvilinearly, which results in a non-conventional layup as shown in Figure 1.2 and aides designers with wide design space to spatially distribute the stiffness such that it gives optimum structure performance under general loading.

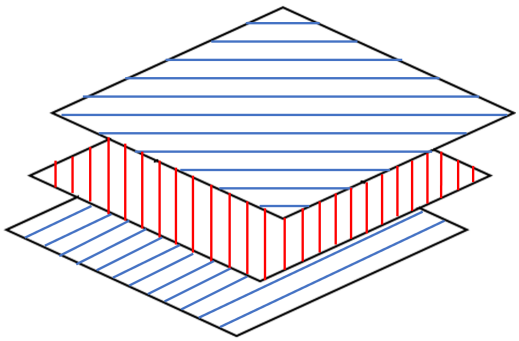

Figure 1.1: Conventional Layup

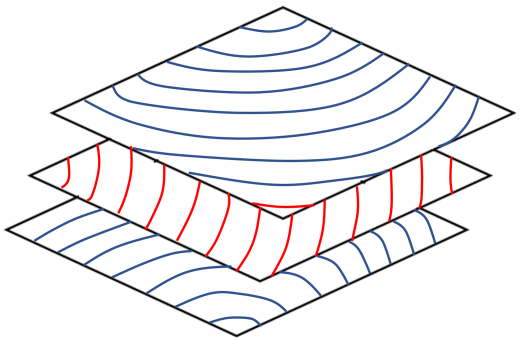

Figure 1.2: Non-conventional Layup

Gurdal and Olmedo [7] were among the first who introduced the "Variable stiffness Panel" concept by studying the in-plane response of the laminate with spatially varying fiber orientations where the effects of the variable fiber orientation on the displacement fields, stress resultants, and the global stiffness were presented

for univariate fiber orientations. Later they studied the buckling response in the subsequent for the same univariate fiber orientation (either function of x or y) where semi-analytical solutions were developed using Ritz-method and results showed better buckling response as compared to the constant stiffness panel [15]. This idea was expanded by a generalizing direction of fiber orientation angle variation to be rotated with respect to the coordinate direction x to study the buckling behavior and get the optimum buckling load [8].

There are two popular methods to optimize a composite panel for the buckling load. The first is stiffness variation-based optimization, and the second is fiber variation-based optimization. In the stiffness variation-based optimization approach, lamination parameters are introduced, representing the laminate stiffness properties ($ABD-matrix$) using fewer parameters and allowing for a continuous laminate stiffness formulation within a convex solution space. In this approach, the number of parameters remains the same even when the laminate thickness is increased [1] [9] [17]. Furthermore, since the formulation is within a conservative convex solution space, an efficient gradient-based optimizer such as a Gradient Decent(GD) method can be used to determine the optimal stiffness distribution to maximize structural performance. However, a secondary framework is still required to find the optimal fiber angle distribution after the optimum lamination parameters are found. However, it is no longer a convex problem as multiple stacking sequences and fiber directions can result in the same ABD matrix distribution. A further limitation of the stiffness-based optimization or Lamination parameter-based framework is that it is difficult to implement strength constraints in the optimization procedure. Despite these limitations, this optimization approach is efficient when the number of lamina in laminates(or laminates thickness) is high.

On the other hand, the fiber angle variation-based optimization framework directly defines the distinct fiber angle orientation throughout the domain of each ply, which results in stiffness variation [3] and does not require any post-processing. Furthermore, this approach also uses manufacturing constraint, strength constraint, stiffness constraint, curvature constraint efficiently during the optimization routine, which is difficult to implement in a purely stiffness-based optimization framework. However, fiber angle variation-based optimization framework may result in non-convex solution space; therefore, it is necessary to verify that the optimized result is a global optimum solution. Furthermore, this framework is efficient when the number of ply in the laminates(or laminate thickness) is few because the number of design variables increases with the increasing laminate thickness or ply.

As there is no closed-form solution available to calculate the buckling load for bivariate variable stiffness composite panel, numerical methods like FEM are used to find the buckling load. However, FEM discretizes the domain of the panel into sub-domain(sections) and assigns the stiffness properties section or sub-domain, which results in discontinuous stiffness variation. Therefore a semi-analytical approximation proposed by Tang [11] can be used to calculate the in-plane loading distribution and buckling. In this thesis, a mesh-less optimization approach is proposed, which uses a semi-analytical method to optimize the buckling load by a continuous distribution of stiffness as compared to a discrete approach of FEM. In the proposed method, fiber angle distribution is represented as a double Fourier series approximation that gives high fidelity in fiber angle variation.

1.2 Thesis Outline

The thesis presented here is divided into a total of seven chapters. Chapter 1 provides the motivation of the thesis and its structure. In chapter 2, a detailed derivation of governing equations [20] [16], the stability equation, and the Boundary value problem for a variable stiffness plate studied here is provided.

Chapter 3 describes the FEM and closed-form solution [20] for the reference problem of the constant stiffness plate. FEM problem definition for the stability or buckling load is established for an 8-ply composite laminate plate under investigation, and a mesh convergence study is performed for buckling load. Subsequently, the constant stiffness laminate modeled using FEM is optimized for the buckling load using Genetic algorithm(GA) to set a benchmark buckling load. The optimized results are verified with the analytical closed-form solution. Chapter 4 describes the framework(MFEM-framework) to achieve variable stiffness through the domain of the plate defined in FEM. Further, buckling load is optimized for univariate variable stiffness plate (angle variation in either x or y direction) and bivariate variable stiffness composite plate using Genetic algorithm(GA) and BFGS methods. Chapter 5 provides the derivation for a semi-analytical method to evaluate in-plane loading distribution and buckling load, utilizing double Fourier series approximation as a description of fiber angle distribution. A convergence study is performed to decide which double Fourier series approximation(either sine or cosine) represents the fiber angle distribution effectively. Finally, the buckling load is optimized using semi-analytical method independently for different cases of Fourier series expansion which represents the fiber angle distribution. BFGS method is used as an optimizer formulation to optimize the buckling load. Finally, optimized buckling load achieved using the different methods is reported and compared in Chapter 6. As the study presented in the thesis is still an open area of research, some future aspects of this study are discussed in Chapter 7.

Chapter 2

Governing equations and Boundary Value Problem

In this section, the kinematic quantities, constitutive equations and governing equations are formulated for variable stiffness plate based on procedure given by Whitney [20].

2.1 Basic Assumptions

In most practical applications of thin plates since the magnitude of the stresses acting on the surface parallel to the middle plane are small compared to the bending and membrane stresses therefore for a thin plate the traction on any surface parallel to the mid-plane are relatively small and consequently an approximate state of plane stress can be assumed.

A standard, x, y, z coordinate system, as shown in figure 2.1, is used in deriving the governing equations. The displacements in the x, y, z directions are denoted u, v, w respectively. The following basic assumptions are made:

1. The plate is constructed of an arbitrary number of layers of orthotropic sheets bonded together. However, the orthotropic axes of material symmetry of an individual layer need not coincide with the $x - y$ axis of the plate.
2. Each layer is of constant thickness. Consequently the plate has constant thickness h.
3. The plate is thin, i.e., the thickness h is much smaller than the other physical dimensions. Hence, transverse shear strains ϵ_{xz} and ϵ_{yz} are negligible, and transverse normal strain ϵ_z is negligible.
4. The displacements u, v, and w are small compared to the plate thickness.Similarly, In-plane strains ϵ_x, ϵ_y and ϵ_{xy} are small compared to unity.
5. Tangential displacements u and v are linear functions of the z coordinate.
6. Transverse shear stresses σ_{xz} and σ_{yz} vanish on the top and bottom surfaces of the plate(at $z = \pm h/2$, σ_{xz}=σ_{yz}=0).
7. In order to include in-plane force effects, nonlinear terms in the equations of motion involving products of stresses and plate slopes are retained. All other nonlinear terms are neglected.
8. Each ply obeys Hook's law.
9. There are no body forces such as gravitational or magnetic forces.
10. All the derivation are for static case, so all the inertia terms and time related parameters are neglected. Rotatory inertia terms are negligible.

It should be noted that assumption 3 is a direct consequence of plane stress, and constitute the classical assumptions of Kirchhoff.

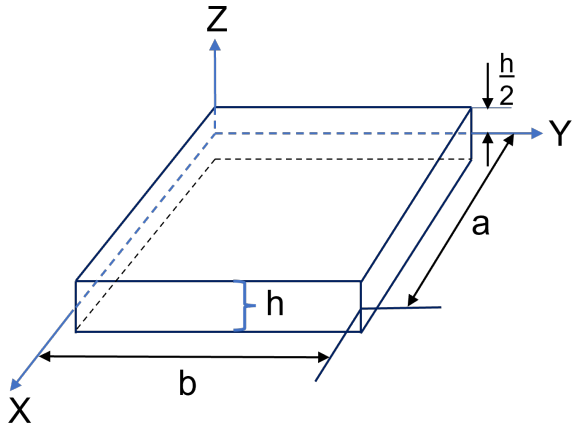

Figure 2.1: Coordinate system of plate.

2.2 Strain-displacement relations

Based on the assumptions made in Section 2.1, tangential or in-plane displacements at any location of plate are given as,

$$\begin{aligned} w &= w(x,y) \\ u &= u^0(x,y) - zw_{,x} \\ v &= v^0(x,y) - zw_{,y} \end{aligned} \tag{2.1}$$

where u^0 and v^0 are tangential displacements of the middle-plane. Strain-displacement relations can be written as,

$$\begin{aligned} \epsilon_x &= \epsilon_x^0 + z\kappa_x \\ \epsilon_y &= \epsilon_y^0 + z\kappa_y \\ \epsilon_{xy} &= \epsilon_{xy}^0 + z\kappa_{xy} \end{aligned} \tag{2.2}$$

where,

$$\epsilon_x^0 = u_{,x}^0 \qquad \epsilon_y^0 = v_{,x}^0 \qquad \epsilon_{xy}^0 = u_{,y}^0 + v_{,x}^0 \tag{2.3}$$

$$\kappa_x = -w_{,xx} \qquad \kappa_y = -w_{,yy} \qquad \kappa_{xy} = -2w_{,xy} \tag{2.4}$$

Equations 2.2,2.3 and 2.4 coincide with those of classical homogeneous plate theory.

2.3 Equations of Motion

Assumption 3 cannot be satisfied unless the resultant shear vanishes, which is not physically correct. However, this apparent inconsistency in classical plate theory is recognized and accepted, and resultant shears are considered when developing the equations of motions which are given for k^{th} laminate as,

$$\frac{\partial \sigma_x^k}{\partial x} + \frac{\partial \sigma_{xy}^k}{\partial y} + \frac{\partial \sigma_{xz}^k}{\partial z} = 0 \tag{2.5}$$

$$\frac{\partial \sigma_{xy}^k}{\partial x} + \frac{\partial \sigma_y^k}{\partial y} + \frac{\partial \sigma_{yz}^k}{\partial z} = 0 \tag{2.6}$$

$$\frac{\partial}{\partial x}(\sigma_{xx}^k + \sigma_x^k w_{,x} + \sigma_{xy}^k w_{,y}) + \frac{\partial}{\partial y}(\sigma_{yz}^k + \sigma_{xy}^k w_{,x} + \sigma_y^k w_{,y}) + \frac{\partial}{\partial z}(\sigma_x^k + \sigma_{xz}^k w_{,x} + \sigma_{yz}^k w_{,y}) = 0 \tag{2.7}$$

Stress and moment resultants are defined as follows:

$$(N_x, N_y, N_{xy}) = \int_{-h/2}^{h/2} (\sigma_x^k, \sigma_y^k, \sigma_{xy}^k)\, dz$$

$$(Q_x, Q_y) = \int_{-h/2}^{h/2} (\sigma_{xz}^k, \sigma_{yz}^k)\, dz \tag{2.8}$$

$$(M_x, M_y, M_{xy}) = \int_{-h/2}^{h/2} (\sigma_x^k, \sigma_y^k, \sigma_{xy}^k) z\, dz$$

These resultants are illustrated in figure 2.2a,2.2b.

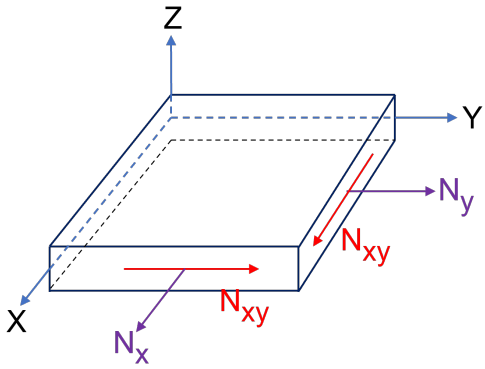

(a) Resultant stress nomenclature

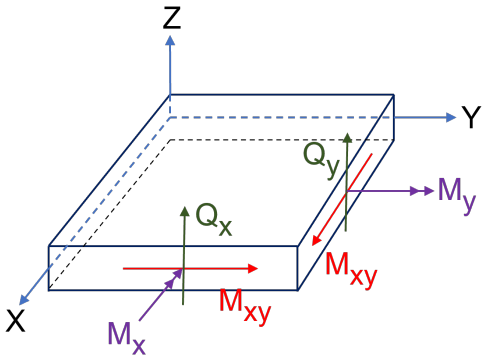

(b) Nomenclature for moment and transverse shear resultant

Figure 2.2: Nomenclature of resultants

Integrating Equations 2.5-2.7 with respect to z and then Substituting Equation 2.8, yields;

$$N_{x,x} + N_{xy,y} = 0 \tag{2.9}$$

$$N_{xy,x} + N_{y,y} = 0 \tag{2.10}$$

$$N_x w_{,xx} + 2N_{xy} w_{,xy} + N_y w_{,yy} + Q_{x,x} + Q_{y,y} + w_{,x}(N_{x,x} + N_{xy,y}) + w_{,y}(N_{xy,x} + N_{y,y}) + q = 0 \tag{2.11}$$

where;

$$q = \sigma_x^k(\frac{h}{2}) - \sigma_x^k(\frac{-h}{2}) \tag{2.12}$$

For static case, 2.9 and 2.10 can be substituted in equations 2.11, to give,

$$N_x w_{,xx} + 2N_{xy} w_{,xy} + N_y w_{,yy} + Q_{x,x} + Q_{y,y} + q = 0 \tag{2.13}$$

Now multiplying equations 2.5 and 2.6 by z, integrating with respect to z over the plate thickness, and taking equation 2.8 into account yields,

$$M_{x,x} + M_{xy,y} - Q_x = 0 \tag{2.14}$$

$$M_{xy,x} + M_{y,y} - Q_y = 0 \tag{2.15}$$

Differentiating equations 2.14 and 2.15 with respect to x and y respectively and then taking equation 2.13 into account yields,

$$M_{x,xx} + 2M_{xy,xy} + M_{y,yy} + N_x w_{,xx} + 2N_{xy} w_{,xy} + N_y w_{,yy} + q = 0 \tag{2.16}$$

equation 2.9, 2.10 and 2.16 together constitute the equations of motion and are identical to those of classical homogeneous plate theory.

2.4 Constitutive Equations

For a laminated composite plate, the plane stress constitutive equation for the k^{th} layer is defined as,

$$\begin{bmatrix} \sigma_x^k \\ \sigma_y^k \\ \sigma_{xy}^k \end{bmatrix} = \begin{bmatrix} Q_{11}^k & Q_{12}^k & Q_{16}^k \\ Q_{12}^k & Q_{22}^k & Q_{26}^k \\ Q_{16}^k & Q_{26}^k & Q_{66}^k \end{bmatrix} \begin{bmatrix} \epsilon_x \\ \epsilon_y \\ \epsilon_{xy} \end{bmatrix} \tag{2.17}$$

Where Q_{ij}^k are reduced stiffness terms for k^{th} layer [16]. Using equation 2.17 in conjunction with equation 2.2, the stress resultant, and moment resultant definitions, yield the following constitutive relation for a laminated composite plate:

$$\begin{bmatrix} N_x \\ N_y \\ N_{xy} \\ M_x \\ M_y \\ M_{xy} \end{bmatrix} = \begin{bmatrix} A_{11} & A_{12} & A_{16} & B_{11} & B_{12} & B_{16} \\ A_{12} & A_{22} & A_{26} & B_{12} & B_{22} & B_{26} \\ A_{16} & A_{26} & A_{66} & B_{16} & B_{26} & B_{66} \\ B_{11} & B_{12} & B_{16} & D_{11} & D_{12} & D_{16} \\ B_{12} & B_{22} & B_{26} & D_{12} & D_{22} & D_{26} \\ B_{16} & B_{26} & B_{66} & D_{16} & D_{26} & D_{66} \end{bmatrix} \begin{bmatrix} \epsilon_x^0 \\ \epsilon_y^0 \\ \epsilon_{xy}^0 \\ \kappa x \\ \kappa y \\ \kappa_{xy} \end{bmatrix} \tag{2.18}$$

where,

$$(A_{ij}, B_{ij}, D_{ij}) = \int_{-h/2}^{h/2} Q_{ij}^k (1, z, z^2)\, dz \tag{2.19}$$

It should be noted that for Variable Stiffness composite, with fiber angle is spatially varied, Q_{ij}^k is not constant within a ply, therefore,

$$Q_{ij}^k = Q_{ij}^k(x, y) \tag{2.20}$$

Thus, from equation 2.19 and 2.20 we find that the ABD matrix is a function of spatial dimensions x and y,

$$A_{ij} = A_{ij}(x, y) \qquad B_{ij} = B_{ij}(x, y) \qquad D_{ij} = D_{ij}(x, y) \tag{2.21}$$

2.5 Equation of Motion in terms of Displacements

In the following derivation the effect of in-plane forces on bending is neglected. In particular, it is assumed that large membrane forces are not applied externally to the plate.

After substituting equation 2.18 in equation 2.9,2.10 and 2.16 respectively and neglecting in-plane force effect on bending we get,

$$\begin{aligned} A_{11}u^0_{,xx} + 2A_{16}u^0_{,xy} + A_{66}u^0_{,yy} + A_{16}v^0_{,xx} + (A_{12} + A_{66})v^0_{,xy} + A_{26}v^0_{,yy} - B_{11}w_{,xxx} - 3B_{16}w_{,xxy} - B_{26}w_{,yyy} - \\ (B_{12} + 2B_{66})w_{,yyx} + (\frac{\partial A_{16}}{\partial y} + \frac{\partial A_{11}}{\partial x})u^0_{,x} + (\frac{\partial A_{66}}{\partial y} + \frac{\partial A_{16}}{\partial x})u^0_{,y} + (\frac{\partial A_{66}}{\partial y} + \frac{\partial A_{16}}{\partial x})v^0_{,x} + (\frac{\partial A_{26}}{\partial y} + \frac{\partial A_{12}}{\partial x})v^0_{,y} - \\ (\frac{\partial B_{16}}{\partial y} + \frac{\partial B_{11}}{\partial x})w_{,xx} - 2(\frac{\partial B_{66}}{\partial y} + \frac{\partial B_{16}}{\partial x})w_{,xy} - (\frac{\partial B_{26}}{\partial y} + \frac{\partial B_{12}}{\partial x})w_{,yy} = 0 \end{aligned} \tag{2.22}$$

similarly,

$$\begin{aligned} A_{16}u^0_{,xx} + (A_{12} + A_{66})u^0_{,xy} + A_{26}u^0_{,yy} + A_{66}v^0_{,xx} + 2A_{26}v^0_{,xy} + A_{22}v^0_{,yy} - B_{16}w^0_{,xxx} - (B_{12} + 2B_{66})w_{,xxy} - \\ B_{22}w_{,yyy} - 3B_{26}w_{,yyx} + (\frac{\partial A_{12}}{\partial y} + \frac{\partial A_{16}}{\partial x})u^0_{,x} + (\frac{\partial A_{26}}{\partial y} + \frac{\partial A_{66}}{\partial x})u^0_{,y} + (\frac{\partial A_{26}}{\partial y} + \frac{\partial A_{66}}{\partial x})v^0_{,x} + (\frac{\partial A_{22}}{\partial y} + \frac{\partial A_{26}}{\partial x})v^0_{,y} - \\ (\frac{\partial B_{12}}{\partial y} + \frac{\partial B_{16}}{\partial x})w_{,xx} - 2(\frac{\partial B_{26}}{\partial y} + \frac{\partial B_{66}}{\partial x})w_{,xy} - (\frac{\partial B_{22}}{\partial y} + \frac{\partial B_{26}}{\partial x})w_{,yy} = 0 \end{aligned} \tag{2.23}$$

and,

$$\begin{aligned} D_{11}w_{,xxxx} + 4D_{16}w_{,xxxy} + (2D_{12} + 4D_{66})w_{,xxyy} + 4D_{26}w_{,yyyx} + D_{22}w_{,yyyy} - B_{11}u^0_{,xxx} - 3B_{16}u^0_{,xxy} - \\ (B_{12} + 2B_{66})u^0_{,yyx} - B_{26}u^0_{,yyy} - B_{16}v^0_{,xxx} - (B_{12} + 2B_{66})v^0_{,xxy} - 3B_{26}v^0_{,yyx} - B_{22}v^0_{,yyy} - 2(\frac{\partial B_{16}}{\partial y} + \frac{\partial B_{11}}{\partial x})u^0_{,xx} - \\ (4\frac{\partial B_{16}}{\partial x} + 2\frac{\partial B_{12}}{\partial y} + 2\frac{\partial B_{66}}{\partial y})u^0_{,xy} - 2(\frac{\partial B_{26}}{\partial y} + \frac{\partial B_{66}}{\partial x})u^0_{,yy} - 2(\frac{\partial B_{66}}{\partial y} + \frac{\partial B_{16}}{\partial x})v^0_{,xx} - (2\frac{\partial B_{12}}{\partial x} + 2\frac{\partial B_{66}}{\partial x} + 4\frac{\partial B_{26}}{\partial y})v^0_{,xy} - \\ 2(\frac{\partial B_{22}}{\partial y} + \frac{\partial B_{26}}{\partial x})v^0_{,yy} + 2(\frac{\partial D_{16}}{\partial y} + \frac{\partial D_{11}}{\partial x})w_{,xxx} + (6\frac{\partial D_{16}}{\partial x} + 2\frac{\partial D_{12}}{\partial y} + 4\frac{\partial D_{66}}{\partial y})w_{,xxy} + 2(\frac{\partial D_{22}}{\partial y} + \frac{\partial D_{26}}{\partial x})w_{,yyy} + \\ (2\frac{\partial D_{12}}{\partial x} + 4\frac{\partial D_{66}}{\partial x} + 6\frac{\partial D_{26}}{\partial y})w_{,yyx} - (\frac{\partial^2 B_{12}}{\partial y\,\partial y} + 2\frac{\partial^2 B_{16}}{\partial x\,\partial y} + \frac{\partial^2 B_{11}}{\partial x\,\partial x})u^0_{,x} - (\frac{\partial^2 B_{26}}{\partial y\,\partial y} + 2\frac{\partial^2 B_{66}}{\partial x\,\partial y} + \frac{\partial^2 B_{16}}{\partial x\,\partial x})u^0_{,y} - \\ (\frac{\partial^2 B_{26}}{\partial y\,\partial y} + 2\frac{\partial^2 B_{66}}{\partial x\,\partial y} + \frac{\partial^2 B_{16}}{\partial x\,\partial x})v^0_{,x} - (\frac{\partial^2 B_{22}}{\partial y\,\partial y} + 2\frac{\partial^2 B_{26}}{\partial x\,\partial y} + \frac{\partial^2 B_{12}}{\partial x\,\partial x})v^0_{,y} + (\frac{\partial^2 D_{12}}{\partial y\,\partial y} + 2\frac{\partial^2 D_{16}}{\partial x\,\partial y} + \frac{\partial^2 D_{11}}{\partial x\,\partial x})w_{,xx} + \\ (2\frac{\partial^2 D_{26}}{\partial y\,\partial y} + 4\frac{\partial^2 D_{66}}{\partial x\,\partial y} + 2\frac{\partial^2 D_{16}}{\partial x\,\partial x})w_{,xy} + (\frac{\partial^2 D_{22}}{\partial y\,\partial y} + 2\frac{\partial^2 D_{26}}{\partial x\,\partial y} + \frac{\partial^2 D_{12}}{\partial x\,\partial x})w_{,yy} = q \end{aligned}$$

(2.24)

Equations 2.22,2.23 and 2.24 are governing equation for variable stiffness plate. Note that, if A, B and D were constant, all the derivatives in the above equations will be zero, which is the governing equation for constant stiffness plate. These equation can be simplified for specially orthotropic laminate where $A_{16}, A_{26}, D_{16}, D_{26}$ and B_{ij} are zero over the domain.

The force and moment resultants are obtained from the constitutive relations as shown in Eqaution 2.18.

$$N_x = A_{11}u^0_{,x} + A_{16}(u^0_{,y} + v^0_{,x}) + A_{12}v^0_{,y} - B_{11}w_{,xx} - 2B_{16}w_{,xy} - B_{12}w_{,yy} \tag{2.25}$$

$$N_y = A_{12}u^0_{,x} + A_{26}(u^0_{,y} + v^0_{,x}) + A_{22}v^0_{,y} - B_{12}w_{,xx} - 2B_{26}w_{,xy} - B_{22}w_{,yy} \tag{2.26}$$

$$N_{xy} = A_{16}u^0_{,x} + A_{66}(u^0_{,y} + v^0_{,x}) + A_{26}v^0_{,y} - B_{16}w_{,xx} - 2B_{66}w_{,xy} - B_{26}w_{,yy} \tag{2.27}$$

$$M_x = B_{11}u^0_{,x} + B_{16}(u^0_{,y} + v^0_{,x}) + B_{12}v^0_{,y} - D_{11}w_{,xx} - 2D_{16}w_{,xy} - D_{12}w_{,yy} \tag{2.28}$$

$$M_y = B_{12}u^0_{,x} + B_{26}(u^0_{,y} + v^0_{,x}) + B_{22}v^0_{,y} - D_{12}w_{,xx} - 2D_{26}w_{,xy} - D_{22}w_{,yy} \tag{2.29}$$

$$M_{xy} = B_{16}u^0_{,x} + B_{66}(u^0_{,y} + v^0_{,x}) + B_{26}v^0_{,y} - D_{16}w_{,xx} - 2D_{66}w_{,xy} - D_{26}w_{,yy} \tag{2.30}$$

From equations 2.28, 2.29, 2.30 and equation (2.14-2.15) the following shear resultants are obtained.

$$\begin{aligned} Q_x = {} & B_{11}u^0_{,xx} + 2B_{16}u^0_{,xy} + B_{66}u^0_{,yy} + B_{16}v^0_{,xx} + (B_{12} + B_{66})v^0_{,xy} + B_{26}v^0_{,yy} - D_{11}w_{,xxx} - 3D_{16}w_{,xxy} - \\ & (D_{12} + 2D_{66})w_{,yyx} - D_{26}w_{,yyy} + (\frac{\partial B_{16}}{\partial y} + \frac{\partial B_{11}}{\partial x})u^0_{,x} + (\frac{\partial B_{66}}{\partial y} + \frac{\partial B_{16}}{\partial x})u_{,y} + (\frac{\partial B_{66}}{\partial y} + \frac{\partial B_{16}}{\partial x})v^0_{,x} + \\ & (\frac{\partial B_{26}}{\partial y} + \frac{\partial B_{12}}{\partial x})v^0_{,y} - (\frac{\partial D_{16}}{\partial y} + \frac{\partial D_{11}}{\partial x})w_{,xx} - 2(\frac{\partial D_{66}}{\partial y} + \frac{\partial D_{16}}{\partial x})w_{,xy} - (\frac{\partial D_{26}}{\partial y} + \frac{\partial D_{12}}{\partial x})w_{,yy} \end{aligned} \tag{2.31}$$

$$\begin{aligned} Q_y = {} & B_{16}u^0_{,xx} + (B_{12} + B_{66})u^0_{,xy} + B_{26}u^0_{,yy} + B_{66}v^0_{,xx} + 2B_{26}v^0_{,xy} + B_{22}v^0_{,yy} - D_{16}w_{,xxx} - (D_{12} + 2D_{66})w_{,xxy} \\ & -3D_{26}w_{,yyx} - D_{22}w_{,yyy} + (\frac{\partial B_{12}}{\partial y} + \frac{\partial B_{16}}{\partial x})u^0_{,x} + (\frac{\partial B_{26}}{\partial y} + \frac{\partial B_{66}}{\partial x})u^0_{,y} + (\frac{\partial B_{26}}{\partial y} + \frac{\partial B_{66}}{\partial x})v_{0,x} + \\ & (\frac{\partial B_{22}}{\partial y} + \frac{\partial B_{26}}{\partial x})v^0_{,y} - (\frac{\partial D_{12}}{\partial y} + \frac{\partial D_{16}}{\partial x})w_{,xx} - 2(\frac{\partial D_{26}}{\partial y} + \frac{\partial D_{66}}{\partial x})w_{,xy} - (\frac{\partial D_{22}}{\partial y} + \frac{\partial D_{26}}{\partial x})w_{,yy} \end{aligned} \tag{2.32}$$

Using the constitutive equation (2.24) the following stresses are obtained within each layer:

$$\sigma^k_x = Q^k_{11}u^0_{,x} + Q^k_{16}(u^0_{,y} + v^0_{,x}) + Q^k_{12}v^0_{,y} - z(Q^k_{11}w_{,xx} + 2Q^k_{16}w_{,xy} + Q^k_{12}w_{,yy}) \tag{2.33}$$

$$\sigma^k_y = Q^k_{12}u^0_{,x} + Q^k_{26}(u^0_{,y} + v^0_{,x}) + Q^k_{22}v^0_{,y} - z(Q^k_{12}w_{,xx} + 2Q^k_{26}w_{,xy} + Q^k_{22}w_{,yy}) \tag{2.34}$$

$$\sigma^k_{xy} = Q^k_{16}u^0_{,x} + Q^k_{66}(u^0_{,y} + v^0_{,x}) + Q^k_{26}v^0_{,y} - z(Q^k_{16}w_{,xx} + 2Q^k_{66}w_{,xy} + Q^k_{26}w_{,yy}) \tag{2.35}$$

2.6 Governing Equation in Terms of a stress function and transverse displacement

For certain static and dynamic problems, where the in-plane inertia terms can be neglected, a stress function formulation of the in-plane loading can be defined using a stress function Φ such that,

$$N_x = \Phi_{,yy} \qquad N_y = \Phi_{,xx} \qquad N_{xy} = -\Phi_{,xy} \tag{2.36}$$

Equation 2.9 and 2.10 are exactly satisfied by equation 2.36. Using an abbreviated form of equation 2.18;

$$\begin{bmatrix} N \\ M \end{bmatrix} = \begin{bmatrix} A & B \\ B & D \end{bmatrix} \begin{bmatrix} \epsilon^0 \\ \kappa \end{bmatrix} \tag{2.37}$$

Equation 2.37 can be rewritten as,

$$\begin{bmatrix} \epsilon^0 \\ M \end{bmatrix} = \begin{bmatrix} A^* & B^* \\ (-B^*)^T & D^* \end{bmatrix} \begin{bmatrix} N \\ \kappa \end{bmatrix} \tag{2.38}$$

where the superscript T denotes a transpose matrix, and

$$A^* = A^{-1} \qquad B^* = -A^{-1}B \qquad D^* = D - BA^{-1}B \tag{2.39}$$

In the general A^* and D^* are symmetric while B^* is not. Substituting equation 2.38 into equation 2.16, and neglecting in plane force effects, yields,

$$\begin{aligned} &D^*_{11}w_{,xxxx} + 4D^*_{16}w_{,xxxy} + (2D^*_{12} + 4D^*_{66})w_{,xxyy} + 4D^*_{26}w_{,yyyx} + D^*_{22}w_{,yyyy} + B^*_{21}\Phi_{,xxxx} + (2B^*_{26} - B^*_{61})\Phi_{,xxxy} + \\ &(B^*_{11} + B^*_{22} - 2B^*_{66})\Phi_{,xxyy} + (2B^*_{16} - B^*_{62})\Phi_{,yyyx} + B^*_{12}\Phi_{,yyyy} + 2(\frac{\partial D^*_{16}}{\partial y} + \frac{\partial D^*_{11}}{\partial x})w_{,xxx} + \\ &(6\frac{\partial D^*_{16}}{\partial x} + 2\frac{\partial D^*{}_{12}}{\partial y} + 4\frac{\partial D^*_{66}}{\partial y})w_{,xxy} + 2(\frac{\partial D^*_{22}}{\partial y} + \frac{\partial D^*_{26}}{\partial x})w_{,yyy} + (2\frac{\partial D^*_{12}}{\partial x} + 4\frac{\partial D^*_{66}}{\partial x} + 6\frac{\partial D^*_{26}}{\partial y})w_{,yyx} + \\ &(\frac{\partial^2 D^*_{12}}{\partial y\,\partial y} + 2\frac{\partial^2 D^*_{16}}{\partial x\,\partial y} + \frac{\partial^2 D^*_{11}}{\partial x\,\partial x})w_{,xx} + (2\frac{\partial^2 D^*_{26}}{\partial y\,\partial y} + 4\frac{\partial^2 D^*_{66}}{\partial x\,\partial y} + 2\frac{\partial^2 D^*_{16}}{\partial x\,\partial x})w_{,xy} + (\frac{\partial^2 D^*_{22}}{\partial y\,\partial y} + 2\frac{\partial^2 D^*_{26}}{\partial x\,\partial y} + \frac{\partial^2 D^*_{12}}{\partial x\,\partial x})w_{,yy} + \\ &2(\frac{\partial B^*_{26}}{\partial y} + \frac{\partial B^*_{21}}{\partial x})\Phi_{,xxx} + 2(\frac{\partial B^*_{26}}{\partial x} - \frac{\partial B^*_{61}}{\partial x} + \frac{\partial B^*_{22}}{\partial y} - \frac{\partial B^*_{66}}{\partial y})\Phi_{,xxy} + 2(\frac{\partial B^*_{12}}{\partial y} + \frac{\partial B^*_{16}}{\partial x})\Phi_{,yyy} + \\ &2(\frac{\partial B^*_{11}}{\partial x} - \frac{\partial B^*_{66}}{\partial x} + \frac{\partial B^*_{16}}{\partial y} - \frac{\partial B^*_{62}}{\partial y})\Phi_{,yyx} + (\frac{\partial^2 B^*_{22}}{\partial y\,\partial y} + 2\frac{\partial^2 B^*_{26}}{\partial x\,\partial y} + \frac{\partial^2 B^*_{21}}{\partial x\,\partial x})\Phi_{,xx} - (\frac{\partial^2 B^*_{62}}{\partial y\,\partial y} + 2\frac{\partial^2 B^*_{66}}{\partial x\,\partial y} + \frac{\partial^2 B^*_{61}}{\partial x\,\partial x})\Phi_{,xy} + \\ &(\frac{\partial^2 B^*{}_{12}}{\partial y\,\partial y} + 2\frac{\partial^2 B^*{}_{16}}{\partial x\,\partial y} + \frac{\partial^2 B^*{}_{11}}{\partial x\,\partial x})\Phi_{,yy} = q \end{aligned} \tag{2.40}$$

Equation 2.6 involves two unknowns; thus a second relationship is necessary. So, the strain-displacement equations [20] is given as,

$$\epsilon^0_{x,yy} + \epsilon^0_{y,xx} - \epsilon^0_{xy,xy} = 0 \tag{2.41}$$

Substituting equation 2.38 into equation 2.41 and taking into account Equation 2.36 and equation 2.4 leads to following compatibility equation,

$$A^*_{22}\Phi_{,xxxx} - 2A^*_{26}\Phi_{,xxxy} + (2A^*_{12} + A^*_{66})\Phi_{,xxyy} - 2A^*_{16}\Phi_{,yyyx} + A^*_{11}\Phi_{,yyyy} - B^*_{21}w_{,xxxx} + (B^*_{61} - 2B^*_{26})w_{,xxxy} +$$
$$(2B^*_{66} - B^*_{22} - B^*_{11})w_{,xxyy} + (B^*_{62} - 2B^*_{16})w_{,yyyx} - B^*_{12}w_{,yyyy} + (\frac{\partial B^*_{61}}{\partial y} - 2\frac{\partial B^*_{21}}{\partial x})w_{,xxx} +$$
$$(\frac{\partial B^*_{61}}{\partial x} - 4\frac{\partial B^*_{26}}{\partial x} - 2\frac{\partial B^*_{11}}{\partial y} + 2\frac{\partial B^*_{66}}{\partial y})w_{,xxy} - (2\frac{\partial B^*_{12}}{\partial y} - \frac{\partial B^*_{62}}{\partial x})w_{,yyy} +$$
$$(2\frac{\partial B^*_{66}}{\partial x} - 2\frac{\partial B^*_{22}}{\partial x} - 4\frac{\partial B^*_{16}}{\partial y} + \frac{\partial B^*_{62}}{\partial y})w_{,yyx} - (\frac{\partial^2 B^*_{11}}{\partial y\,\partial y} - \frac{\partial^2 B^*_{61}}{\partial x\,\partial y} + \frac{\partial^2 B^*_{21}}{\partial x\,\partial x})w_{,xx} -$$
$$2(\frac{\partial^2 B^*_{16}}{\partial y\,\partial y} - \frac{\partial^2 B^*_{66}}{\partial x\,\partial y} + \frac{\partial^2 B^*_{26}}{\partial x\,\partial x})w_{,xy} - (\frac{\partial^2 B^*_{12}}{\partial y\,\partial y} - \frac{\partial^2 B^*_{62}}{\partial x\,\partial y} + \frac{\partial^2 B^*_{22}}{\partial x\,\partial x})w_{,yy} - (\frac{\partial A^*_{26}}{\partial y} - \frac{\partial A^*_{22}}{\partial x})\Phi_{,xxx} +$$
$$(2\frac{\partial A^*_{12}}{\partial y} - 3\frac{\partial A^*_{26}}{\partial x} + \frac{\partial A^*_{66}}{\partial y})\Phi_{,xxy} + (2\frac{\partial A^*_{11}}{\partial y} - \frac{\partial A^*_{16}}{\partial x})\Phi_{,yyy} + (2\frac{\partial A^*_{12}}{\partial x} + \frac{\partial A^*_{66}}{\partial x} - 3\frac{\partial A^*_{16}}{\partial y})\Phi_{,yyx} +$$
$$(\frac{\partial^2 A^*_{12}}{\partial y\,\partial y} - \frac{\partial^2 A^*_{26}}{\partial x\,\partial y} + \frac{\partial^2 A^*_{22}}{\partial x\,\partial x})\Phi_{,xx} - (\frac{\partial^2 A^*_{16}}{\partial y\,\partial y} - \frac{\partial^2 A^*_{66}}{\partial x\,\partial y} + \frac{\partial^2 A^*_{26}}{\partial x\,\partial x})\Phi_{,xy} + (\frac{\partial^2 A^*_{11}}{\partial y\,\partial y} - \frac{\partial^2 A^*_{16}}{\partial x\,\partial y} + \frac{\partial^2 A^*_{12}}{\partial x\,\partial x})\Phi_{,yy} = 0 \tag{2.42}$$

The moment resultants are obtained from the constitutive relations as shown in equation 2.38:

$$M_x = -\left(B^*_{21}\Phi_{,xx} - B^*_{61}\Phi_{,xy} + B^*_{11}\Phi_{,yy} + D^*_{11}w_{,xx} + 2D^*_{16}w_{,xy} + D^*_{12}w_{,yy}\right) \tag{2.43}$$

$$M_y = -\left(B^*_{22}\Phi_{,xx} - B^*_{62}\Phi_{,xy} + B^*_{12}\Phi_{,yy} + D^*_{12}w_{,xx} + 2D^*_{26}w_{,xy} + D^*_{22}w_{,yy}\right) \tag{2.44}$$

$$M_{xy} = -\left(B^*_{26}\Phi_{,xx} - B^*_{66}\Phi_{,xy} + B^*_{16}\Phi_{,yy} + D^*_{16}w_{,xx} + 2D^*_{66}w_{,xy} + D^*_{26}w_{,yy}\right) \tag{2.45}$$

And, from equations 2.14,2.14, and 2.6 the following shear resultants are obtained:

$$Q_x = -[B^*_{21}\Phi_{,xxx} + (B^*_{26} - B^*_{61})\Phi_{,xxy} + (B^*_{11} - B^*_{66})\Phi_{,yyx} + B^*_{16}\Phi_{,yyy} +$$
$$D^*_{11}w_{,xxx} + 3D^*_{16}w_{,xxy} + (D^*_{12} + 2D^*_{66})w_{,yyx} + D^*_{26}w_{,yyy} +$$
$$(\frac{\partial D^*_{16}}{\partial y} + \frac{\partial D^*_{11}}{\partial x})w_{,xx} + 2(\frac{\partial D^*_{66}}{\partial y} + \frac{\partial D^*_{16}}{\partial x})w_{,xy} + (\frac{\partial D^*_{26}}{\partial y} + \frac{\partial D^*_{12}}{\partial x})w_{,yy} +$$
$$(\frac{\partial B^*_{26}}{\partial y} + \frac{\partial B^*_{21}}{\partial x})\Phi_{,xx} - (\frac{\partial B^*_{66}}{\partial y} + \frac{\partial B^*_{61}}{\partial x})\Phi_{,xy} + (\frac{\partial B^*_{16}}{\partial y} + \frac{\partial B^*_{11}}{\partial x})\Phi_{,yy}] \tag{2.46}$$

$$Q_y = -[B^*_{26}\Phi_{,xxx} + (B^*_{22} - B^*_{66})\Phi_{,xxy} + (B^*_{16} - B^*_{62})\Phi_{,yyx} + B^*_{12}\Phi_{,yyy} +$$
$$D^*_{16}w_{,xxx} + (D^*_{12} + 2D^*_{66})w_{,xxy} + 3D^*_{26}w_{,yyx} + D^*_{22}w_{,yyy} +$$
$$(\frac{\partial D^*_{12}}{\partial y} + \frac{\partial D^*_{16}}{\partial x})w_{,xx} + 2(\frac{\partial D^*_{26}}{\partial y} + \frac{\partial D^*_{66}}{\partial x})w_{,xy} + (\frac{\partial D^*_{22}}{\partial y} + \frac{\partial D^*_{26}}{\partial x})w_{,yy} +$$
$$(\frac{\partial B^*_{22}}{\partial y} + \frac{\partial B^*_{26}}{\partial x})\Phi_{,xx} - (\frac{\partial B^*_{62}}{\partial y} + \frac{\partial B^*_{66}}{\partial x})\Phi_{,xy} + (\frac{\partial B^*_{12}}{\partial y} + \frac{\partial B^*_{16}}{\partial x})\Phi_{,yy}] \tag{2.47}$$

2.7 Stability of Variable stiffness composite Plates

In the two previous sections it was assumed that no large external in-plane forces were applied to the plate. However, plate buckling occurs only under large in-plane loads. Thus a stability analysis must include the effect of in-plane forces on plate bending. If equation 2.16 is used in its present form, then for unsymmetrical laminates ($B_{ij} \neq 0$) the problem becomes nonlinear. Since our concept of a critical buckling load is based on a linear analysis, an altered form of equation 2.16 must be obtained. This can be done in a manner directly analogous to procedures in classical shell theory.

Consider the displacement field,

$$u^0 = u^{0i} + \lambda u^0 \qquad v^0 = v^{0i} + \lambda v^0 \qquad w = w^i + \lambda w \tag{2.48}$$

where the superscript i denotes the pre-buckling displacements and λ is an infinitesimally small perturbation. Therefore, a critical load is sought which causes an infinitesimally small shift in the equilibrium position. In classical stability theory this is referred to as the "Adjacent equilibrium method". Using equation 2.48 in conjunction with the constitutive relations given in equation 2.37 leads to the following matrix equations,

$$\begin{aligned} N &= A\epsilon^{0i} + B\kappa^i + \lambda(A\epsilon + B\kappa) = N^i + \lambda N \\ M &= B\epsilon^{0i} + D\kappa^i + \lambda(B\epsilon + D\kappa) = M^i + \lambda M \end{aligned} \tag{2.49}$$

Substituting, equation 2.48 and 2.49 into equation 2.16, collecting terms of like powers in λ, and neglecting second order terms in λ leads to the following post-buckling equation,

$$M_{x,xx} + 2M_{xy,xy} + M_{y,yy} + N_x^i w_{,xx} + N_x w_{,xx}^i + 2N_{xy}^i w_{,xy} + 2N_{xy} w_{,xy}^i + N_y^i w_{,yy} + N_y w_{,yy}^i + q = 0 \tag{2.50}$$

Since w^i, Ny, and N^i are obtained from the solutions for the initial equilibrium position equation 2.50 is linear. However difficulty is still encountered as the nonlinear version of equation 2.16 is used to determine the initial configuration. A common simplification can be introduced by using linear theory to determine solutions corresponding to the initial equilibrium position. This assumption is the distinguishing feature of a linear stability analysis. Since the initial configuration is determined from linear theory, the terms in equation 2.50 containing initial curvatures can be neglected. Thus equation 2.50 becomes,

$$M_{x,xx} + 2M_{xy,xy} + M_{y,yy} + N_x^i w_{,xx} + 2N_{xy}^i w_{,xy} + N_y^i w_{,yy} + q = 0 \tag{2.51}$$

For the displacement formulation of the stability problem, the governing Equations include 2.22 and 2.23. Taking 2.51 into account. Equation 2.24 becomes,

$$\begin{aligned} &D_{11}w_{,xxxx} + 4D_{16}w_{,xxxy} + (2D_{12} + 4D_{66})w_{,xxyy} + 4D_{26}w_{,yyyx} + D_{22}w_{,yyyy} - B_{11}u^0_{,xxx} - 3B_{16}u^0_{,xxy} - \\ &(B_{12} + 2B_{66})u^0_{,yyx} - B_{26}u^0_{,yyy} - B_{16}v^0_{,xxx} - (B_{12} + 2B_{66})v^0_{,xxy} - 3B_{26}v^0_{,yyx} - B_{22}v^0_{,yyy} - 2(\frac{\partial B_{16}}{\partial y} + \frac{\partial B_{11}}{\partial x})u^0_{,xx} - \\ &(4\frac{\partial B_{16}}{\partial x} + 2\frac{\partial B_{12}}{\partial y} + 2\frac{\partial B_{66}}{\partial y})u^0_{,xy} - 2(\frac{\partial B_{26}}{\partial y} + \frac{\partial B_{66}}{\partial x})u^0_{,yy} - 2(\frac{\partial B_{66}}{\partial y} + \frac{\partial B_{16}}{\partial x})v^0_{,xx} - (2\frac{\partial B_{12}}{\partial x} + 2\frac{\partial B_{66}}{\partial x} + 4\frac{\partial B_{26}}{\partial y})v^0_{,xy} - \\ &2(\frac{\partial B_{22}}{\partial y} + \frac{\partial B_{26}}{\partial x})v^0_{,yy} + 2(\frac{\partial D_{16}}{\partial y} + \frac{\partial D_{11}}{\partial x})w_{,xxx} + (6\frac{\partial D_{16}}{\partial x} + 2\frac{\partial D_{12}}{\partial y} + 4\frac{\partial D_{66}}{\partial y})w_{,xxy} + 2(\frac{\partial D_{22}}{\partial y} + \frac{\partial D_{26}}{\partial x})w_{,yyy} + \\ &(2\frac{\partial D_{12}}{\partial x} + 4\frac{\partial D_{66}}{\partial x} + 6\frac{\partial D_{26}}{\partial y})w_{,yyx} - (\frac{\partial^2 B_{12}}{\partial y\,\partial y} + 2\frac{\partial^2 B_{16}}{\partial x\,\partial y} + \frac{\partial^2 B_{11}}{\partial x\,\partial x})u^0_{,x} - (\frac{\partial^2 B_{26}}{\partial y\,\partial y} + 2\frac{\partial^2 B_{66}}{\partial x\,\partial y} + \frac{\partial^2 B_{16}}{\partial x\,\partial x})u^0_{,y} - \\ &(\frac{\partial^2 B_{26}}{\partial y\,\partial y} + 2\frac{\partial^2 B_{66}}{\partial x\,\partial y} + \frac{\partial^2 B_{16}}{\partial x\,\partial x})v^0_{,x} - (\frac{\partial^2 B_{22}}{\partial y\,\partial y} + 2\frac{\partial^2 B_{26}}{\partial x\,\partial y} + \frac{\partial^2 B_{12}}{\partial x\,\partial x})v^0_{,y} + (\frac{\partial^2 D_{12}}{\partial y\,\partial y} + 2\frac{\partial^2 D_{16}}{\partial x\,\partial y} + \frac{\partial^2 D_{11}}{\partial x\,\partial x})w_{,xx} + \\ &(2\frac{\partial^2 D_{26}}{\partial y\,\partial y} + 4\frac{\partial^2 D_{66}}{\partial x\,\partial y} + 2\frac{\partial^2 D_{16}}{\partial x\,\partial x})w_{,xy} + (\frac{\partial^2 D_{22}}{\partial y\,\partial y} + 2\frac{\partial^2 D_{26}}{\partial x\,\partial y} + \frac{\partial^2 D_{12}}{\partial x\,\partial x})w_{,yy} = N_x^i w_{,xx} + 2N_{xy}^i w_{,xy} + N_y^i w_{,yy} + q \end{aligned} \tag{2.52}$$

For the stress function formulation the governing Equations include 2.6 and2.6 which becomes, after taking 2.51 into account,

$$D^*_{11}w_{,xxxx} + 4D^*_{16}w_{,xxxy} + (2D^*_{12} + 4D^*_{66})w_{,xxyy} + 4D^*_{26}w_{,yyyx} + D^*_{22}w_{,yyyy} + B^*_{21}\Phi_{,xxxx} +$$
$$(2B^*_{26} - B^*_{61})\Phi_{,xxxy} + (B^*_{11} + B^*_{22} - 2B^*_{66})\Phi_{,xxyy} + (2B^*_{16} - B^*_{62})\Phi_{,yyyx} + B^*_{12}\Phi_{,yyyy} +$$
$$2(\frac{\partial D^*_{16}}{\partial y} + \frac{\partial D^*_{11}}{\partial x})w_{,xxx} + (6\frac{\partial D^*_{16}}{\partial x} + 2\frac{\partial D^{*}{}_{12}}{\partial y} + 4\frac{\partial D^*_{66}}{\partial y})w_{,xxy} + 2(\frac{\partial D^*_{22}}{\partial y} + \frac{\partial D^*_{26}}{\partial x})w_{,yyy} +$$
$$(2\frac{\partial D^*_{12}}{\partial x} + 4\frac{\partial D^*_{66}}{\partial x} + 6\frac{\partial D^*_{26}}{\partial y})w_{,yyx} + (\frac{\partial^2 D^*_{12}}{\partial y\,\partial y} + 2\frac{\partial^2 D^*_{16}}{\partial x\,\partial y} + \frac{\partial^2 D^*_{11}}{\partial x\,\partial x})w_{,xx} +$$
$$(2\frac{\partial^2 D^*_{26}}{\partial y\,\partial y} + 4\frac{\partial^2 D^*_{66}}{\partial x\,\partial y} + 2\frac{\partial^2 D^*_{16}}{\partial x\,\partial x})w_{,xy} + (\frac{\partial^2 D^*_{22}}{\partial y\,\partial y} + 2\frac{\partial^2 D^*_{26}}{\partial x\,\partial y} + \frac{\partial^2 D^*_{12}}{\partial x\,\partial x})w_{,yy} + 2(\frac{\partial B^*_{26}}{\partial y} + \frac{\partial B^*_{21}}{\partial x})\Phi_{,xxx} +$$
$$2(\frac{\partial B^*_{26}}{\partial x} - \frac{\partial B^*_{61}}{\partial x} + \frac{\partial B^*_{22}}{\partial y} - \frac{\partial B^*_{66}}{\partial y})\Phi_{,xxy} + 2(\frac{\partial B^*_{12}}{\partial y} + \frac{\partial B^*_{16}}{\partial x})\Phi_{,yyy} +$$
$$2(\frac{\partial B^*_{11}}{\partial x} - \frac{\partial B^*_{66}}{\partial x} + \frac{\partial B^*_{16}}{\partial y} - \frac{\partial B^*_{62}}{\partial y})\Phi_{,yyx} + (\frac{\partial^2 B^*_{22}}{\partial y\,\partial y} + 2\frac{\partial^2 B^*_{26}}{\partial x\,\partial y} + \frac{\partial^2 B^*_{21}}{\partial x\,\partial x})\Phi_{,xx} -$$
$$(\frac{\partial^2 B^*_{62}}{\partial y\,\partial y} + 2\frac{\partial^2 B^*_{66}}{\partial x\,\partial y} + \frac{\partial^2 B^*_{61}}{\partial x\,\partial x})\Phi_{,xy} + (\frac{\partial^2 B^{*}{}_{12}}{\partial y\,\partial y} + 2\frac{\partial^2 B^{*}{}_{16}}{\partial x\,\partial y} + \frac{\partial^2 B^{*}{}_{11}}{\partial x\,\partial x})\Phi_{,yy} = N^i_x w_{,xx} + 2N^i_{xy}w_{,xy} + N^i_y w_{,yy} + q \tag{2.53}$$

Equations 2.52 and 2.53, are the two governing differential equations for the stability of a VS plate. These equations provide a general formulation, and can be simplified for specific cases, like symmetric laminates where $[B_{ij}] = 0$. The constant stiffness cases is obtained by setting the derivative of $[A], [B], [D]$ to zero.

2.8 Boundary Value Problem

In this thesis a simply supported composite plate under uni-axial loading is optimized for the buckling load. The dimension of the plate are $aXb = 1000mmX1000mm$ result in unit aspect ratio($R = 1$).The unidirectional carbon-epoxy IM7-8552 lamina [13] was selected as a for present study where properties of the material is given in the Table 2.1. The composite plate is made up of 8-ply laminates as shown in Figure 2.3b. The loading and boundary condition are shown in Figure 2.3a.

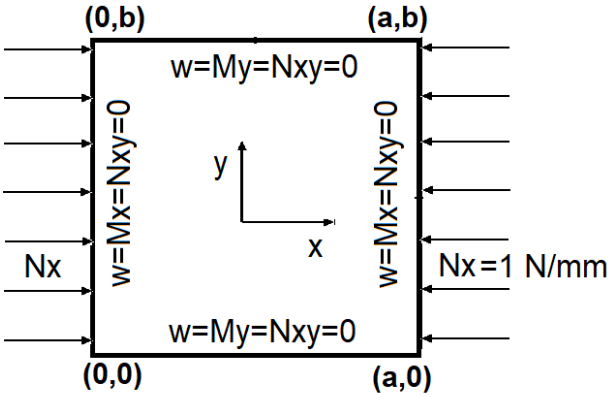

(a) Plate under uni-axial compression load

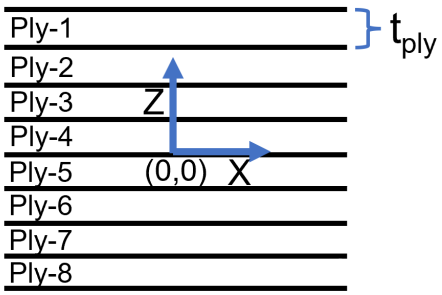

(b) Stack-up of the laminate plate under consideration

Figure 2.3: Boundary value problem under investigation

Modulus, E(MPa)		Poisson's ratio, v(-)		Shear Modulus, G(MPa)		Ply thickness, t_{ply}(mm)
$E1$	171,420	v_{12}	0.32	G_{12}	5290	0.125
$E2$	9080	v_{13}	0.32	G_{13}	5290	
$E3$	9080	v_{23}	0.5	G_{23}	3974	

Table 2.1: Material properties of IM7-8552.

The Loading boundary condition can be written mathematically as,

$$N_x = 1N/mm, N_{xy} = 0 \quad \text{(on x=0,a)} \tag{2.54}$$

$$N_y = 0, N_{xy} = 0 \quad \text{(on y=0,b)} \tag{2.55}$$

And since, plate under study is simply supported, the essential and natural boundary condition can be written mathematically as,

$$w = 0, M_x = 0, M_{xy} = 0, M_z = 0 \quad \text{(on x=0,a)} \tag{2.56}$$

$$w = 0, M_y = 0, M_{xy} = 0, M_z = 0 \quad \text{(on y=0,b)} \tag{2.57}$$

Chapter 3

Buckling Load Optimization of CS composite plate using FEM

As a first step, the case of constant stiffness (CS) composite plate was studied. The aim of this study is to; first establish a finite element framework and perform mesh convergence. Second, to verify Genetic Algorithm (GA) [5] (refer Appedix-A) optimization method against analytical closed form solution. Third, to establish a benchmark buckling load to assess performance of variable stiffness plate.

3.1 Stability of Constant stiffness Plates

The derivation follows the procedure outlined by Whitney [20]. Consider a simply-supported bi-axially compressed, constant stiffness angle-ply laminated plate, with following boundary condition,

For, $x = 0$:

$$u^0 = 0, N_{xy} = 0, w = 0, M_x = 0 \tag{3.1}$$

For, $x = a$:

$$u^0 = C_1, N_{xy} = 0, w = 0, M_x = 0 \tag{3.2}$$

For, $y = 0$:

$$v^0 = 0, N_{xy} = 0, w = 0, M_y = 0 \tag{3.3}$$

For, $y = b$:

$$v^0 = C_2, N_{xy} = 0, w = 0, M_y = 0 \tag{3.4}$$

For this particular case, stability equation can be solved into a closed form solution [20] where initial pre-buckling displacement field is assumed to be linear functions,

$$u^{0i} = \frac{c_1}{a}x \qquad v^{0i} = \frac{c_2}{b}y \qquad w^i = 0 \tag{3.5}$$

which satisfy all the boundary condition simultaneously for $q = 0$. The constant c_1 and c_2 are determined by assuming

$$N_x^i = -N_0 = constant \qquad N_y^i = -kN_0, N_0 > 0 \tag{3.6}$$

where k is a load proportionality constant in case of bi-axial loading. Substituting equation (3.5-3.6) into equation (2.25-2.26) c_1 and c_2 can be determined as follows,

$$c_1 = \frac{(A_{12}k - A22)N_0}{A_{11}A_{22} - A_{12}^2} \qquad c_2 = \frac{(A_{12}k - A11)N_0}{A_{11}A_{22} - A_{12}^2} \tag{3.7}$$

The post-buckling equations can be determined using Equation (2.22-2.23) and equation 2.52 for constant stiffness laminate as,

$$A_{11}u^0_{,xx} + A_{66}u^0_{,yy} + (A_{12} + A_{66})v^0_{,xy} - 3B_{16}w_{,xxy} - B_{26}w_{,yyy} = 0 \tag{3.8}$$

similarly,

$$(A_{12} + A_{66})u^0_{,xy} + A_{66}v^0_{,xx} + A_{22}v^0_{,yy} - B_{16}w^0_{,xxx} - 3B_{26}w_{,yyx} = 0 \tag{3.9}$$

and,

$$\begin{aligned} D_{11}w_{,xxxx} + (2D_{12} + 4D_{66})w_{,xxyy} + D_{22}w_{,yyyy} - 3B_{16}u^0_{,xxy} - B_{26}u^0_{,yyy} \\ -B_{16}v^0_{,xxx} - 3B_{26}v^0_{,yyx} - B_{22}v^0_{,yyy} + N_0(w_{,xx} + kw, yy) = 0 \end{aligned} \tag{3.10}$$

Equation(3.8-**??**) and boundary condition equation(3.1-3.4) are satisfied by following displacement field,

$$\begin{aligned} u^0 &= Asin(\frac{m\pi x}{a})cos(\frac{n\pi y}{b}) \\ v^0 &= Bcos(\frac{m\pi x}{a})sin(\frac{n\pi y}{b}) \\ w &= Csin(\frac{m\pi x}{a})sin(\frac{n\pi y}{b}) \end{aligned} \tag{3.11}$$

After substituting equation 3.11 into equations(3.8-**??**) and collecting like terms leads to following homogeneous equation

$$\begin{bmatrix} A_{mn} & B_{mn} & C_{mn} \\ B_{mn} & D^{mn} & E_{mn} \\ C_{mn} & E_{mn} & (F_{mn} - \lambda) \end{bmatrix} = \begin{bmatrix} 0 \\ 0 \\ 0 \end{bmatrix} \tag{3.12}$$

In order to solve Equation 3.12, and to obtain non-trivial solution, the determinant of the matrix should be zero. Equating the determinant of the matrix to zero, the equation of λ and ultimately buckling load N_0 can be found in closed form,

$$\begin{aligned} N_0 = \frac{\pi^2}{R^2b^2(m^2 + kn^2R^2)}[D_{11}m^4 + 2(D_{12} + 2D_{66})m^2n^2R^2 + D_{22}n^4R^4] \\ -\frac{1}{J_1}[m(B_{16}m^2 + 3B_{26}n^2R^2)J_2 + nR(3B_{16}m^2 + B_{26}n^2R^2)J_3] \end{aligned} \tag{3.13}$$

where,

$$\begin{aligned} J_1 &= (A_{11}m^2 + A_{66}n^2R^2)(A_{66}m^2 + A_{22}n^2R^2) - (A_{12} + A_{66})^2m^2n^2R^2 \\ J_2 &= (A_{11}m^2 + A_{66}n^2R^2)(B_{16}m^2 + 3B_{26}n^2R^2) - n^2R^2(A_{12} + A_{66})(3B_{16}m^2 + 3B_{26}n^2R^2) \\ J_3 &= (A_{66}m^2 + A_{22}n^2R^2)(3B_{16}m^2 + B_{26}n^2R^2) - n^2R^2(A_{12} + A_{66})(B_{16}m^2 + 3B_{26}n^2R^2) \end{aligned} \tag{3.14}$$

The buckling load for uni-axial load case can be found by setting $k = 0$. In the above equation, the following observations can be made; first, the maximum load is obtained when the second term in the equation is less than or equal to zero. The second term is equal to zero when $B_{16} = B_{26} = 0$, which indicates that maximum buckling load is achieved for symmetric laminates.

3.2 FEM Mesh Convergence Study

A square plate of size 1000mm x 1000mm is considered with applied in-plane uni-axial compressive load as illustrated in the Figure 3.1. The plate is simply supported on all the edges and The unidirectional carbon-epoxy IM7-8552 was selected for the present study where properties of the material is given in Table-2.1 [13].

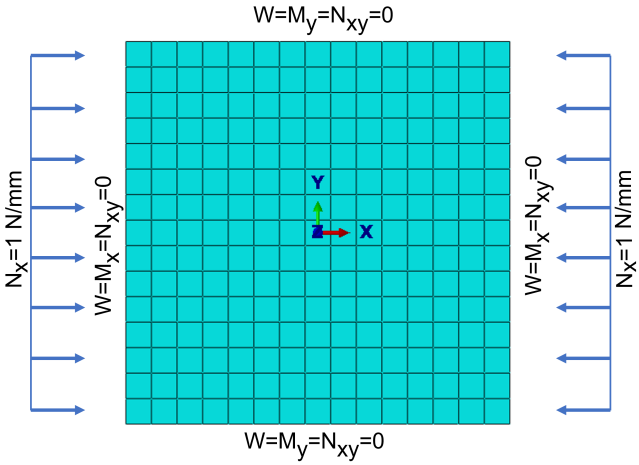

Figure 3.1: Plate under uni-axial compression load
FEM stress-element $M\times$ N= 15×15

The Finite element procedure is an eigenvalue problem of form [16],

$$\left[K - \lambda_i G\right] v_i = 0 \tag{3.15}$$

where, K is assembled stiffness matrix, G is geometric stiffness matrix, v_i is $i'th$ eigenvector associated with $i'th$ eigenvalue, from which lowest eigenvalue is sought for critical buckling load. A 8-ply composite plate with quasi-isotropic symmetric laminate $[0\ 45\ 90\ -45]_s$, was modeled in a commercial FEA software Abaqus [18] with boundary and loading condition, shown in Figure 3.1. The plate was discretized along x and y (mesh $M \times N$) respectively using S4 element, which is a 4-node quadrilateral conventional shell element with full integration scheme. The convergence study of the buckling load vs mesh size are shown in Table-3.1.

Mesh(M × N)	Buckling Load(N/mm), N_0	Decrease(%)
5×5	0.21378	-
10×10	0.20305	5.019
15×15	0.20114	0.94
20×20	0.20045	0.343

Table 3.1: Mesh convergence study of the buckling load N_0

The convergence study shown above, indicates that the plate with mesh(15×15) has sufficiently converged (0.94% variation), hence was chosen as the minimum mesh size for further analysis and optimization in all case.

3.3 Optimization Results

To set the reference buckling load and to verify the GA-based optimization approach, a study on maximum buckling load of a constant stiffness plate was conducted. A brief note on GA is provided in Appendix-A. Here again, an eight ply composite was modeled in FEM, where the angles of each ply are the optimization variable. The optimization problem can be written as;

$$min - \lambda(\theta_k)\ \forall\ \theta_k \in [-90, 90],\ k = 1, 2, ..8 \tag{3.16}$$

Parameters for GA [5] algorithms are shown in Table-3.2. For optimization, two cases were studied. First, where the minimum step size of angle variation was kept to 1°. Second, where the variation was fixed at 45°.

For the optimization, at each iteration the FEM model was call and evaluated. The buckling load is then post processed and the results are fed to the GA routine. The complete process is automated using python scripting.

GA Parameter	Value
Generation	40
Population	150
Mutation Probability	0.2 (20%)
Crossover Probability	0.5 (50%)
Crossover type	Uniform
Parents Portion	0.3 (30%)
Elit ratio	0.01 (1%)
Variable bound	$[-90°, 90°]$

Table 3.2: GA Parameters for the optimization of CS Plate

By tracking the GA parameter population, it is possible to see the evolution of ABD matrices. Figures 3.2,3.3 and 3.4, show the GA function evaluation parameters versus the buckling load. It can be noticed from that GA tries to make all element of $[B_{ij}]$ and D_{26} and D_{16} zero. This observation is also evident from Equation 3.13 which shows that buckling load would be higher if these elements of $[ABD]$ matrix are zero. Also it can be noted that, D_{12} and D_{26} evolves to maximum which can be reasoned from Equation 3.13 as buckling load is proportional to these two parameters. From this optimization study, it can be concluded that, to get laminate which gives high buckling load, it at-least need to be symmetric which means $[B_{ij}]$ should be zero.

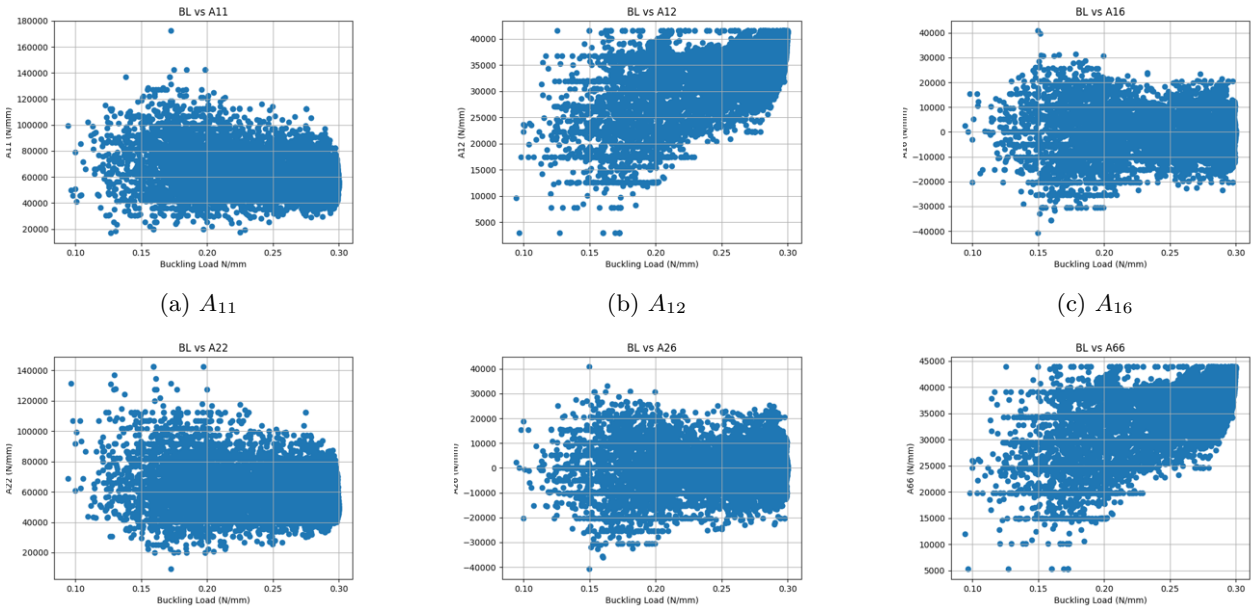

(a) A_{11} (b) A_{12} (c) A_{16}

(d) A_{22} (e) A_{26} (f) A_{66}

Figure 3.2: GA Evolution plot of $[A_{ij}]$

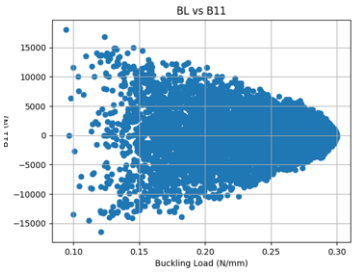

(a) B_{11}

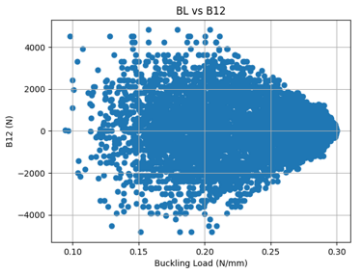

(b) B_{12}

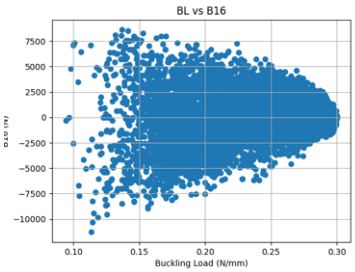

(c) B_{16}

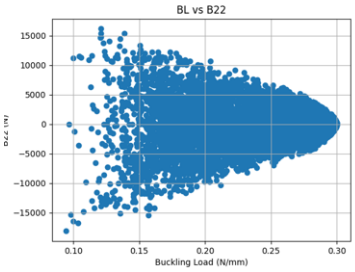

(d) B_{22}

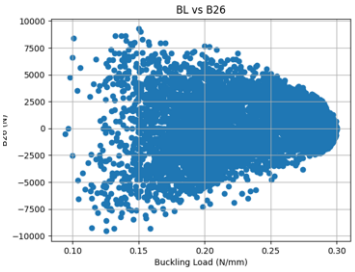

(e) B_{26}

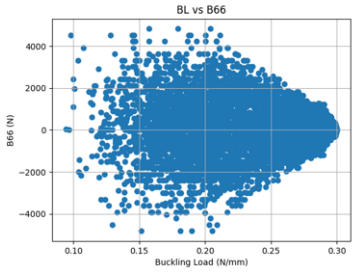

(f) B_{66}

Figure 3.3: GA Evolution plot of $[B_{ij}]$

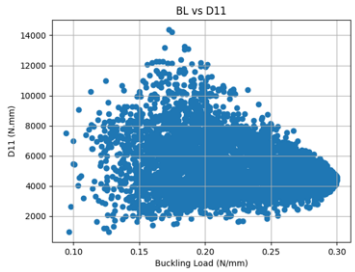

(a) D_{11}

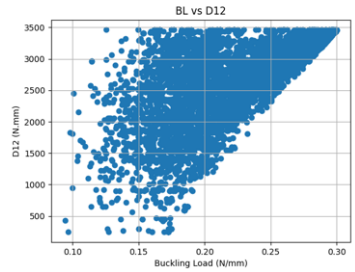

(b) D_{12}

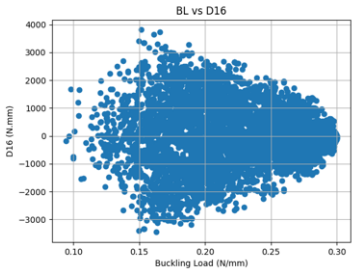

(c) D_{16}

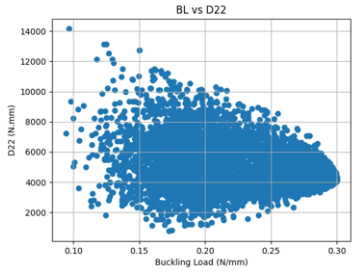

(d) D_{22}

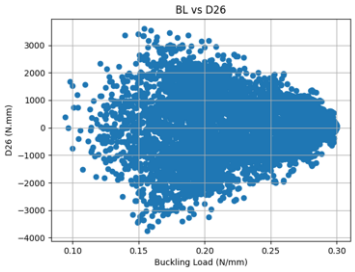

(e) D_{26}

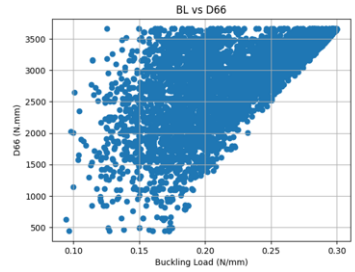

(f) D_{66}

Figure 3.4: GA Evolution plot of $[D_{ij}]$

Table 3.3, lists the optimization results for the two cases. From the results, it can be concluded that among all the possible laminates balanced anti-symmetric layup (layup [-45 45 45 -45 45 -45 -45 45]) is the best for the buckling. Since, there is an analytical-closed form solution for the constant stiffness composite laminate as shown in Section 3.2, the optimized buckling load achieved using FEM can also be verified. The analytical solution is found by setting $B_{ij} = D_{26} = D_{16} = 0$ (balanced-anti symmetric) in equation 3.13, to get the closed form solution 3.3. The result of the closed form solution is also listed in table 3.3.

$$N_0 = \frac{\pi^2}{R^2 b^2 (m^2 + kn^2 R^2)} [D_{11} m^4 + 2(D_{12} + 2D_{66}) m^2 n^2 R^2 + D_{22} n^4 R^4] \tag{3.17}$$

Layup	Type	Variable Steps(°)	(GA) Optimized Result	Buckling Load(N/mm), N_0
Test:1	General	1	[-44 46 42 -44 43 -46 -43 45]	0.2998
Test:2	General	45	[-45 45 45 -45 45 -45 -45 45]	0.3007
Eqn 3.16	General	-	[-45 45 45 -45 45 -45 -45 45]	0.2985

Table 3.3: Optimized buckling load for CS Plate.

Figure 3.5 and Figure 3.6 shows the comparison of first two buckling mode are compared calculated using FEM and Analytical method .

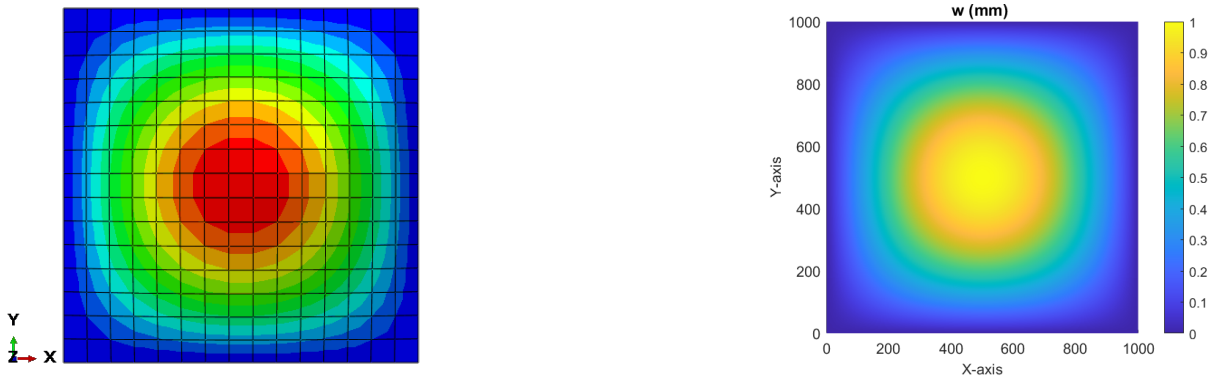

(a) $FEM(stress - element : 15X15)$ $(Eigenvalue = 0.3007)$

(b) Analytical solution $(Eigenvalue = 0.2985)$

Figure 3.5: First Buckling-mode comparison: FEM Vs Analytical

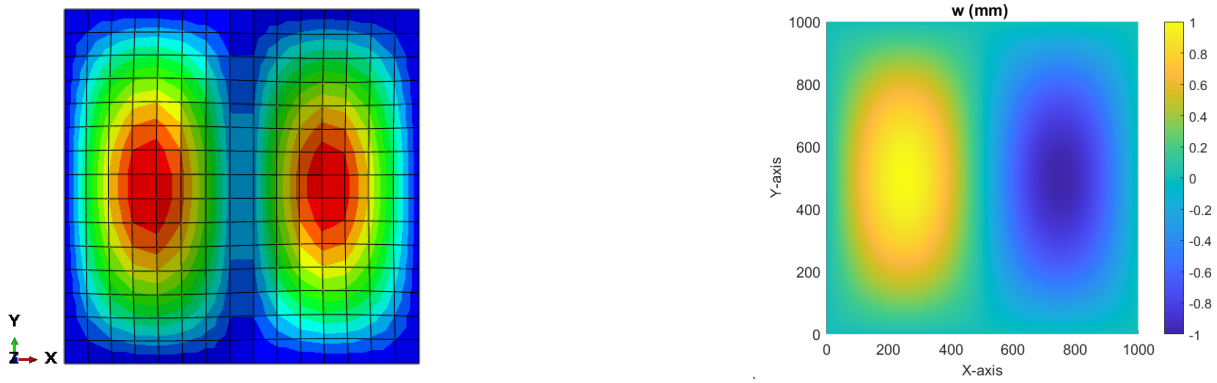

(a) $FEM(stress - element : 15X15)$ $(Eigenvalue = 0.4013)$

(b) Analytical solution $(Eigenvalue = 0.3950)$

Figure 3.6: Second Buckling-mode comparison: FEM Vs Analytical

3.4 Summary

From the analysis of constant stiffness plate, the following can be summarized. First, the maximum mesh size to obtain a converged solution is 15. Second, the optimum ply stack up for a constant stiffness plate is a balanced anti-symmetric [-45 45 45 -45 45 -45 -45 45]. Third, the optimization results using GA is reasonable and is verified using closed form solution.

Chapter 4

Buckling Load Optimization Of VS Composite Plate using FEM

The first approach taken to study the buckling of variable stiffness composite is using a FEM framework, where in the spatial variation of angle is provided as an input at each integration point. The question then becomes of how the angles are to be distributed across the plies. The most general approach would be to randomly define fiber angles $\theta^k(x, y)$ at centroidal location of each FEM stress-mesh element, as shown in Figure(2.1). However the main problem with this approach is large number of input or control parameters (fiber angle $\theta(x, y)$ for each stress-mesh element in each ply) for the optimization. Also randomness of fiber angle distribution can causes high stiffness discontinuity between two adjacent elements which may causes error in FEM approximation. Additionally, fiber angle distribution for each ply would be impossible to manufacture using AFP.

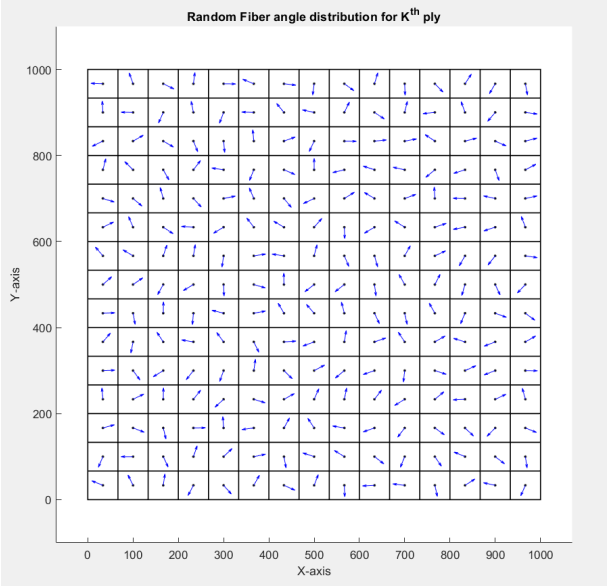

Figure 4.1: Random fiber angle distribution for K^{th} ply.

This problem can be addressed by using interpolation technique which reduce the number of input or control parameters for the optimization. There may be many techniques for the interpolation however, in this thesis, the fiber steering are achieved using Lagrangian interpolation where the domain of each ply is meshed using very coarse mesh which is called as MM (Manufacturing Mesh) and this interpolation framework is referred as MFEM(manufacturing finite element mesh)-framework [3]. The MFEM approach helps to reduce the optimization parameters by using fine stress-mesh for FEM calculations and coarser Manufacturing-mesh to obtain optimum fiber path throughout the domain independently.

In this section, the MFEM framework is described, followed by buckling load optimization studies for the different cases of variable stiffness composite plate. First study is on the buckling load optimization for univariate variable stiffness composite plate (fiber angle or direction as a function of x or y) is performed. Later, bivariate variable stiffness composite plate (fiber angle or direction as a function of both x and y) is optimized for the buckling using Genetic Algorithm (GA) and BFGS algorithm.

4.1 MFEM-Framework

A manufacturing mesh is a coarse 4-nodes quadrilateral element with only 1 degree of freedom per node per ply which represents fiber direction or angle $\theta(x, y)$ in k^{th} ply at j^{th} node. The fiber direction at the j^th node are then used to obtain the fiber direction or angle at the centroidal location of the stress-mesh elements which falls in the domain of each manufacturing mesh element. Consider the Figure 4.2, where stress-mesh is shown in green with centroids in black and manufacturing-mesh is shown red with angle at each node in black. Figure 4.3 shows the enlarged representation of e^{th} manufacturing-mesh element of k^{th} ply having angles θ_1^e to θ_4^e at the respective nodes and centroids of all the stress-mesh elements which falls in it's domain.

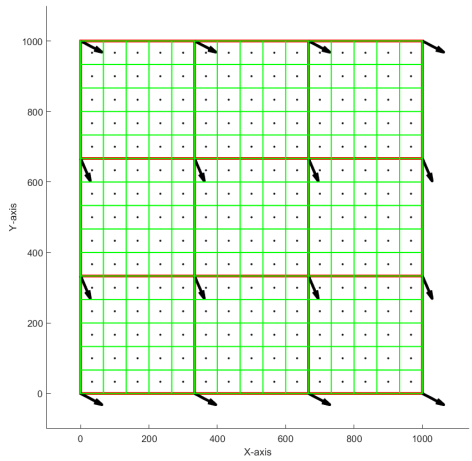

Figure 4.2: Manufacturing-Mesh with stress-mesh for k^{th} ply.

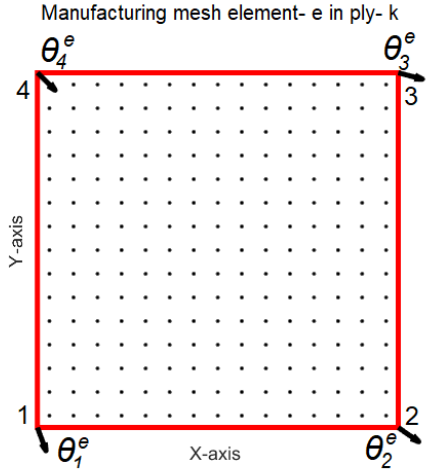

Figure 4.3: e^{th} Manufacturing mesh element of k^{th} ply.

The fiber directions of the manufacturing-mesh element at each node are interpolated at the centroidal location of stress-mesh elements using set of four Lagrangian's interpolation functions which are,

$$\begin{aligned} N_1 &= \frac{1}{4ab}(x - x_2)(y - y_4) \\ N_2 &= \frac{1}{4ab}(x - x_1)(y - y_3) \\ N_3 &= \frac{1}{4ab}(x - x_4)(y - y_2) \\ N_4 &= \frac{1}{4ab}(x - x_3)(y - y_1) \end{aligned} \tag{4.1}$$

where,

$$a = \frac{x_2 - x_1}{2} \qquad\qquad b = \frac{y_2 - y_1}{2} \tag{4.2}$$

subsequently, the fiber direction or angle $\theta(x, y)$ at the centroid located at (x, y) can be given as,

$$\theta^{e,k}(x, y) = \sum_{j=1}^{4} N_j^{(e)} \theta_j^{e,k} \tag{4.3}$$

here, fiber direction $\theta_j^{e,k}$ at each nodal point of manufacturing-mesh elements are design variables for the optimization. Once, the fiber direction $\theta_j^{e,k}$ from the nodal point of manufacturing-mesh element are mapped at the centroidal location of the stress-mesh element, FEM calculations such as stresses, strains and displacements are performed.

4.2 Univariate variable stiffness composite plate

When fiber angle distribution, throughout the domain of plate, is a function of only x, it results in stiffness as a function of variable x. Similarly for fiber angle distribution as a function of y. Univariate fiber angle distribution as a function of x can be achieved using following linear equation provided by Gurdal et al [8],

$$\theta(x) = \frac{2(T_1 - T_0)}{a}|x| + T_0 \tag{4.4}$$

Similarly, univariate fiber angle distribution as a function of y can be given as,

$$\theta(y) = \frac{2(T_1 - T_0)}{a}|y| + T_0 \tag{4.5}$$

Where, $< T_0, T_1 >$ is a set of initial and final angle of the fiber distribution.

4.2.1 Stiffness as a function of-x

To achieve the fiber angle as a function of x, only a 2×2 manufacturing-mesh is needed where T_0 are the angles at the nodes in the centers and T_1 are the angles at the left and right and edges of the plate as shown in Figure 5.1. Here, balanced anti-symmetric 8-ply laminate $[\pm < T_0, T_1 > \ \mp < T_0, T_1 >_2 \ \pm < T_0, T_1 >]$ ($A_{16} = A_{26} = D_{16} = D_{26} = B_{ij} = 0$) is chosen, which results in only two input parameters for the optimization. Since, there are only two input variables T_0 and T_1, the results can be plotted and the maximum buckling load can be ontained graphically, negating the requirement for optimization algorithm. The bound for each input parameters are $[0°, 90°]$ at $3°$ steps.

Figure 4.4 represents the plot of buckling load for different combination of T_0 and T_1. The plot is shown for T_0 at $6°$ steps for convenience. It can be concluded form the plot that buckling load is highest for $< T_0, T_1 > = < 3°, 54° >$ at 0.3249 N/mm. The corresponding fiber angle distribution $\theta(x)$ for $< 3°, 54° >$ is shown in Figure 4.6 and first two buckling mode for the optimized laminate are shown in Figure 4.7 . Note that, optimized buckling load is 8.05% higher as compared to the optimum buckling load of constant stiffness composite plate.

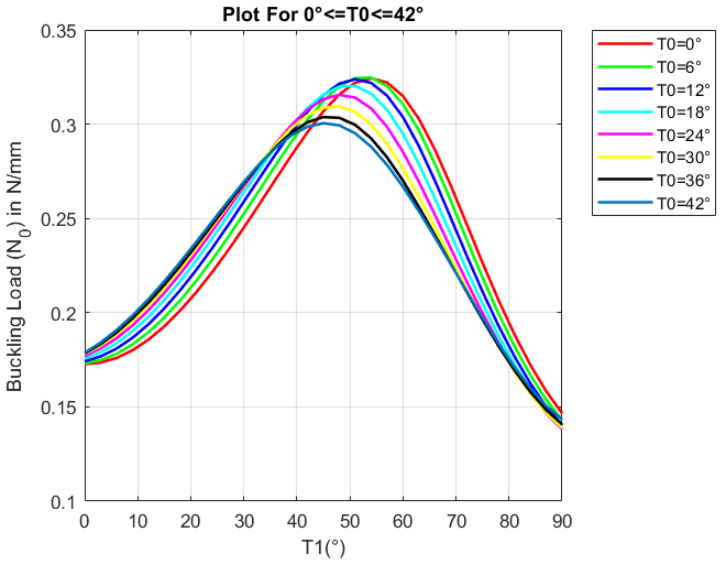

(a) For $0° \leq T_0 \leq 42°$

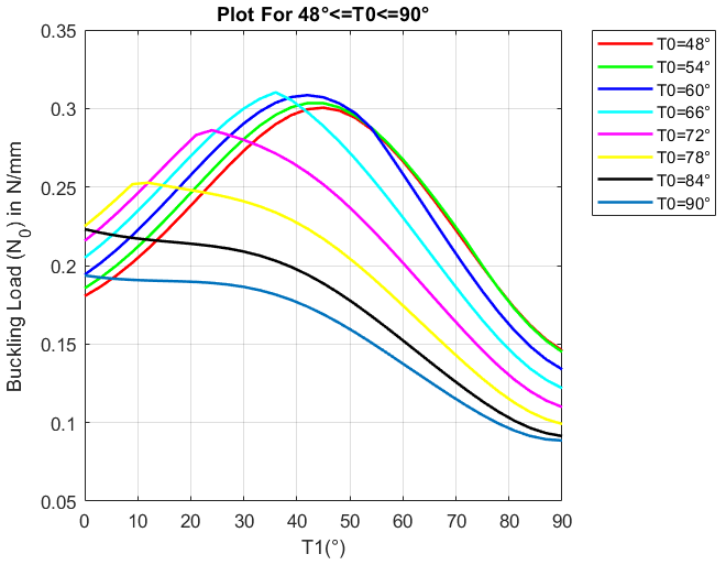

(b) For $48° \leq T_0 \leq 90°$

Figure 4.4: Buckling load vs Angle $\theta(x) =< T_0, T_1 >$

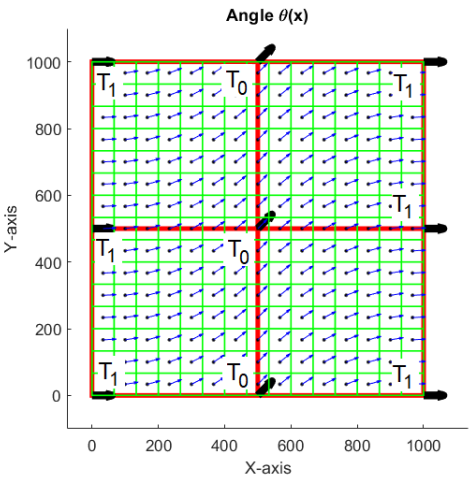

Figure 4.5: Angle variation $\theta(x)$ using MFEM-framework.

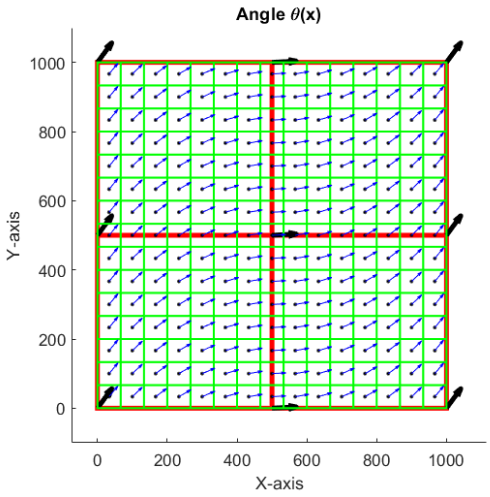

Figure 4.6: Optimized fiber Angle distribution $\theta(x) < 3°, 54° >$,

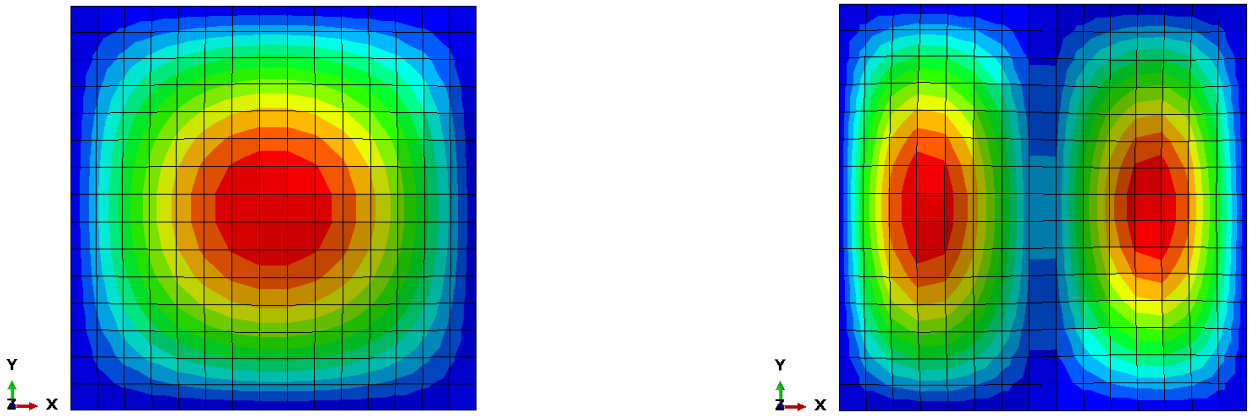

(a) $BucklingMode : 1(Eigenvalue = 0.3249)$

(b) $BucklingMode : 2(Eigenvalue = 0.5014)$

Figure 4.7: Buckling Mode of optimized Univariate variable stiffness when $\theta(x)$

4.2.2 Stiffness as a function of-y

Similarly, to achieve the fiber angle as a function of y, only 2×2 manufacturing-mesh is needed where T_0 are the angles at the nodes which are at the centers and T_1 are the angles at the top and bottom and edges of the plate as shown in Figure 4.9.

Figure 4.8 represents the plot of buckling load for different combination of T_0 and T_1. The plot is shown for T_0 at 6° steps for convenience. It can be concluded form the plot that buckling load is highest for $< T_0, T_1 > = < 66°, 27° >$ which is 0.3968 N/mm. The fiber angle distribution $\theta(y)$ for $< 66°, 27° >$ is shown in Figure 4.10 for the top ply and and first two buckling mode for the optimized laminate are shown in Figure 4.11. Also note that optimized buckling load is 31.96% higher as compared to the optimum buckling load of constant stiffness composite plate.

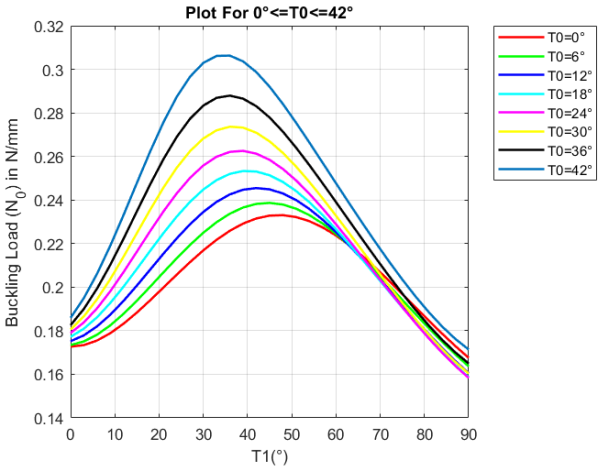

(a) For $0° \leq T_0 \leq 42°$

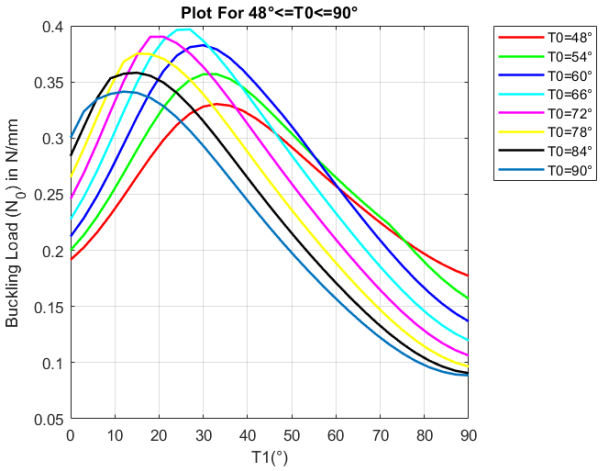

(b) For $48° \leq T_0 \leq 90°$

Figure 4.8: Buckling load vs Angle $\theta(y) =< T_0, T_1 >$

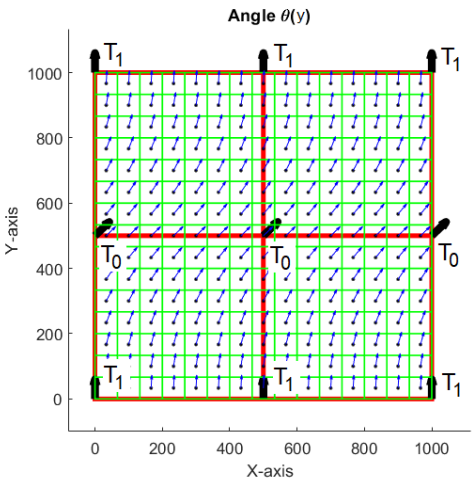

Figure 4.9: Angle variation $\theta(y)$ using MM-framework.

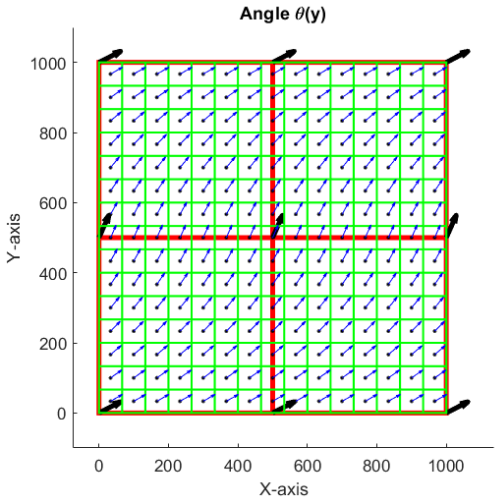

Figure 4.10: Optimized fiber Angle distribution $\theta(y) < 66°, 27° >$,

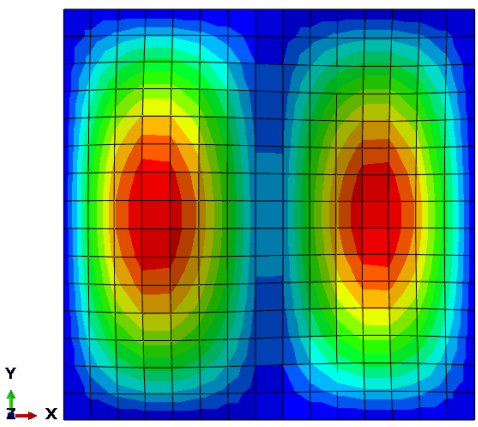

(a) $BucklingMode : 1(Eigenvalue = 0.3968)$

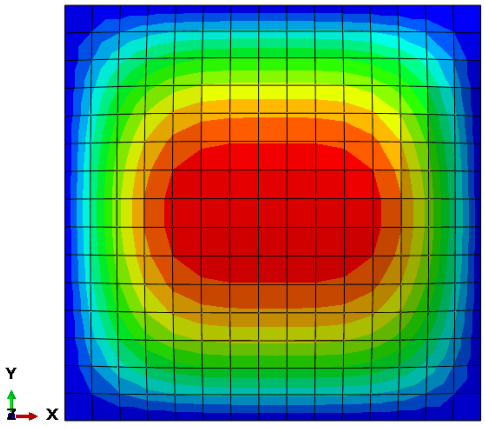

(b) $BucklingMode : 2(Eigenvalue = 0.3989)$

Figure 4.11: Buckling Mode of optimized unidirectional variable stiffness when $\theta(y)$

4.3 Bivariate variable stiffness composite plate : Using GA

In this section, bivariate stiffness composite plate is optimized for buckling using MFEM-framework for different number of manufacturing-mesh. To achieve bivariate variable stiffness composite plate, each nodes of manufacturing-mesh elements in each ply needs to be treated independently as an input which results in bivariate distribution of fiber directions or angle $\theta(x, y)$. Here, the layup to be optimized for the buckling load is 8-ply symmetric layup ($B_{ij} = 0$ thought the plate domain) which means only 4-ply(either from top or bottom of the laminate) needs to be meshed using manufacturing-mesh to keep minimum number of input parameters for the optimization. Since input parameters associated with this optimization is large, optimization using different combination of this parameters is not preferable. Also, there could be many local minimum(local optimal solution for the buckling load) possible, optimization using Gradient-decent(GD) may not give the global optimum(Global optimal solution for the buckling load). Therefore, Genetic-algorithm(GA) used for the optimization in this case which is elite in finding global optimal solution.

Here, three different cases of manufacturing-mesh sizes, 2×2,3×3, and 5×5 are chosen to discretize 4-ply for the optimization of the buckling load of the 8-ply symmetric layup. There are 36, 64 and 144 input parameters for optimization using 2×2,3×3, and 5×5 manufacturing mesh respectively. The GA Parameter taken for all the three cases are shown in Table-4.1. The population size taken in case of 5×5 manufacturing mesh double the population size taken in case of 2×2 and 3×3 manufacturing mesh as the number of input parameter in case of 5×5 manufacturing mesh is large.

GA Parameter	Value
Generation	100
Population	600 (For MM:2×2 & MM:3×3)
Population	1200 (For MM:5×5)
Mutation Probability	0.2 (20%)
Crossover Probability	0.5 (50%)
Crossover type	Uniform
Parents Portion	0.3 (30%)
Elit ratio	0.01 (1%)
Variable Bound	$[-90°, 90°]$

Table 4.1: GA Parameters for the Optimization of buckling load of bivariate VS composite Plate .

The input parameters for 2×2,3×3, and 5×5 manufacturing mesh for k^{th} ply is shown in Figure 4.12. Also, convergence plot of the optimization using GA for all the three cases are shown in Figure 4.13,

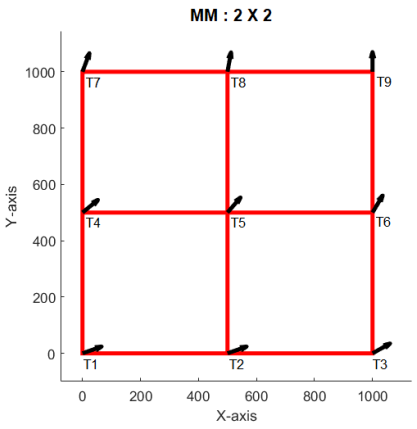

(a) For Manufacturing Mesh : 2×2

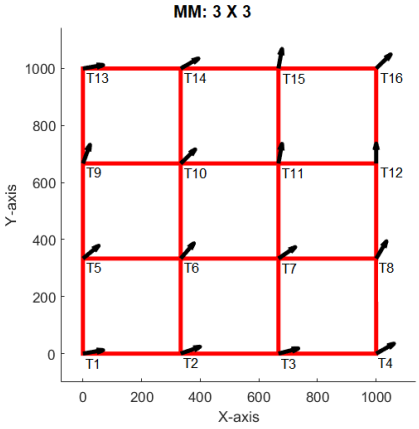

(b) For Manufacturing Mesh : 3×3

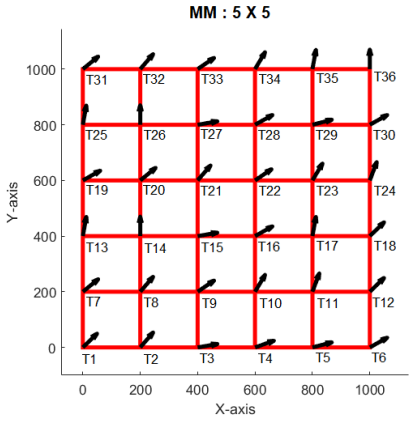

(c) For Manufacturing Mesh : 5×5

Figure 4.12: Input Parameters for k^{th} ply

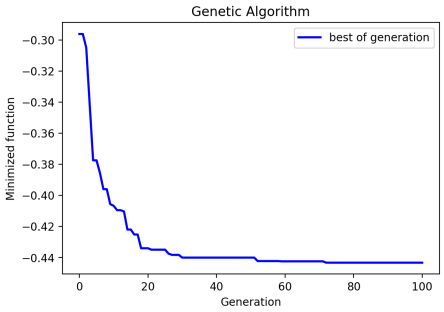

(a) For Manufacturing Mesh : 2×2

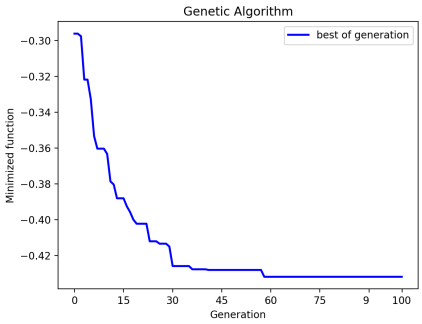

(b) For Manufacturing Mesh : 3×3

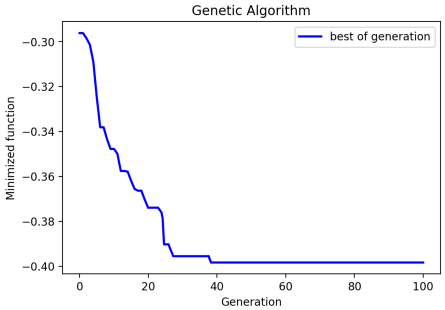

(c) For Manufacturing Mesh : 5×5

Figure 4.13: GA convergence graph

4.3.1 Optimized Results Comparison : Ply

In this section, the optimized fiber angle or direction for optimized buckling load are compared for each ply as shown in Figure 4.14-4.17. It can be noticed from the fiber angle distribution that, fiber angles are arranged in approximately -45° or 45° angle away from the center of the plate. The results(S-shaped fiber angle distribution) are similar to Tatting and Gurdal [11] but due to GA is poor in searching converged solution, the optimal distribution of fiber angle $\theta(x, y)$ is not converged.

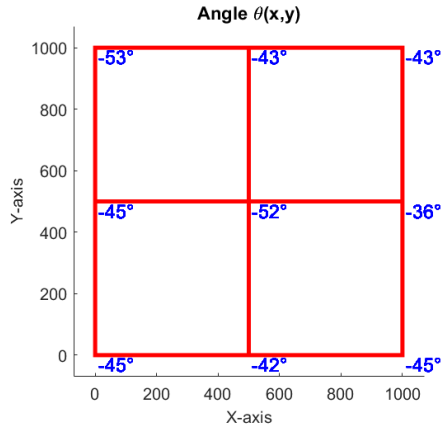

(a) Manufacturing Mesh : 2×2

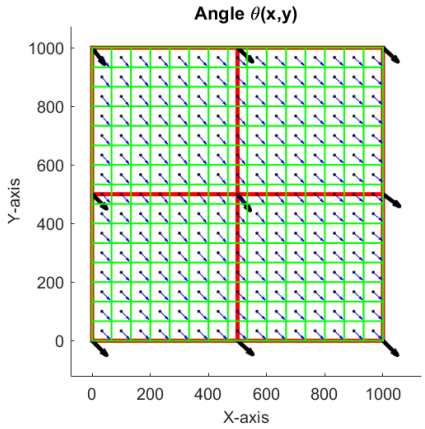

(b) Fiber angle distribution MM: 2×2

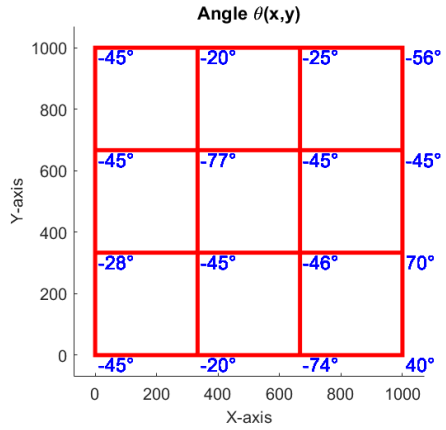

(c) Manufacturing Mesh : 3×3

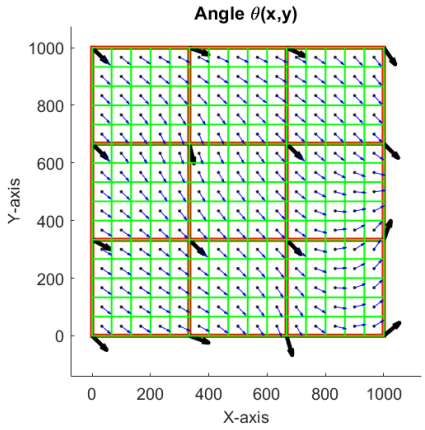

(d) Fiber angle distribution MM: 3×3

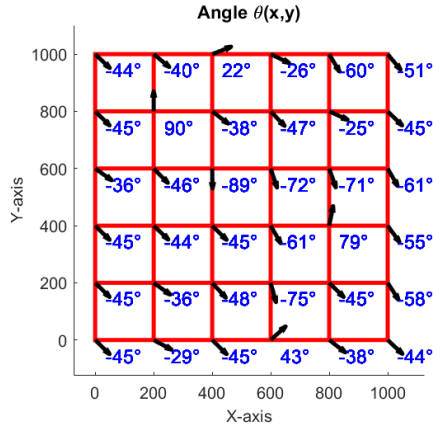

(e) Manufacturing Mesh : 5×5

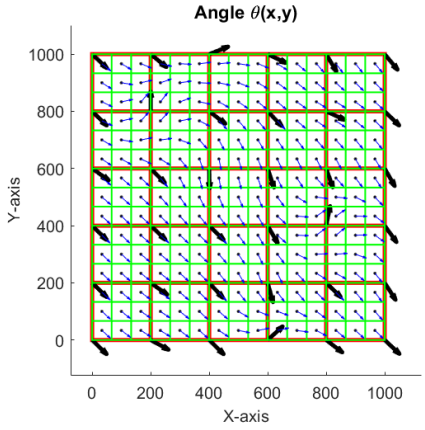

(f) Fiber angle distribution MM: 5×5

Figure 4.14: Optimized result Comparison of: Ply-1

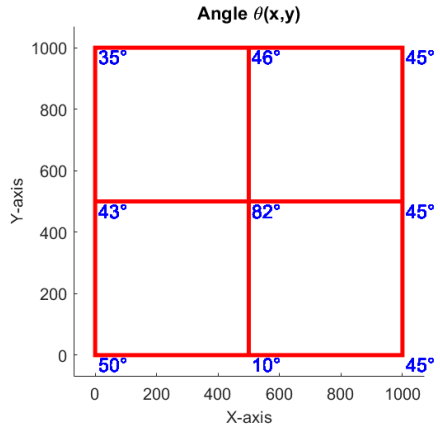

(a) Manufacturing Mesh : 2×2

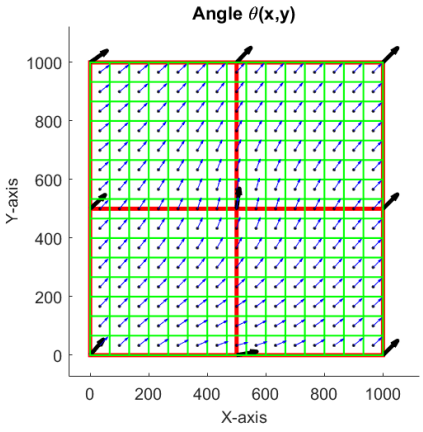

(b) Fiber angle distribution MM: 2×2

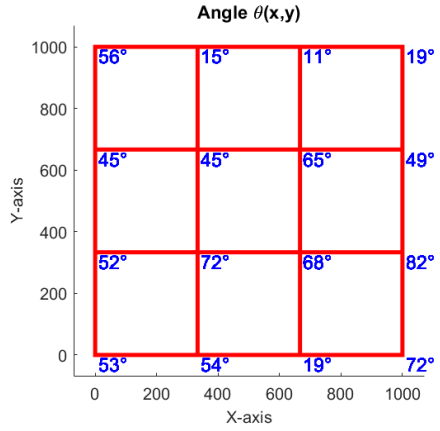

(c) Manufacturing Mesh : 3×3

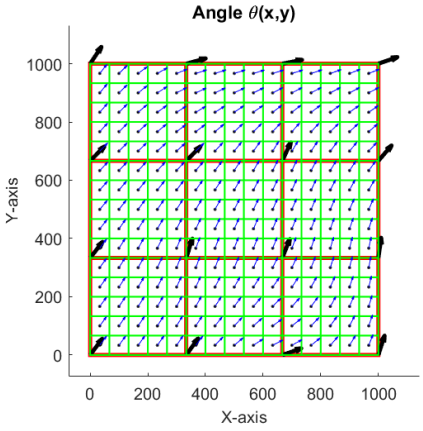

(d) Fiber angle distribution MM: 3×3

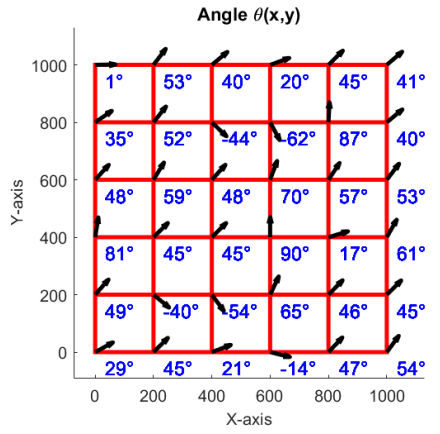

(e) Manufacturing Mesh : 5×5

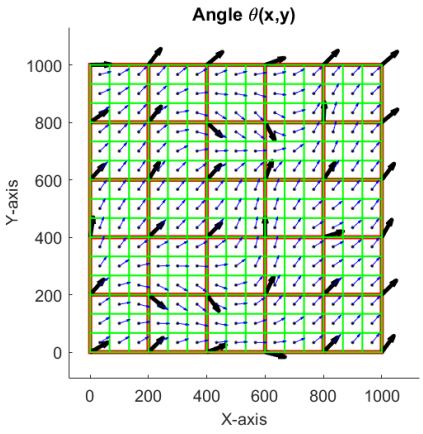

(f) Fiber angle distribution MM: 5×5

Figure 4.15: Optimized result Comparison of: Ply-2

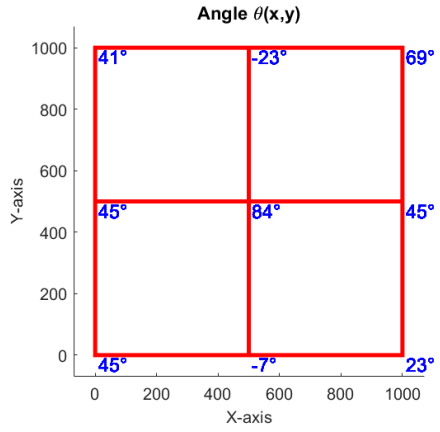

(a) Manufacturing Mesh : 2×2

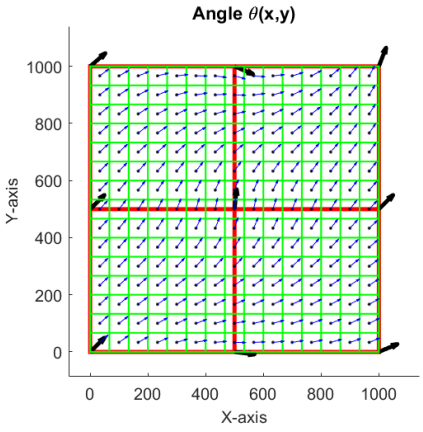

(b) Fiber angle distribution MM: 2×2

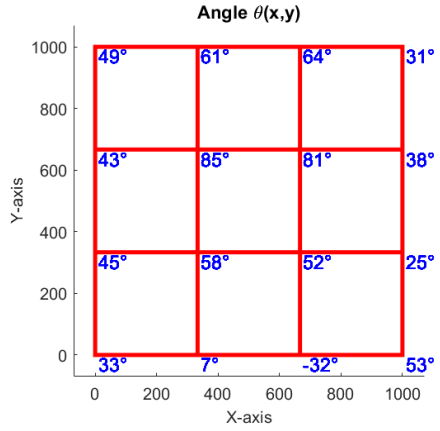

(c) Manufacturing Mesh : 3×3

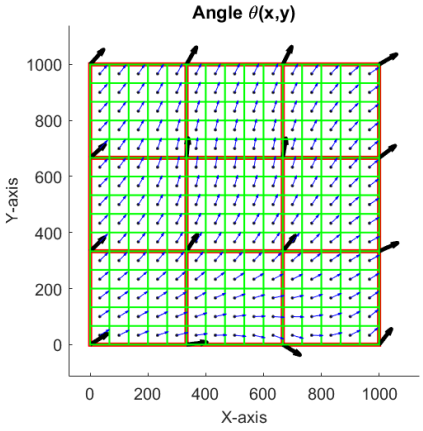

(d) Fiber angle distribution MM: 3×3

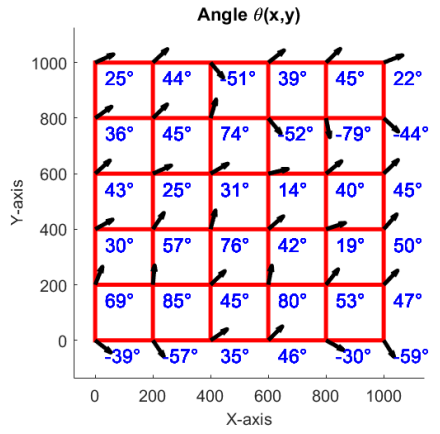

(e) Manufacturing Mesh : 5×5

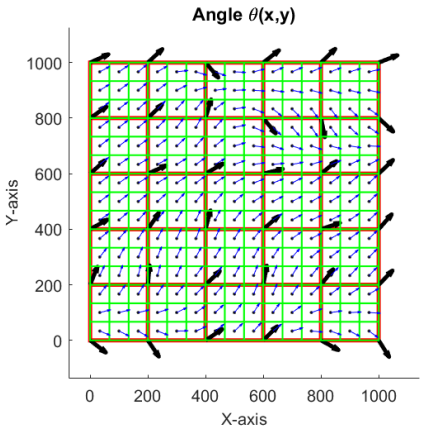

(f) Fiber angle distribution MM: 5×5

Figure 4.16: Optimized result Comparison of: Ply-3

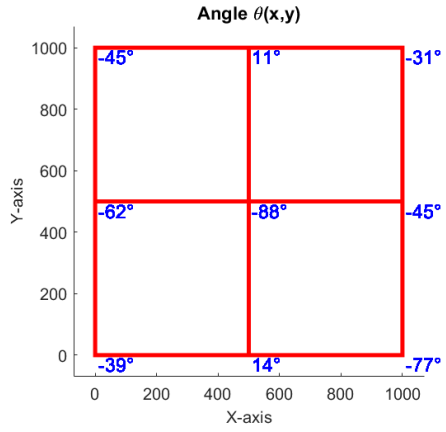

(a) Manufacturing Mesh : 2×2

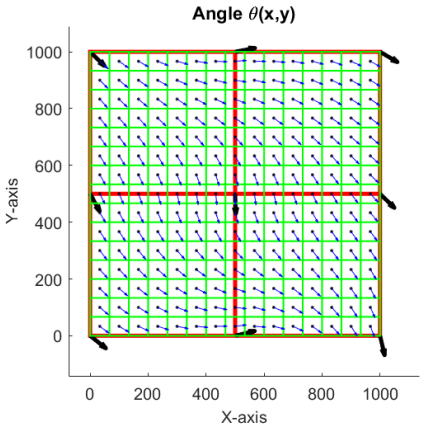

(b) Fiber angle distribution MM: 2×2

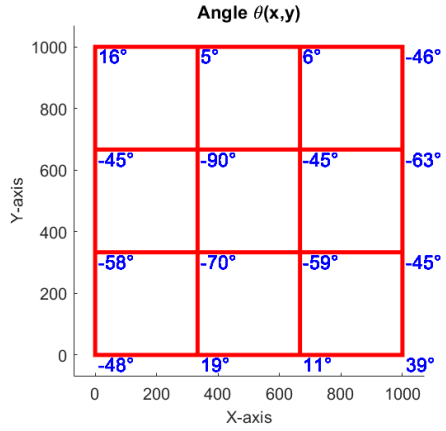

(c) Manufacturing Mesh : 3×3

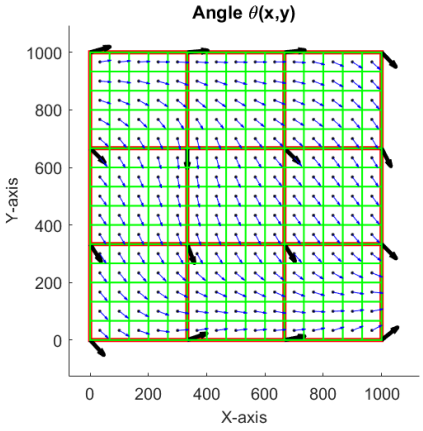

(d) Fiber angle distribution MM: 3×3

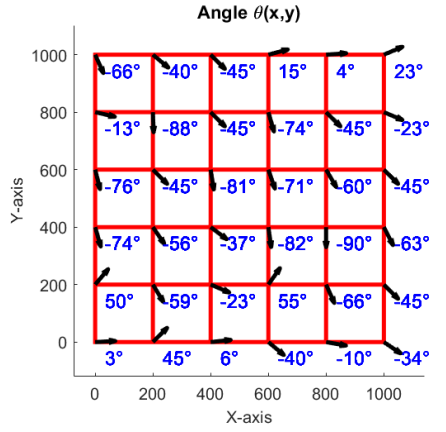

(e) Manufacturing Mesh : 5×5

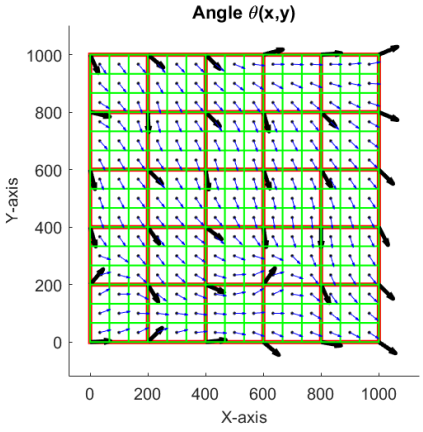

(f) Fiber angle distribution MM: 5×5

Figure 4.17: Optimized result Comparison of: Ply-4

4.3.2 Optimized Results Comparison : Buckling Mode

Here first two buckling mode or eigenvectors are compared for optimized results achieved using MM:2×2, MM:3×3 and MM:5×5 mesh in Figure 4.18 and 4.19. It can be observed from figure that first two eigenvalues are nearly equal in each of the case.

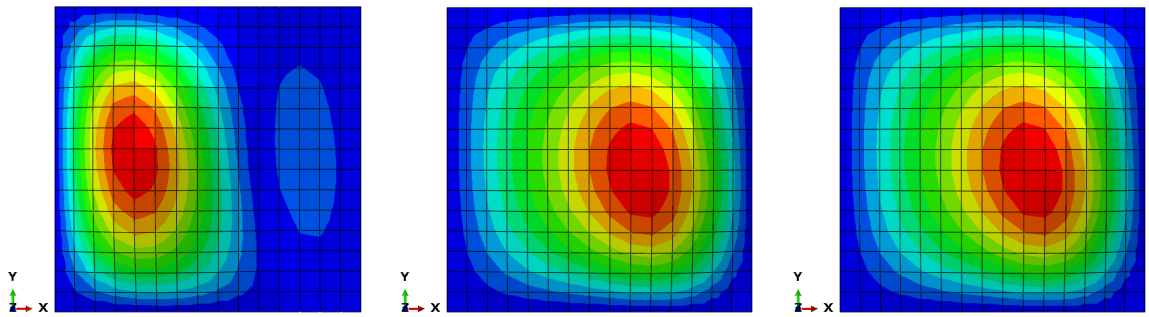

(a) MM: 2×2
Eigenvalue = 0.4432

(b) MM: 3×3
Eigenvalue = 0.4318

(c) MM: 5×5
Eigenvalue = 0.3983

Figure 4.18: Comparison of Buckling Mode-1

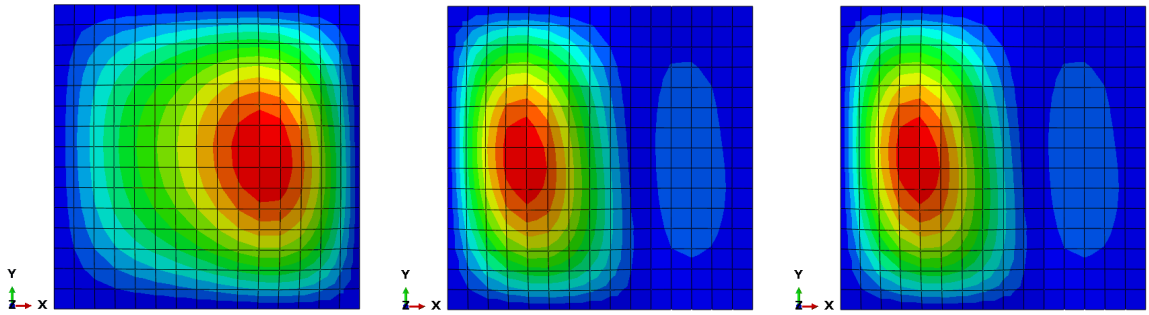

(a) MM: 2×2
Eigenvalue = 0.4476

(b) MM: 3×3
Eigenvalue = 0.4429

(c) MM: 5×5
Eigenvalue = 0.4172

Figure 4.19: Comparison of Buckling Mode-2

4.3.3 Convergence study of optimized result

Since the FEM mesh chosen for buckling load optimization consist 15X15 mesh (total 225 stress-mesh elements), the optimized buckling load is verified for convergence by refining the FEM model further with fine stress-mesh using the optimized fiber angle distribution achieved using 15×15 stress-mesh (total 225 stress-mesh elements). The convergence study for each case,namely MM:2×2, MM:3×3 and MM:5×5 are shown in Table-4.2, 4.3 and 4.4 respectively. It can be seen from the table that change in the buckling load is not large even if the model is refined with fine stress-mesh elements.

Stress-Mesh(M×N)	Buckling Load(N/mm), N_0	Decrease(%)
15×15	0.4432	-
30×30	0.4362	1.58
45×45	0.4348	0.32
60×60	0.4343	0.11

Table 4.2: Convergence study on optimized 2×2 MM case.

Stress-Mesh(M×N)	Buckling Load(N/mm), N_0	Decrease(%)
15×15	0.4318	-
30×30	0.4257	1.41
45×45	0.4245	0.28
60×60	0.4240	0.12

Table 4.3: Convergence study on optimized 3×3 MM case.

Stress-Mesh(M×N)	Buckling Load(N/mm), N_0	Decrease(%)
15×15	0.3983	-
30×30	0.3949	0.85
45×45	0.3942	0.18
60×60	0.3939	0.076

Table 4.4: Convergence study on optimized 5×5 MM case.

4.4 Bivariate variable stiffness composite plate : Using BFGS

The parameter for BFGS optimizer chosen here is shown in Table-4.5, where gradient tolerance (g_{tol}) represents the stopping criteria which means if gradient evaluated at the k^{th} iterate is less than the specified gradient tolerance(g_{tol}) it stops evaluating further. The input parameters for MM:2×2, MM:3×3 and MM:5×5 manufacturing mesh for k^{th} ply is shown in Figure 4.12.Also, convergence plot of the optimization using BFGS for all the three cases are shown in Figure 4.20,

BFGS Parameter	Value
c_1	1e-4
c_2	0.9
ϵ	1° $(forward - difference)$
g_{tol}	1e-5
Variable Bound	$[-90^\circ, 90^\circ]$
Initial Guess	$[-45^\circ, 45^\circ, 45^\circ, -45^\circ]_s$

Table 4.5: BFGS Parameters for the Optimization of buckling load of bidirectional VS composite Plate .

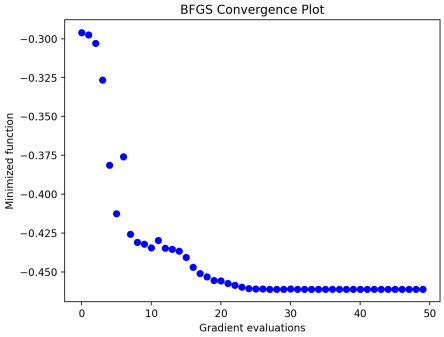

(a) For Manufacturing Mesh : 2×2

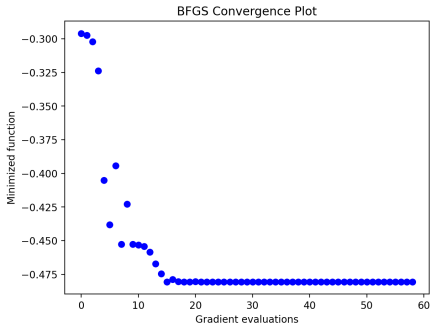

(b) For Manufacturing Mesh : 3×3

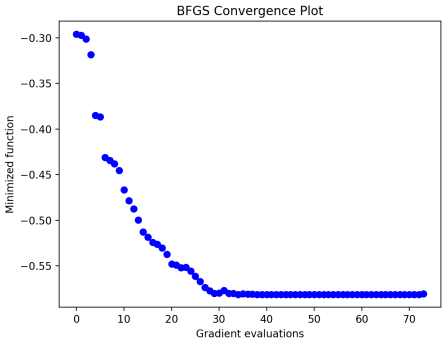

(c) For Manufacturing Mesh : 5×5

Figure 4.20: BFGS convergence plot for each cases of MM

4.4.1 Optimized Results Comparison : Ply

In this section, the optimized fiber angle or direction for optimized buckling load are compared for each ply as shown from Figure 4.21 to Figure 4.24. It can be noticed from the fiber angle distribution that, fiber angles

are arranged in approximately -45° or 45° angle away from the center of the plate. The results(S-shaped fiber angle distribution) are similar to Tatting and Gurdal [11] and the optimal distribution of fiber angle $\theta(x, y)$ is converged.

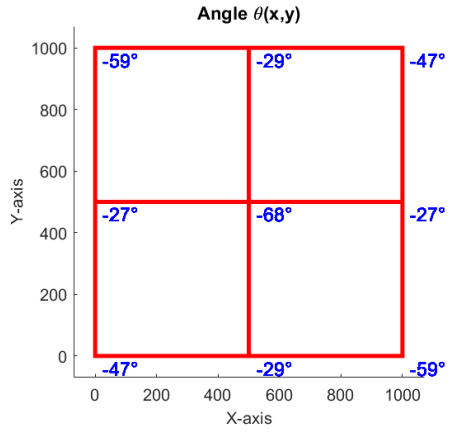

(a) Manufacturing Mesh : 2×2

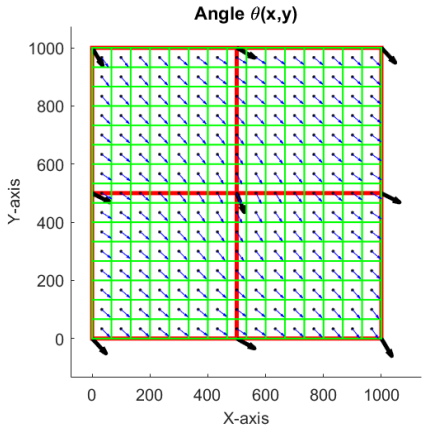

(b) Fiber angle distribution MM: 2×2

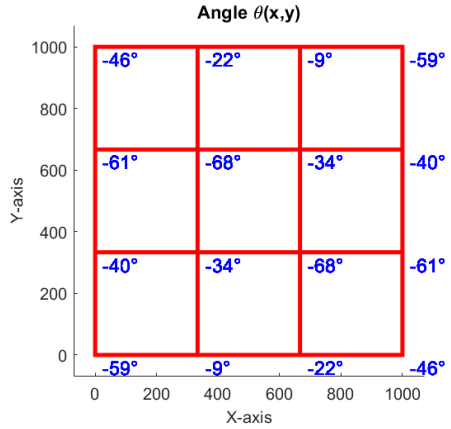

(c) Manufacturing Mesh : 3×3

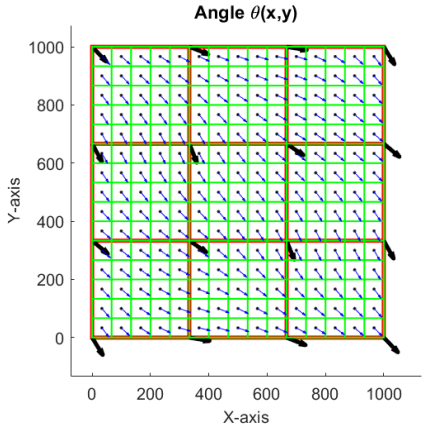

(d) Fiber angle distribution MM: 3×3

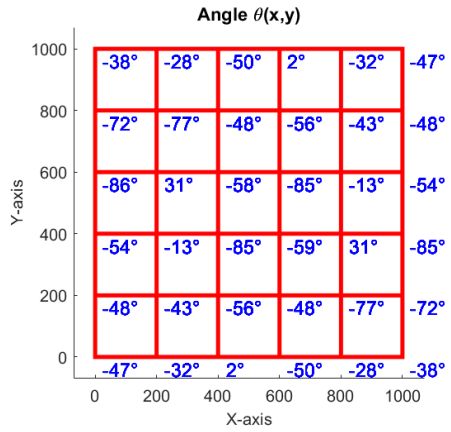

(e) Manufacturing Mesh : 5×5

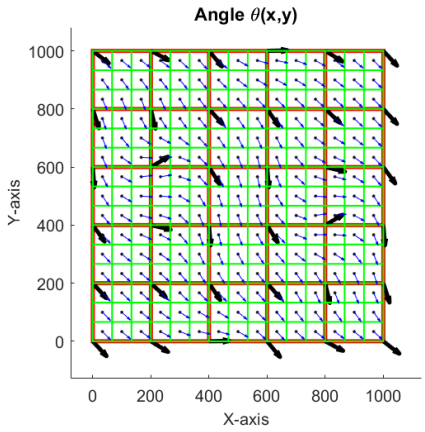

(f) Fiber angle distribution MM: 5×5

Figure 4.21: Optimized result Comparison of: Ply-1

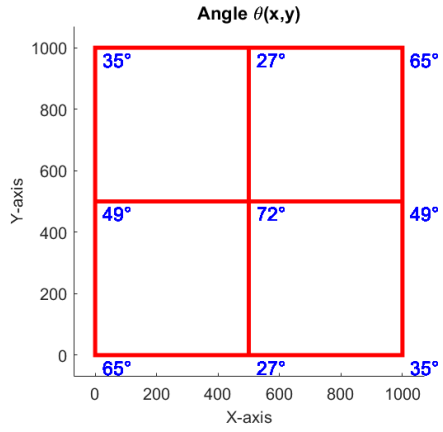

(a) Manufacturing Mesh : 2×2

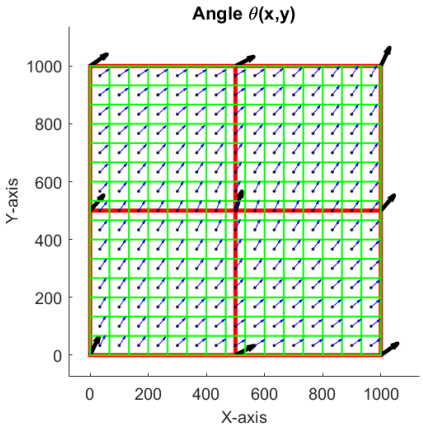

(b) Fiber angle distribution MM: 2×2

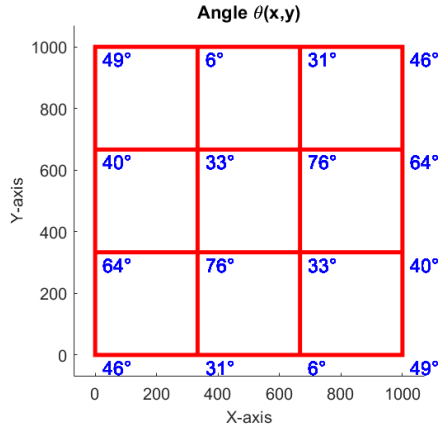

(c) Manufacturing Mesh : 3×3

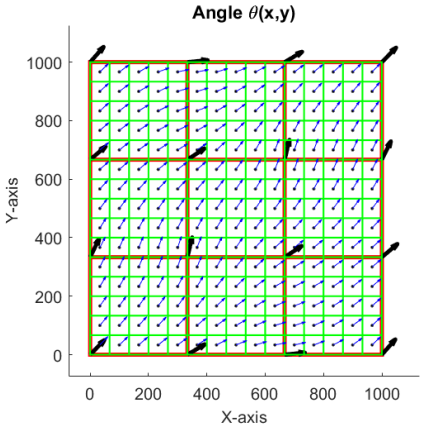

(d) Fiber angle distribution MM: 3×3

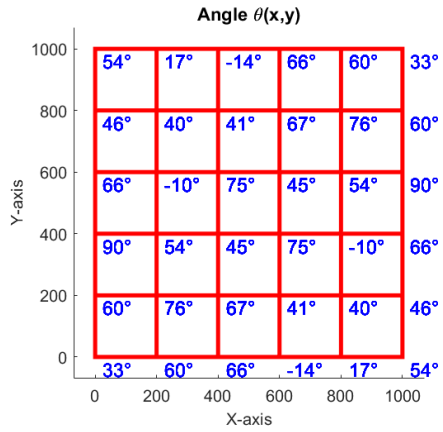

(e) Manufacturing Mesh : 5×5

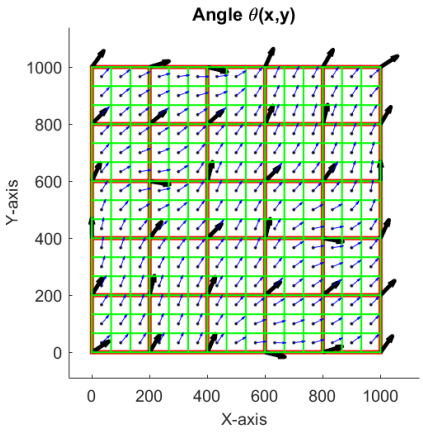

(f) Fiber angle distribution MM: 5×5

Figure 4.22: Optimized result Comparison of: Ply-2

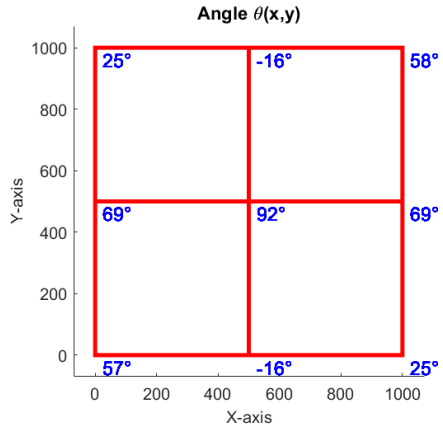

(a) Manufacturing Mesh : 2×2

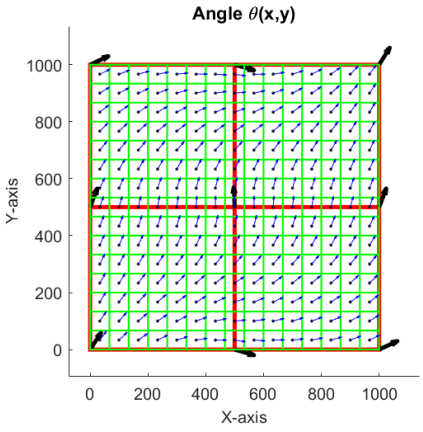

(b) Fiber angle distribution MM: 2×2

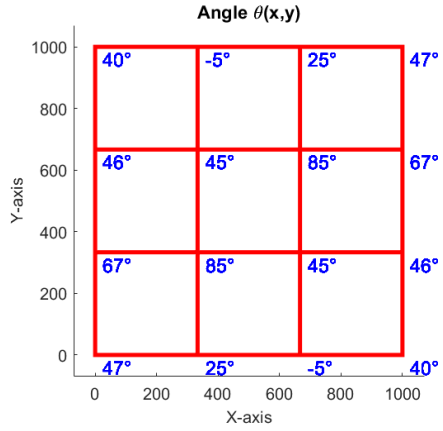

(c) Manufacturing Mesh : 3×3

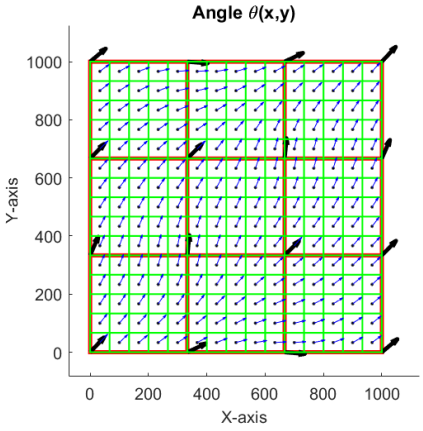

(d) Fiber angle distribution MM: 3×3

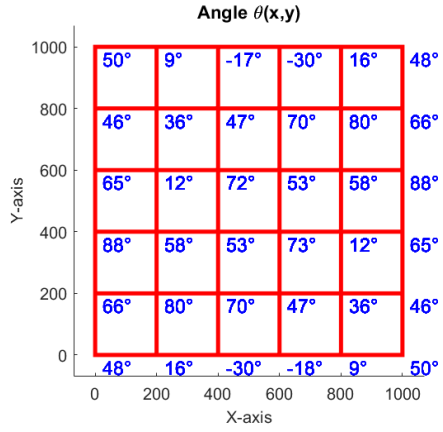

(e) Manufacturing Mesh : 5×5

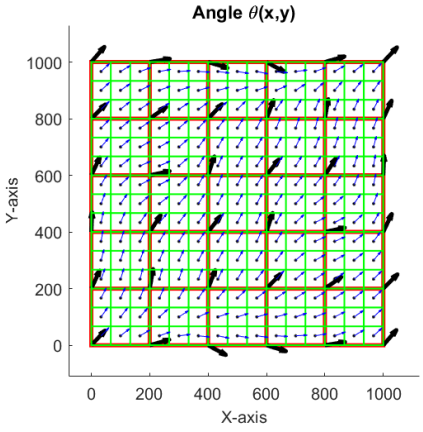

(f) Fiber angle distribution MM: 5×5

Figure 4.23: Optimized result Comparison of: Ply-3

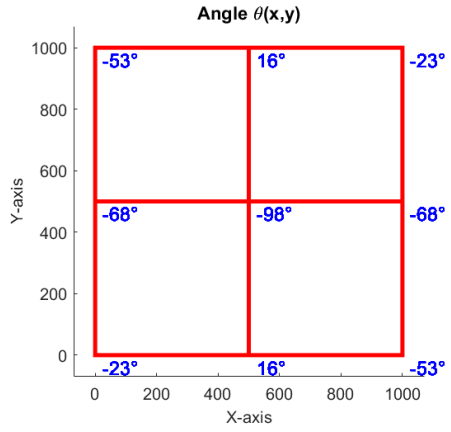

(a) Manufacturing Mesh : 2×2

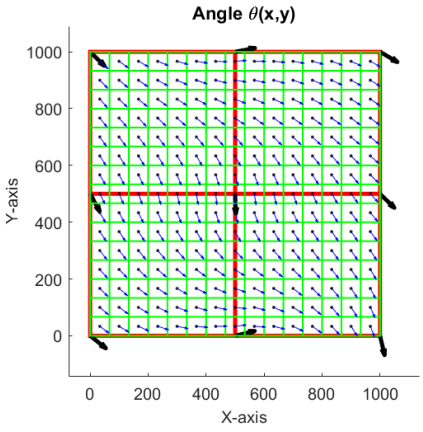

(b) Fiber angle distribution MM: 2×2

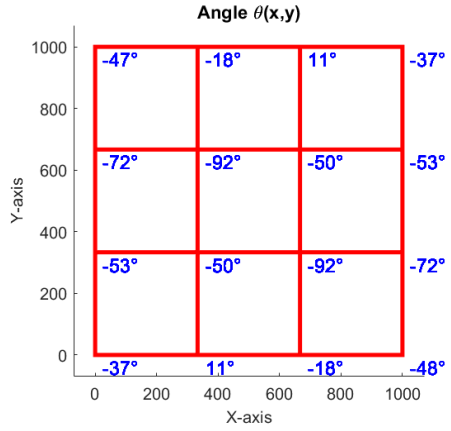

(c) Manufacturing Mesh : 3×3

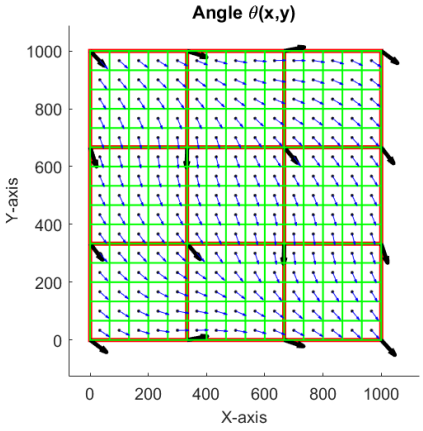

(d) Fiber angle distribution MM: 3×3

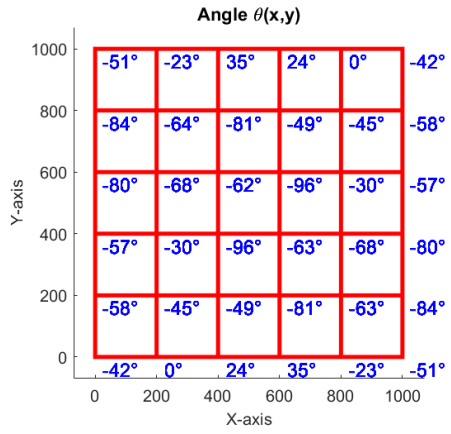

(e) Manufacturing Mesh : 5×5

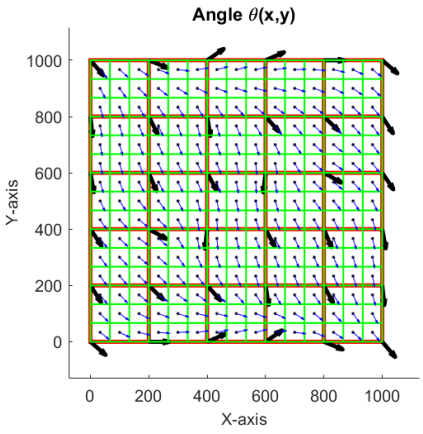

(f) Fiber angle distribution MM: 5×5

Figure 4.24: Optimized result Comparison of: Ply-4

4.4.2 Optimized Results Comparison : Buckling Mode

Here first two buckling mode or eigenvectors are compared for optimized results achieved using MM:2×2,MM:3×3 and MM:5×5 mesh shown in Figure 4.25 and Figure 4.26 respectively. It can be observed from figure that first two eigenvalues are nearly equal in each of the case.

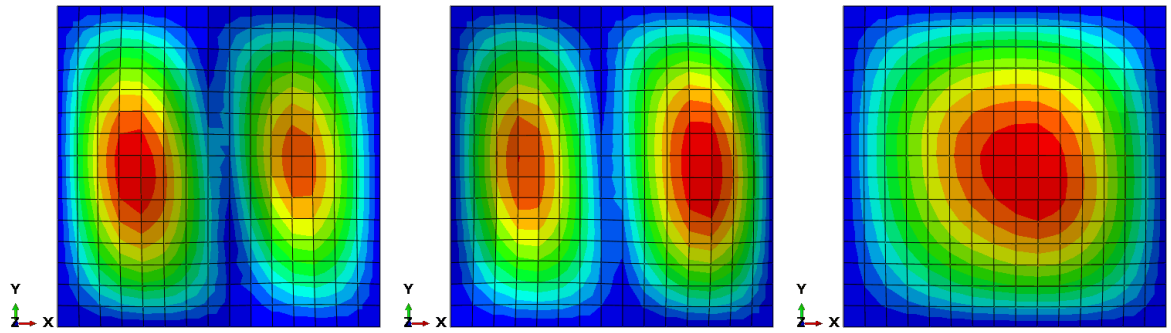

(a) MM: 2×2
Eigenvalue = 0.4611

(b) MM: 3×3
Eigenvalue = 0.4804

(c) MM: 5×5
Eigenvalue = 0.5811

Figure 4.25: Comparison of Buckling Mode-1

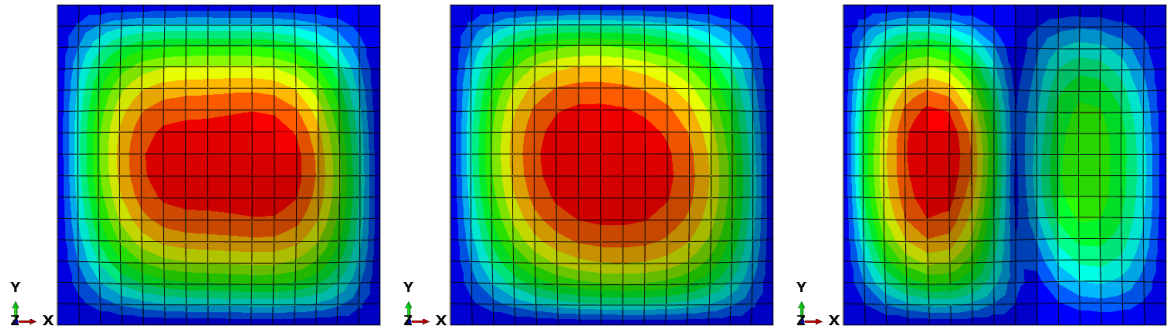

(a) MM: 2×2
Eigenvalue = 0.4618

(b) MM: 3×3
Eigenvalue = 0.4809

(c) MM: 5×5
Eigenvalue = 0.5813

Figure 4.26: Comparison of Buckling Mode-2

4.4.3 Convergence study of optimized result

Since the FEM mesh chosen for buckling load optimization consist 15×15 mesh (total 225 stress-mesh elements), the optimized buckling load is verified for convergence by further refining the FEM model further with fine mesh using the optimized fiber angle distribution achieved using 15×15 mesh (total 225 stress-mesh elements). The convergence study for each case,namely MM:2×2, MM:3×3 and MM:5×5 are shown in Table 4.6, 4.7 and 4.8 respectively. It can be seen from the table that change in the buckling load is not large even if the model is refined with fine stress-mesh elements.

Stress-Mesh(M×N)	Buckling Load(N/mm), N_0	Decrease(%)
15×15	0.4611	-
30×30	0.4537	1.60
45×45	0.4522	0.33
60×60	0.4516	0.13

Table 4.6: Convergence study on optimized 2×2 MM case.

Stress-Mesh(M×N)	Buckling Load(N/mm), N_0	Decrease(%)
15×15	0.4804	-
30×30	0.4711	1.94
45×45	0.4694	0.36
60×60	0.4687	0.15

Table 4.7: Convergence study on optimized 3×3 MM case.

Stress-Mesh(M×N)	Buckling Load(N/mm), N_0	Decrease(%)
15×15	0.5811	-
30×30	0.5681	2.24
45×45	0.5652	0.51
60×60	0.5640	0.21

Table 4.8: Convergence study on optimized 5×5 MM case.

Chapter 5

Buckling Load Optimization Of VS Composite Plate using Semi-Analytical method

One of the main problem using MFEM-framwork is variation of fiber angle distributions

5.1 Ritz-method

Unlike the derivation shown from Section (2.5-2.7), Ritz method bypasses the derivation of the governing differential equations, and goes directly from the variational statements of the problem, such as the principle of minimization of total potential energy, which are equivalent to the governing differential equations and the corresponding natural boundary conditions, where unknown variables such as out-of-plane displacement (w) or Airy-stress function (Φ) is approximated by finite linear combination of shape function with unknown parameters which satisfy the required boundary condition [16], such as

$$\Phi \approx \phi_0 + \sum_{i=1}^{\infty} c_i \phi_i \tag{5.1}$$

Where c_i are the unknown parameters, ϕ_0 and ϕ_i are the shape function. Note that ϕ_0 serves as a particular solution where as ϕ_i serves as a homogeneous solution of the equation. Also, the selected shape function must be such that it meets following requirement [16],

- ϕ_0 must satisfy the specified essential or geometric boundary conditions.
- ϕ_i must satisfy the homogeneous form of the essential boundary condition. also it should be linearly independent and form a complete system of functions.

As compared to Galerking methd, Ritz-method has several advantages, one of which is it is not necessary that chosen shape function has to satisfy the natural boundary condition [2], but if it does, the accuracy of the approximation is substantially better.Morever, in Ritz-method, only essential boundary condition has to satisfied by the shape function [16]. Also, for the computational accuracy, it is better to choose orthogonal shape functions [4]. if chosen shape functions are not orthogonal somehow, it can be orthogonalized using Gram-schmidt orthogonalization process [6].

To apply Ritz-method, the first step is to derive the equation of total complemetry energy of the panel in the prebuckling state to calculate the in-plane stress or load distribution, and then the total energy functional (combination of complementary and strain energy) for the postbuckling state to determine the buckling load and out-of-plane displacement. Note that all the equations shown in this section are for symmetric laminate ($[B_{ij}] = 0$).

5.1.1 Total Complementary energy and Total energy functional

For detailed derivation of Total Complementary energy and Total Potential energy for a panel under general load case, reader is referred to [19]. Consider a free body under general load case as shown in Figure 5.1 where BL represents the boundary of prescribed load and BD represent the boundary of prescribed displacement, so

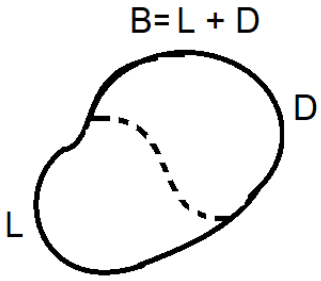

Figure 5.1: Boundary of Free body.

total boundary of the free body under general load case becomes $BT = BL + BD$. For a plate, total boundary is comprised of four straight edge.

Here the free body is considered under prescribed load $\bar{N_x}$,$\bar{N_y}$ and $\bar{N_{xy}}$ on boundary BL and prescribed displacement $\bar{u}$ and $\bar{v}$ on boundary BD,

There for the mechanical boundary conditions are,

$$N_x = \bar{N_x}, N_y = \bar{N_y}, N_{xy} = \bar{N_{xy}} \quad \text{(On boundary BL)} \tag{5.2}$$

similarly, the geometric boundary conditions are ,

$$u = \bar{u}, v = \bar{v} \quad \text{(On boundary BD)} \tag{5.3}$$

The total complementary energy for the body or panel can be given as[28,29,33],

$$\Pi^c_{pre} = U^c_m + V_{BD} \tag{5.4}$$

Where, U^c_m is the membrane complementary energy which can be given as[7,28],

$$U^c_m = \frac{1}{2}\iint [A^*_{11}N_x^2 + 2A^*_{12}N_xN_y + 2A^*_{16}N_xN_{xy} + A^*_{22}N_y^2 + 2A^*_{26}N_yN_{xy} + A^*_{66}N_{xy}^2]\, dx\, dy \tag{5.5}$$

and V_{BD} is the complementary work done by the prescribed displacements on boundary BD which can be given for rectangular plates(as shown in Figure 2.1) as [28,33],

$$V_{BD} = -\int_{BD} [(N_y\bar{v} + N_{xy}\bar{u})_{y=b} - (N_y\bar{v} + N_{xy}\bar{u})_{y=0}]\, dx - \int_{BD} [(N_x\bar{u} + N_{xy}\bar{v})_{x=a} - (N_x\bar{u} + N_{xy}\bar{v})_{x=0}]\, dy \tag{5.6}$$

By by making complementary energy Π^c_{pre} stationary with respect to unknown variable N_x,N_y and N_{xy} , in-plane load distribution can be solved. To solve the in-plane load distribution, it is necessary to satisfy in-plane equilibrium equation as shown in Equation 2.9 and 2.10, which can be addressed by using airy-stress function as shown in Equation 2.36 and shown here for convenience,

$$N_x = \Phi_{,yy} \qquad N_y = \Phi_{,xx} \qquad N_x = -\Phi_{,xy} \tag{5.7}$$

Therefore, the equation for complementary energy Π^c_{pre} can be rewritten as,

$$\begin{aligned}\Pi^c_{pre} = \frac{1}{2}\iint [\phi^T A^*\ \phi]\, dx\, dy - \int_{BD} [(\Phi_{,xx}\bar{v} - \Phi_{,xy}\bar{u})_{y=b} - (\Phi_{,xx}\bar{v} - \Phi_{,xy}\bar{u})_{y=0}]\, dx \\ - \int_{BD} [(\Phi_{,yy}\bar{u} - \Phi_{,xy}\bar{v})_{x=a} - (\Phi_{,yy}\bar{u} - \Phi_{,xy}\bar{v})_{x=0}]\, dy\end{aligned} \tag{5.8}$$

where,

$$\phi = [\Phi_{,yy}\ \Phi_{,xx}\ \Phi_{,xy}]^T \tag{5.9}$$

Similar derivation for Total Potential energy (Π) given in terms of airy-stress function for general load case as [19],

$$\begin{aligned}\Pi = -\frac{1}{2}\iint [\phi^T A^*\ \phi]\, dx\, dy + \frac{1}{2}\iint [\kappa^T D\ \kappa]\, dx\, dy + \iint \phi^T e_n\, dx\, dy \\ + \int_{BD} [(\Phi_{,xx}\bar{v} - \Phi_{,xy}\bar{u})_{y=b} - (\Phi_{,xx}\bar{v} - \Phi_{,xy}\bar{u})_{y=0}]\, dx \\ + \int_{BD} [(\Phi_{,yy}\bar{u} - \Phi_{,xy}\bar{v})_{x=a} - (\Phi_{,yy}\bar{u} - \Phi_{,xy}\bar{v})_{x=0}]\, dy \end{aligned} \tag{5.10}$$

Where,

$$\begin{aligned}\kappa &= [-w_{,xx}\ \ -w_{,yy}\ \ -2w_{,xy}]^T \\ e_n &= [\frac{1}{2}w_{,x}^2\ \ \frac{1}{2}w_{,y}^2\ \ w_{,x}w_y]^T\end{aligned} \tag{5.11}$$

Equation 5.8 and 5.10 are used to solve the in-plane load distribution and stability of the VS panel respectively. Note that Equation 5.10 is mixture of membrane complementary energy(first part of the Equation 5.10) and bending strain energy (second part of the Equation 5.10.Therefore, it is called as Total energy functional instead of Total potential energy.

5.1.2 Semi-analytical equation for Prebuckling-Ritz method

The detailed derivation of the section is presented in [19]. To evaluate the stability of the VS composite plate, it is necessary to calculate in-plate load distribution N_x, N_y and N_{xy} first as these loads will not be the uniform throughout the domain of the plate due to variation of in-plane stiffness $[A^*_{ij}(x,y)]$ and distribution of the in-plane load affect the buckling behaviour of the plate. Here, the boundary conditions for the in-plane loads for the plate under the investigation are shown here for convenience,

$$N_x = \bar{N_x}, N_{xy} = 0 \quad \text{(on x=0,a)} \tag{5.12}$$

$$N_y = 0, N_{xy} = 0 \quad \text{(on y=0,b)} \tag{5.13}$$

since, No prescribed displacement ($\bar{u}$ and $\bar{v}$) applied on any of the four edge of the plate, work done by the prescribed displacement is zero, there for equation of complementary energy Π^c_{pre} reduced from Equation 5.8 to [19],

$$\Pi^c_{pre} = \frac{1}{2}\iint (\phi^T A^*\ \phi)\, dx\, dy \tag{5.14}$$

and from the in-plane boundary condition mentioned in Equation 5.12 and 5.13, the airy-stress function can be assumed as,

$$\Phi(x,y) = \frac{1}{2}\bar{N_x}y^2 + \sum_{kl}^{KL} \Phi_{kl} X_k(x) Y_l(y) \tag{5.15}$$

Where, Φ_{kl} are unknown parameters. It can be noticed from Equation 5.15 that first part ($\frac{1}{2}\bar{N_x}$) serves as a particular solution of the equation and second part ($X_k(x)$ *and* $Y_l(y)$) serves as a homogeneous solution of the equation. After Substituting Equation 5.15 into Equation 5.14 and making complementary energy stationary with respect to unknown parameters Φ_{kl},

$$\frac{\partial \Pi^c_{pre}}{\partial \Phi_{kl}} = 0 \text{ ,(for } k = 1 \text{ to } K,\ l = 1 \text{ to } L) \tag{5.16}$$

leads to KXL linear equation which can be written in terms of matrix as [19],

$$\bar{N_x} C_{kl} + C_a \phi_{kl} = 0 \tag{5.17}$$

Where, ϕ_{kl} is a vector of length KXL,

$$\phi_{kl} = [\Phi_{11}, \Phi_{12}, ..., \Phi_{1L}, \Phi_{21}, ..., \Phi_{kl}, ..., \Phi_{KL}]^T \tag{5.18}$$

C_{kl} is a vector of length KXL where each element of which given as,

$$\iint \begin{bmatrix} A^*_{11} \\ A^*_{12} \\ A^*_{16} \end{bmatrix}^T \begin{bmatrix} X_k Y_l^{''} \\ X_k^{''} Y_l \\ -X_k^{''} Y_l^{''} \end{bmatrix} dx\, dy \tag{5.19}$$

and C_a is a matrix size of KXL by KXL where each element of which given as,

$$\iint \begin{bmatrix} X_k Y_l^{''} \\ X_k^{''} Y_l \\ -X_k^{''} Y_l^{''} \end{bmatrix}^T A^* \begin{bmatrix} X_{k2} Y_{l2}^{''} \\ X_{k2}^{''} Y_{l2} \\ -X_{k2}^{''} Y_{l2}^{''} \end{bmatrix} dx\, dy \tag{5.20}$$

Where, $X_k^{'}$ and $X_k^{''}$ represent the first and second derivative of X_k with respect to x and $Y_l^{'}$ and $Y_l^{''}$ represents the first and second derivative with respect to y respectively. $k2$, $l2$, X_{k2} and Y_{l2} are the counterparts of k, l, X_k and Y_l in quadruple summations [19].

Then the unknown parameter vector ϕ_{kl} can be solved as,

$$\phi_{kl} = -\bar{N_x} C_a^{-1} C_{kl} \tag{5.21}$$

Once, each unknown parameter Φ_{kl} solved, Airy-stress function $\Phi(x, y)$ can be determined using Equation **??** and ultimately in-plane load distribution N_x, N_y and N_{xy} can be calculated using Equation 2.36. It can easily be observed from Equation 5.21 that ϕ_{kl} or subsequently in-plane loads are linearly depended on $\bar{N_x}$, there for buckling initiation can be determined by introducing buckling factor λ to the prescribed load $\bar{N_x}$ as,

$$N_0 = \bar{N_x}^{critical} = \lambda \bar{N_x} \tag{5.22}$$

Where, if λ is greater than 1, prescribed load $\bar{N_x}$ is lower than the critical buckling load of the plate and likewise if the λ is less than 1, the prescribed load is higher than the critical buckling load of the plate.

5.1.3 Semi-analytical equation for Stability-Ritz method

Once, Airy-stress function $\Phi(x, y)$ or in-plane load distribution N_x, N_y and N_{xy} is solved, next step is to solve the buckling load factor λ. For the plate under the loading condition mentioned in Equation 5.12 and 5.13, Total energy functional reduced from Equation 5.10 to ,

$$\Pi = -\frac{1}{2} \iint [\phi^T A^*\ \phi]\, dx\, dy + \frac{1}{2} \iint [\kappa^T D\ \kappa]\, dx\, dy + \iint \phi^T e_n\, dx\, dy \tag{5.23}$$

Where,

$$\begin{aligned}\phi &= [\Phi_{,yy}\ \Phi_{,xx}\ \Phi_{,xy}]^T \\ \kappa &= [-w_{,xx}\ -w_{,yy}\ -2w_{,xy}]^T \\ e_n &= [\frac{1}{2}w_{,x}^2\ \ \frac{1}{2}w_{,y}^2\ \ w_{,x}w_y]^T\end{aligned} \tag{5.24}$$

The out-of-plane displacement is approximated as,

$$w = \sum_{pq}^{PQ} W_{pq} X_p(x) Y_q(y) \tag{5.25}$$

where W_{pq} are unknown parameters and X_p, Y_q are the shape functions different from the shape function used to approximate airy-stress function. To initiate the buckling, buckling load factor is introduced with Airy-stress function as,

$$\Phi(x,y) = \lambda(\frac{1}{2}\bar{N_x}y^2 + \sum_{kl}^{KL} \Phi_{kl} X_k(x) Y_l(y)) \tag{5.26}$$

where the solution for parameters Φ_{kl} are already solved using Equation 5.21. After substituting Equation 5.25 and Equation 5.26 into Equation 5.23 and making total energy functional Π stationary with respect to unknown parameters W_{pq} as,

$$\frac{\partial \Pi}{\partial W_{pq}} = 0 \text{ ,(for } p = 1 \text{ to } P,\ q = 1 \text{ to } P) \tag{5.27}$$

results in PXQ linear equations, which can be written in matrix from as [19],

$$[C_D + \lambda(C_N + C_F)]w_{pq} = 0 \tag{5.28}$$

where, w_{pq} is a vector of length PXQ given as,

$$w_{pq} = [W_{11}, W_{12}, ..., W_{1P}, W_{21}, ..., W_{pq}, ..., W_{PQ}]^T \tag{5.29}$$

C_D is a matrix of dimension PXQ by PXQ of which each element is,

$$\iint \begin{bmatrix} X_p^{''} Y_q \\ X_p Y_q^{''} \\ -2X_p^{'} Y_q^{'} \end{bmatrix}^T D \begin{bmatrix} X_{p2}^{''} Y_{q2} \\ X_{p2} Y_{q2}^{''} \\ -2X_{p2}^{'} Y_{q2}^{'} \end{bmatrix} dx\, dy \tag{5.30}$$

C_N is a matrix of dimension PXQ by PXQ of which each element is,

$$\bar{N_x} \iint (X_p^{'} Y_q X_{p2}^{'} Y_{q2})\, dx\, dy \tag{5.31}$$

and C_F is a matrix of dimension PXQ by PXQ of which each element are,

$$\sum_{kl}^{KL} \Phi_{kl} \iint \begin{bmatrix} X_k Y_l^{''} \\ X_k^{''} Y_l \\ -X_k^{'} Y_l^{'} \end{bmatrix}^T \begin{bmatrix} X_p^{'} X_{p2}^{'} Y_q Y_{q2} \\ X_p X_{p2} Y_q^{'} Y_{q2}^{'} \\ X_p^{'} Y_q X_{p2} Y_{q2}^{'} + X_p Y_q^{'} X_{p2}^{'} Y_{q2} \end{bmatrix} dx\, dy \tag{5.32}$$

Here, $p2$, $q2$, X_{p2} and Y_{q2} are the counterparts of p, q, X_p and Y_q in quadruple summations. For detailed derivation for the stability equation, please refer to [19].

5.2 Double Fourier series approximation of fiber angle distribution

To use Ritz-method approximation(Equation 5.8 and Equation 5.10), it is necessary to precalculate in-plane stiffness $A^*_{ij}(x,y)$ and bending stiffness $D_{ij}(x,y)$ which are functions of fiber angle $\theta(x,y)$ of the k^{th} ply in a laminate. Thus once, fiber angle distribution function $\theta(x,y)$ are known for each ply in the laminate, in-plane stiffness and bending-stiffness and subsequently in-plane load distribution and buckling load can be solved. Out-of-many possible approximation of a function in R^2, Double Fourier series approximation is one of the widely used approximation method which gives infinitely differential continuous approximation of any function in a domain Ω [10]. There are two choices for double Fourier series approximation which are Double sine Fourier series as shown in Equation 5.33 as,

$$\bar{\theta(x,y)} = \sum_{m=1}^{M=\infty}\sum_{n=1}^{N=\infty} \theta_{mn} sin(\frac{m\pi x}{a}) sin(\frac{n\pi y}{b}) \tag{5.33}$$

where,

$$\theta_{mn} = \frac{4}{ab}\int_0^a \int_0^b \theta(x,y) sin(\frac{m\pi x}{a}) sin(\frac{n\pi y}{b})\, dx\, dy \tag{5.34}$$

and Double cosine Fourier series as shown in Equation 5.35 as,

$$\bar{\theta(x,y)} = \sum_{m=0}^{M=\infty}\sum_{n=0}^{N=\infty} \theta_{mn} cos(\frac{m\pi x}{a}) cos(\frac{n\pi y}{b}) \tag{5.35}$$

where,

$$\theta_{mn} = \frac{4}{ab}\int_0^a \int_0^b \theta(x,y) cos(\frac{m\pi x}{a}) cos(\frac{n\pi y}{b})\, dx\, dy \tag{5.36}$$

Here, m and n represents the number of half waves alog x and y directions respectively. Out of these two double Fourier approximation, which approximation should be used can be decided based on the convergence of Root Mean square error(RSME) to zero, which is calculated using true fiber angle distribution $\theta(x,y)$(obtained using MFEM-framework) and approximated fiber angle distribution $\bar{\theta(x,y)}$(approximation using Double Fourier series) as,

$$RSME = \sqrt{\frac{\sum(\theta(x,y) - \bar{\theta(x,y)})^2}{N}} \tag{5.37}$$

where N is the number of samples. In this section, fiber angle distribution is approximated for the optimized fiber angle distribution obtained using MFEM-framework (case : $MM-5X5$, stress-mesh $60X60$) in section 4.4 by double sin Fourier series and double cosine Fourier series separately and RSME convergence plot for each ply are shown in Figure 5.2.

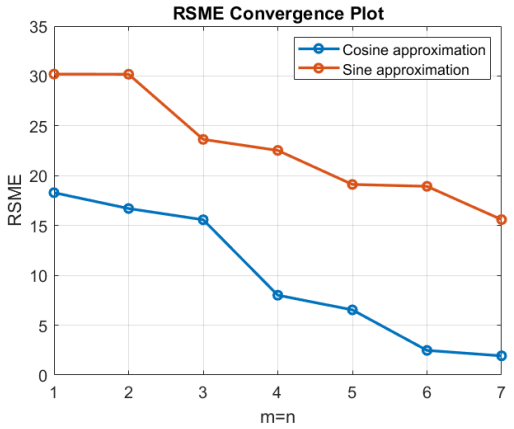

(a) RSME convergence plot : Ply-1

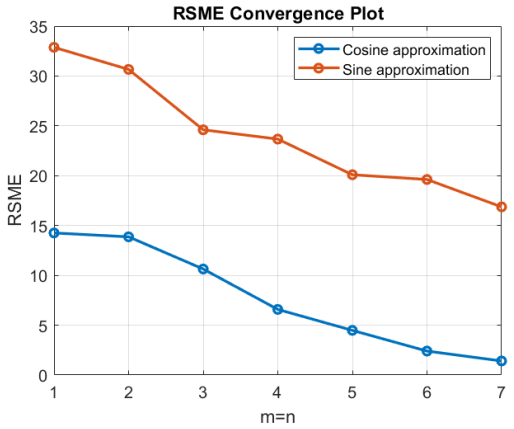

(b) RSME convergence plot : Ply-2

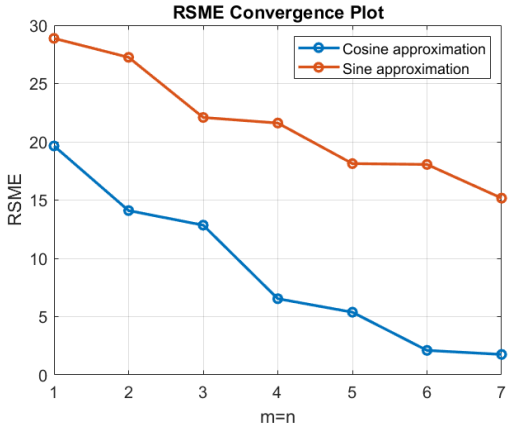

(c) RSME convergence plot : Ply-3

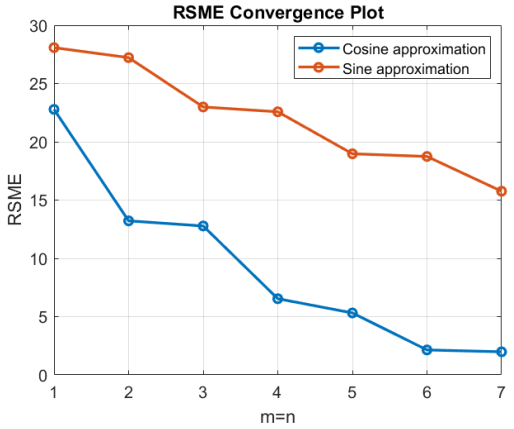

(d) RSME convergence plot : Ply-4

Figure 5.2: RSME convergence plot of fourier approximation

It can be concluded from the RSME convergence plot that Double cosine Fourier series approximation gives better approximation of the optimized fiber angle distribution obtained using MFEM-framework(Case: MM-5X5, stress-mesh 15X15) than the Double sine Fourier series approximation and RSME value converges to zero rapidly if fiber angle distribution is approximated using Double cosine Fourier series. The reason that Double sine Fourier series approximation gives poor approximation of fiber angle distribution is it forces the fiber angle distribution to be zero at all the edges of the plate while it can be seen from the result obtained in Section 4.4 that fiber angles are certainly not zero at the edges or the corner of the plate. Therefore, fiber angle distribution $\theta(x, y)$ is assumed as a Double cosine Fourier series for the buckling load optimization using semi-analytical method as,

$$\theta(\bar{x}, y) = \sum_{m=0}^{M=\infty} \sum_{n=0}^{N=\infty} \theta_{mn} cos(\frac{m\pi x}{a}) cos(\frac{n\pi y}{b}) \tag{5.38}$$

5.2.1 Verification

In this section, solution for in-plane load distribution and stability using ritz method are verified with optimized converged result achieved using MFEM-framework(MM: 5×5, stress-mesh: 60×60) and number of terms(K, L, P, Q) of shape functions needed to approximate in-plane load distribution and buckling are decided based on convergence to the FEM results with convergence error less than 2%.

To approximate the in-plane load distribution, the chosen shape function has to satisfy the mechanical boundary conditions as shown in Equation 5.12 and 5.13 term by term for the loading condition chosen for the study and can be written as,

$$X_k(x) = X_k^{'}(x) = 0 \quad \text{(on x=0,a for } k\text{=1,2,...K)} \tag{5.39}$$

$$Y_l(y) = Y_l^{'}(y) = 0 \quad \text{(on y=0,b for } l\text{=1,2,...L)} \tag{5.40}$$

Therefore, Polynomial shape functions are used to approximate in-plane loading distributions which satisfy the conditions as shown in Equation 5.39 and 5.40 [19].The assumed Polynomial shape function is of fourth order,

$$X(x) = c_0 + c_1 x + c_2 x^2 + c_0 x^3 + c_4 x^4 \tag{5.41}$$

The constant c_0 to c_4 are determined using boundary conditions as shown in Equation 5.39 and Equation 5.40. As there is only four boundary conditions, Only Four out of Five constants can be solved, therefore rest of the constants are arbitrary and can be set to unity. After applying the boundary conditions, Polynomial shape function becomes,

$$X(x) = (\frac{x}{a})^2(\frac{x}{a} - 1)^2 \tag{5.42}$$

Therefore the k^{th} shape function can be written as,

$$X_k(x) = (\frac{x}{a})^{k+1}(\frac{x}{a} - 1)^2 \tag{5.43}$$

The shape functions are then Orthogonalized using Gram-Schmidt process and transformed into the natural coordinates (ζ, η) spanning the interval $[-1, 1]$ to avoid the numerical instability. Finally, The transformed shape functions are written as [19],

$$X_1(\zeta) = \frac{3\sqrt{35}}{16}(\zeta^2 - 1)^2 \tag{5.44}$$

$$X_2(\zeta) = \frac{3\sqrt{385}}{16}\zeta(\zeta^2 - 1)^2 \tag{5.45}$$

$$\begin{matrix} . \\ . \\ . \end{matrix} \tag{5.46}$$

Similar procedure is for shape functions $Y(y)$ in y-direction, where $Y_l(\eta)$ can be written as [19],

$$Y_1(\eta) = \frac{3\sqrt{35}}{16}(\eta^2 - 1)^2 \tag{5.47}$$

$$Y_2(\eta) = \frac{3\sqrt{385}}{16}\eta(\eta^2 - 1)^2 \tag{5.48}$$

$$\begin{matrix} . \\ . \\ . \end{matrix} \tag{5.49}$$

Where,

$$\zeta = \frac{2x-a}{a}$$
$$\eta = \frac{2y-b}{b} \tag{5.50}$$

To approximate, the Out-of-plane displacement in Buckling, It can be assumed as a linear combinations of shape functions as shown in Equation 5.25, As the plate under investigation is simply supported, the boundary condition shape function has to satisfy term by term is written as,

$$\begin{aligned} X_p(x) &= 0 \text{ (on x=0,a)} \\ Y_q(y) &= 0 \text{ (on y=0,b)} \end{aligned} \tag{5.51}$$

$$\begin{aligned} X_p^{'}(x) &= 0 \text{ (on x=0,a)} \\ Y_q^{'}(y) &= 0 \text{ (on y=0,b)} \end{aligned} \tag{5.52}$$

$$\begin{aligned} X_p^{''}(x) &= 0 \text{ (on x=0,a)} \\ Y_q^{''}(y) &= 0 \text{ (on y=0,b)} \end{aligned} \tag{5.53}$$

There is no shape function which can satisfy the boundary shown in Equation 5.2.1 and 5.2.1 simultaneously which result in error in approximation. However, as the number of terms used to approximate the solution are increased, the error in the approximation reduce [19] [16].

Out of many possible shape function, polynomial shape function is used which satisfy the essential boundary condition and written as [19],

$$\begin{aligned} X_p(x) &= (\frac{x}{a})^p(\frac{x}{a}-1) \quad \text{(for p=1,2,..,P)} \\ Y_q(y) &= (\frac{y}{b})^q(\frac{y}{b}-1) \quad \text{(for q=1,2,..,Q)} \end{aligned} \tag{5.54}$$

The shape function shown in Equation 5.2.1 are then transferred to natural coordinates $[-1, 1]$ and after orthogonalized using Gram-Schmidt process, finally $X_p(\zeta)$ can be written as [19],

$$X_1(\zeta) = \frac{\sqrt{15}}{4}(\zeta^2-1)^2 \tag{5.55}$$

$$X_2(\zeta) = \frac{\sqrt{105}}{4}\zeta(\zeta^2-1) \tag{5.56}$$

$$\begin{matrix} . \\ . \\ . \end{matrix} \tag{5.57}$$

Similarly, $Y_q(\eta)$ can be written as [19],

$$Y_1(\eta) = \frac{\sqrt{15}}{4}(\eta^2 - 1)^2 \tag{5.58}$$

$$Y_2(\eta) = \frac{\sqrt{105}}{4}\eta(\eta^2 - 1) \tag{5.59}$$

$$\begin{matrix} . \\ . \\ . \end{matrix} \tag{5.60}$$

Where,

$$\begin{aligned} \zeta &= \frac{2x - a}{a} \\ \eta &= \frac{2y - b}{b} \end{aligned} \tag{5.61}$$

Here, Optimized fiber angle distribution for buckling achieved using MFEM(MM:5×5) in Section 4.4 is first approximated using double cosine Fourier series for each ply and later buckling load is calculated using approximated angle distribution $\theta(x, y)$ by semi-analytical method and verified for convergence as shown in Figure 5.3. All the integration required to evaluate the in-plane loading distribution(Equation 5.19-5.20) and the buckling (Equation 5.30-5.32) are performed numerically using Gaussian quadrature points (N_g).

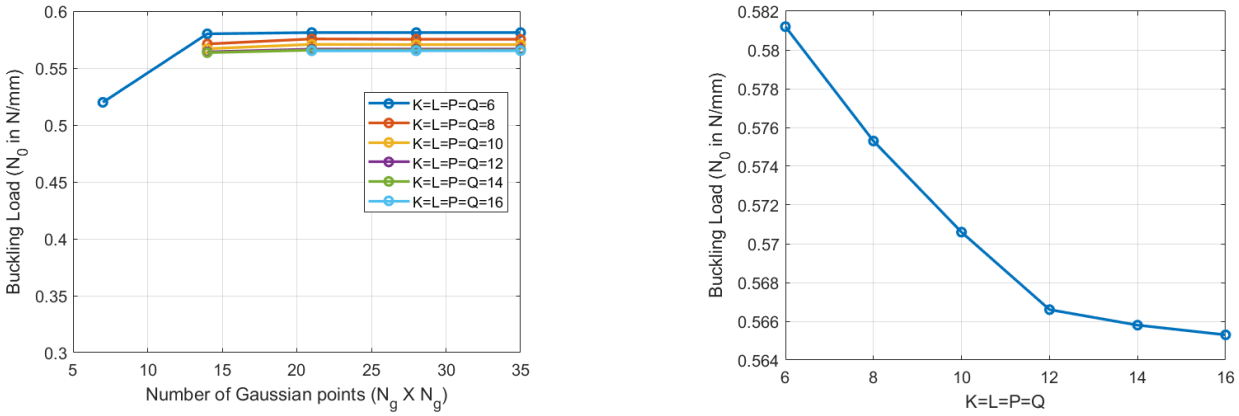

(a) Buckling Load vs Number of Gaussian points

(b) Buckling Load convergence

Figure 5.3: Buckling Load approximation using Ritz method

It can be seen that, semi-analytical method requires only upto 8 terms($K = L = P = Q = 8$) to approximate the buckling load with convergence error less than 2% due to stiffness discontinuity [19]. Further, First two eigenmodes calculated using MFEM-framework(MM: 5×5, stress-mesh: 60×60) and calculated using semi-analytical method (terms $K = L = P = Q = 8$) are compared for the verification which show that semi-analytical method approximate buckling load and buckling mode by using only upto 8 terms (terms $K = L = P = Q = 8$) with convergence error less than 2% and therefore optimization using Semi-analytical method is carried out using $K = L = P = Q = 8$ with 21×21 Gaussian quadrature points($N_g = 21$) in each direction(ζ and η) which captures the buckling behaviour effectively and requires less calculation time.

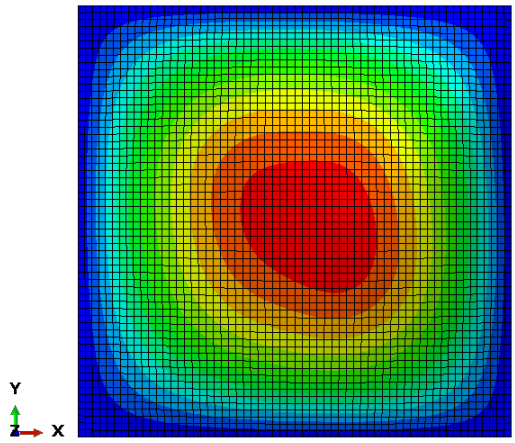

(a) $FEM(stress - element : 60X60)$
$(Eigenvalue = 0.5640)$

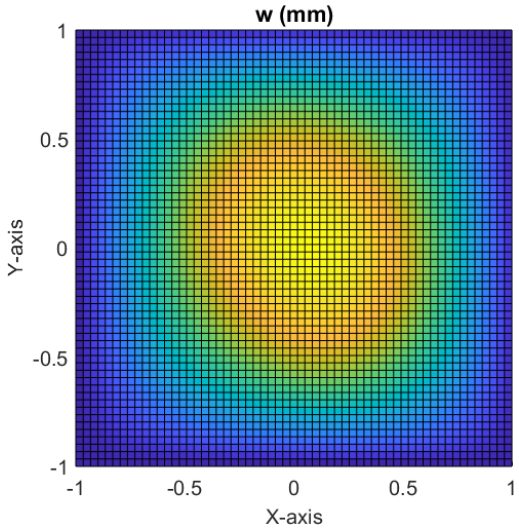

(b) $Ritz$ $(K = L = P = Q = 8)$
$(Eigenvalue = 0.5755)$

Figure 5.4: First Buckling-mode comparison: FEM Vs Semi-analytical

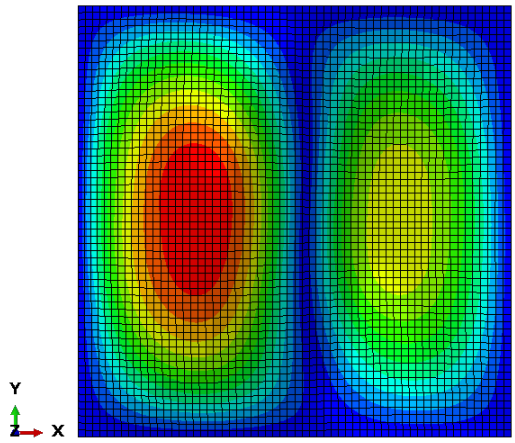

(a) $FEM(stress - element : 60X60)$
$(Eigenvalue = 0.5642)$

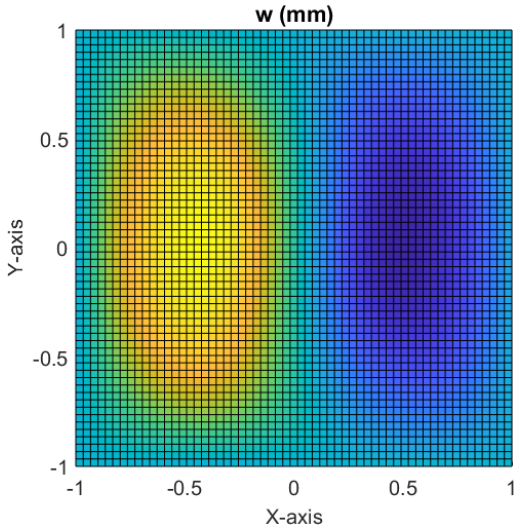

(b) $Ritz$ $(K = L = P = Q = 8)$
$(Eigenvalue = 0.5764)$

Figure 5.5: Second Buckling-mode comparison: FEM Vs Semi-analytical

5.3 Optimization using Semi-analytical equation

In this section Buckling load optimization of bivariate Variable stiffness plate using semi-analytical method has been performed.As explained in Section Appendix-A, The BFGS algorithm [14] is used as an optimization method and its parameters are shown in Table 5.1. The fiber angle distribution $\theta(x, y)$ is assumed as a Double cosine Fourier series for the buckling load optimization using semi-analytical method as,

$$\theta(\bar{x}, y) = \sum_{m=1}^{M=\infty} \sum_{n=1}^{N=\infty} \theta_{mn} cos(\frac{m\pi x}{a}) cos(\frac{n\pi y}{b}) \tag{5.62}$$

where, θ_{mn} are unknown parameters and inputs of the objective function which is being optimized for buckling load.

To start with initial Guess which is $[-45°, 45°, 45°, -45°]_s$, the constant θ_{00} are set with the value $-45°$ or $45°$ according to sequence of laminate, and rest of the amplitude θ_{mn} associated with cosines are set to zero initially for each ply.

Here, buckling load is optimized for three different cases of cosine terms expansion; $Case1 : M = N = 2$, $Case2 : M = N = 3$ and $Case3 : M = N = 5$ separately and BFGS optimization convergence plot is shown for all three cases in Figure 5.6

BFGS Parameter	Value
c_1	1e-4
c_2	0.9
ϵ	$0.01°$ $(forward - difference)$
g_{tol}	1e-5
Variable Bound	$[-90°, 90°]$
Initial Guess	$[-45°, 45°, 45°, -45°]_s$

Table 5.1: BFGS Parameters for the Optimization of buckling load of bi-variate VS composite Plate .

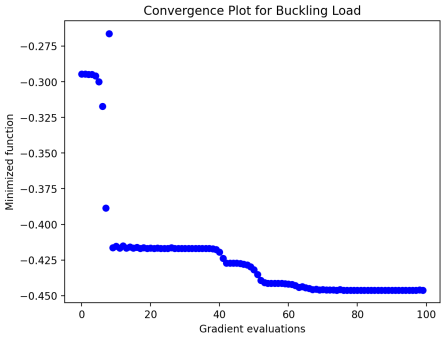

(a) Case: M=N=2

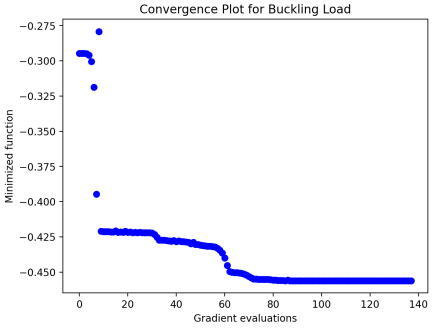

(b) Case: M=N=3

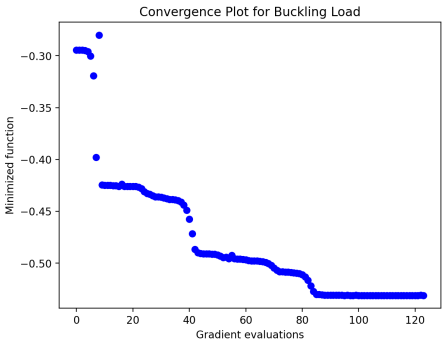

(c) Case: M=N=5

Figure 5.6: BFGS convergence plot for each cases of M=N

5.3.1 Optimized Results Comparison : Ply

In this section, the optimized fiber angle or direction for optimized buckling load are compared for each ply from Figure 5.7 to 5.10. It can be noticed from the fiber angle distribution that, fiber angles are arranged in approximately -45° or 45° angle away from the center of the plate. The results(S-shaped fiber angle distribution) are similar to Tatting and Gurdal [11].

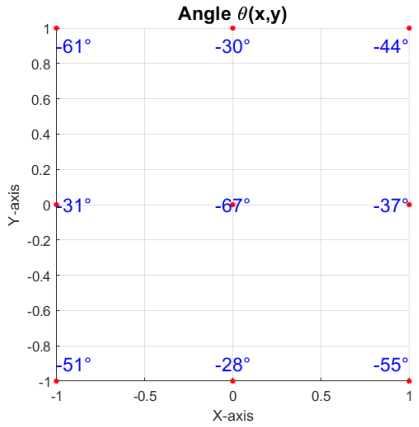

(a) $Case : M = N = 2$

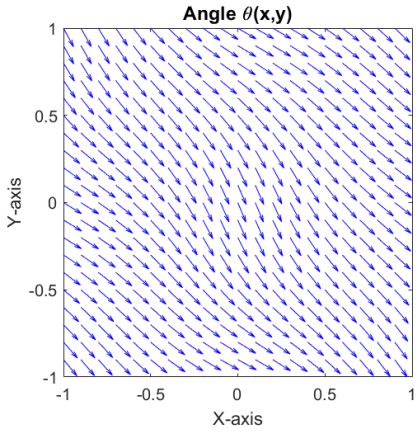

(b) Fiber angle distribution : $M = N = 2$

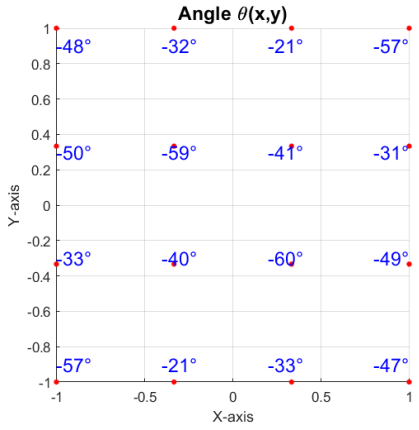

(c) $Case : M = N = 3$

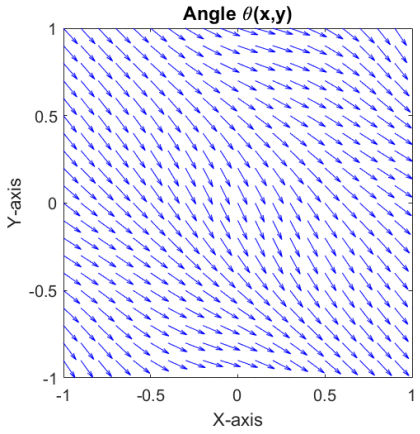

(d) Fiber angle distribution : $M = N = 3$

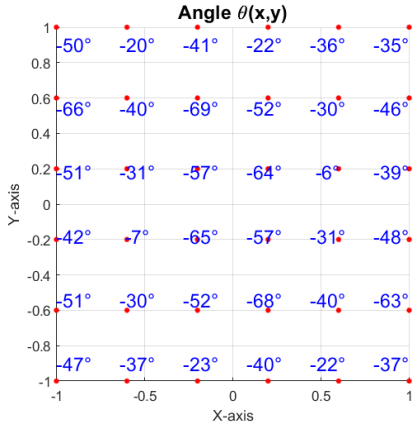

(e) $Case : M = N = 5$

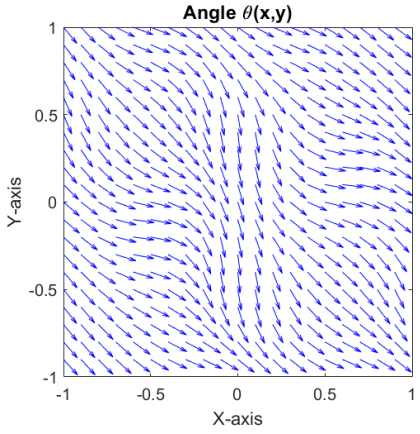

(f) Fiber angle distribution : $M = N = 5$

Figure 5.7: Optimized result Comparison of: Ply-1

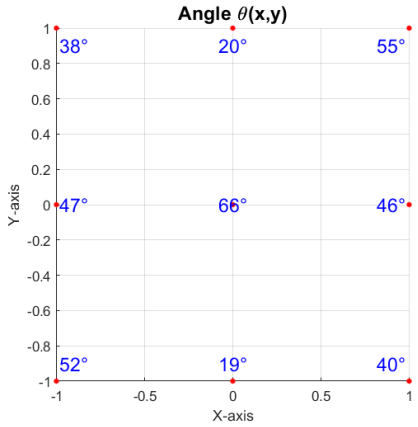

(a) $Case : M = N = 2$

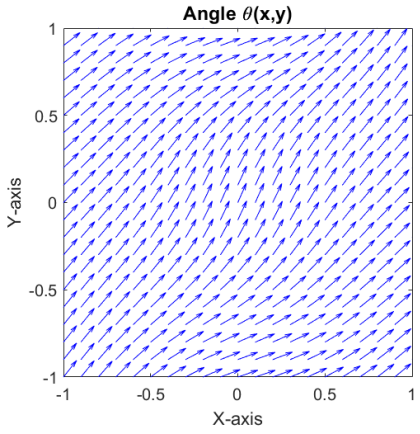

(b) Fiber angle distribution : $M = N = 2$

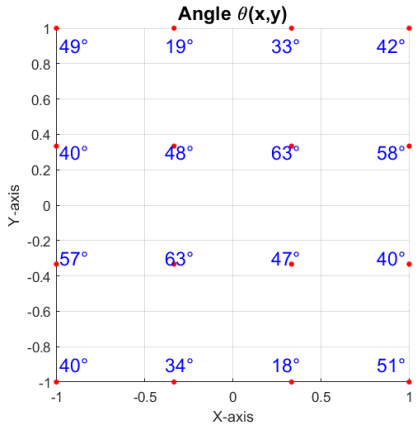

(c) $Case : M = N = 3$

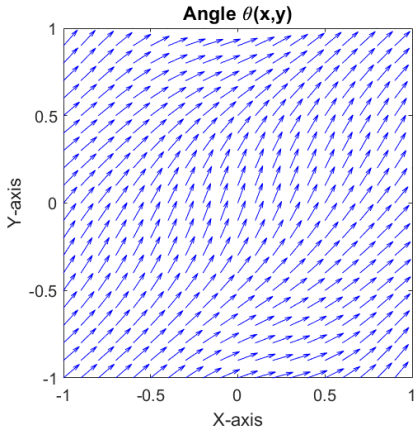

(d) Fiber angle distribution : $M = N = 3$

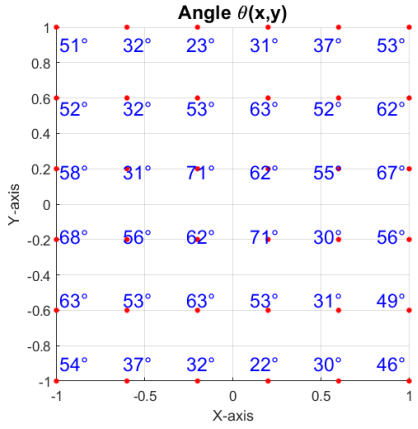

(e) $Case : M = N = 5$

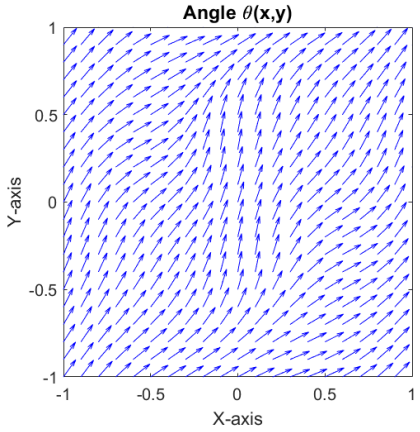

(f) Fiber angle distribution : $M = N = 5$

Figure 5.8: Optimized result Comparison of: Ply-2

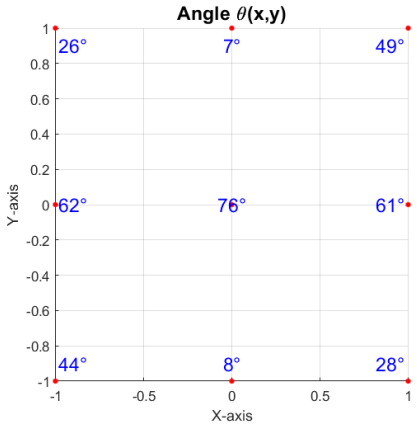

(a) $Case : M = N = 2$

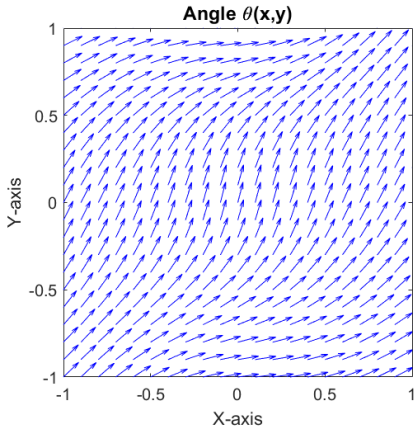

(b) Fiber angle distribution : $M = N = 2$

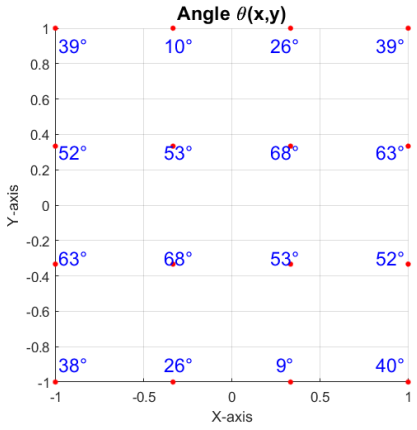

(c) $Case : M = N = 3$

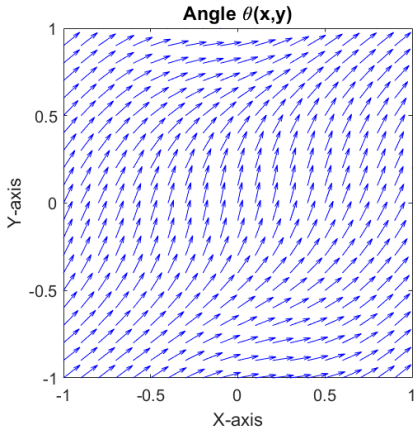

(d) Fiber angle distribution : $M = N = 3$

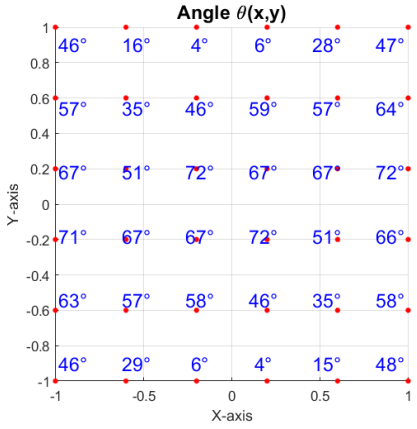

(e) $Case : M = N = 5$

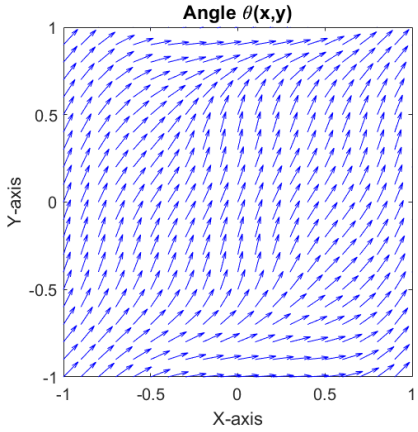

(f) Fiber angle distribution : $M = N = 5$

Figure 5.9: Optimized result Comparison of: Ply-3

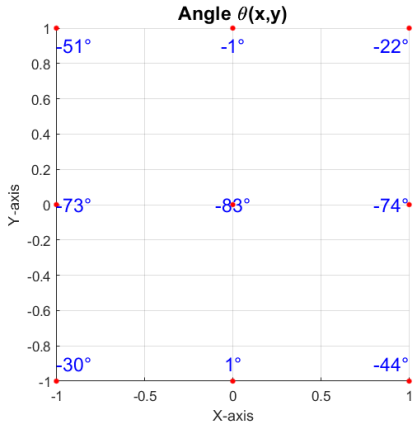

(a) $Case : M = N = 2$

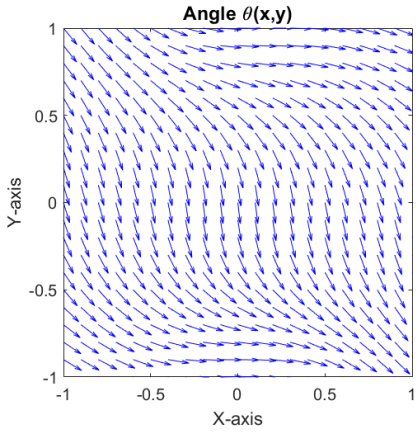

(b) Fiber angle distribution : $M = N = 2$

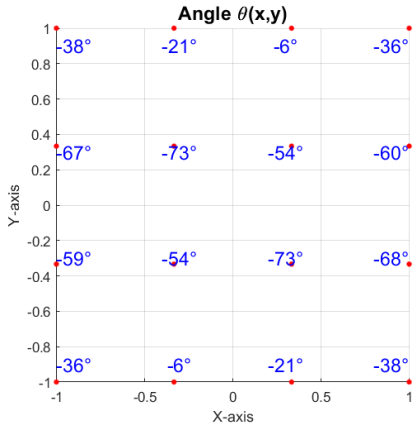

(c) $Case : M = N = 3$

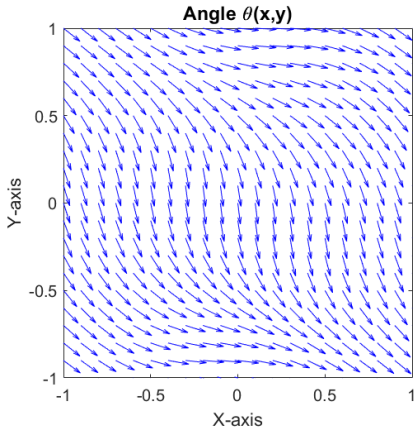

(d) Fiber angle distribution : $M = N = 3$

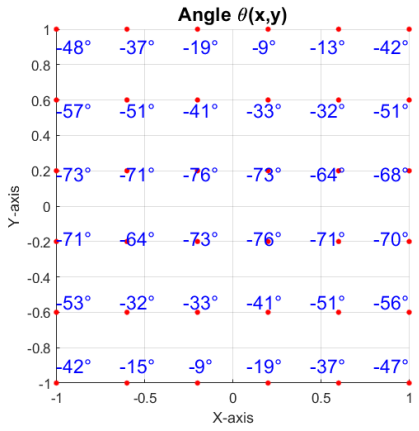

(e) $Case : M = N = 5$

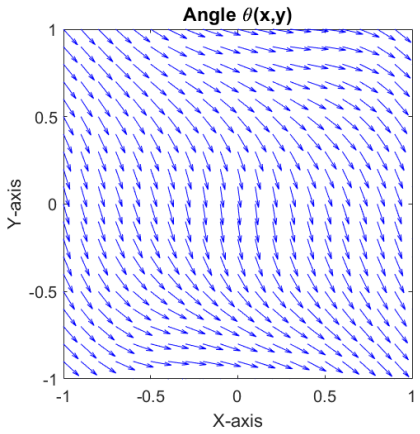

(f) Fiber angle distribution : $M = N = 5$

Figure 5.10: Optimized result Comparison of: Ply-4

5.3.2 Optimized Results Comparison : Buckling Mode

Here first two buckling mode or eigenvectors are compared for optimized results achieved using $M = N = 2$, $M = N = 3$ and $M = N = 5$. It can be observed from Figure 5.11 and 5.12 that first two eigenvalues are nearly equal in each of the case.

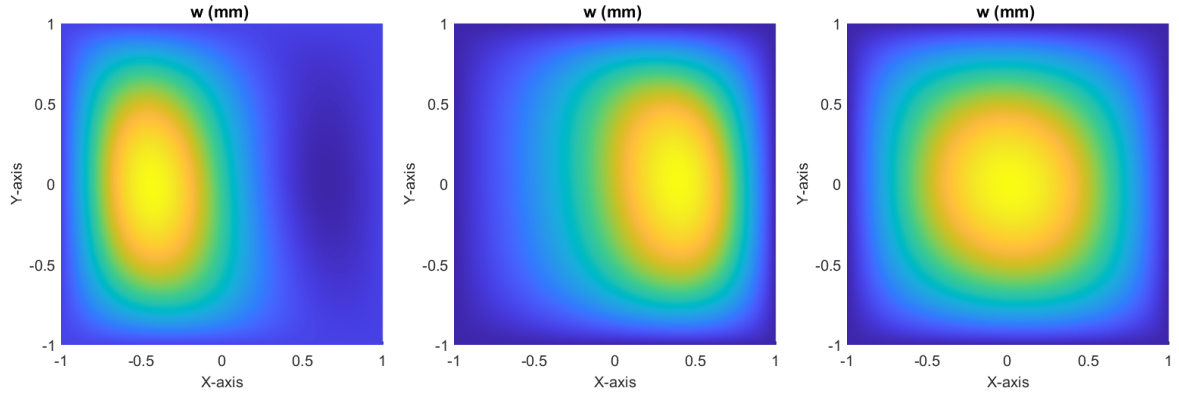

(a) Case: M=N=2
Eigenvalue = 0.4460

(b) Case: M=N=3
Eigenvalue = 0.4560

(c) Case: M=N=5
Eigenvalue = 0.5308

Figure 5.11: Comparison of Buckling Mode-1

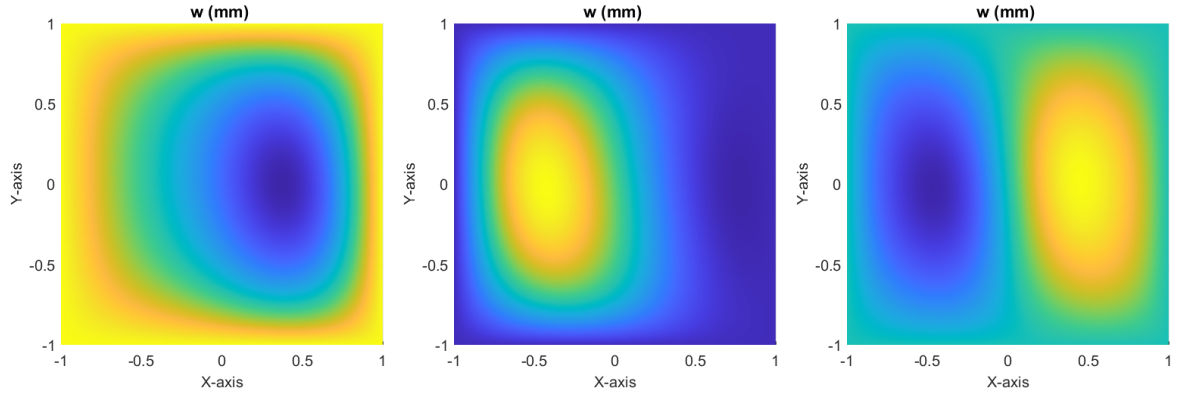

(a) Case: M=N=2
Eigenvalue = 0.4461

(b) Case: M=N=3
Eigenvalue = 0.4560

(c) Case: M=N=5
Eigenvalue = 0.5309

Figure 5.12: Comparison of Buckling Mode-2

5.3.3 Convergence study of optimized result

Since the Number of polynomial approximation(K, L, P, Q) chosen for buckling load optimization upto 8^th order, the optimized buckling load is verified for convergence by adding more polynomial terms further with using the optimized fiber angle distribution achieved using $K, L, P, Q = 8$ terms. The convergence study for each case,namely $M = N = 2$, $M = N = 3$ and $M = N = 5$ are shown in Figure 5.13. It can be seen from the table that change in the buckling load is not noticeably large even if the approximation is refined with adding higher order terms K, L, P and Q .

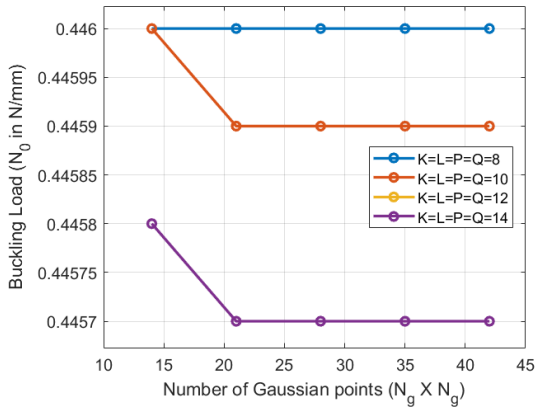

(a) Buckling load vs Gaussian Points
Case: $M = N = 2$

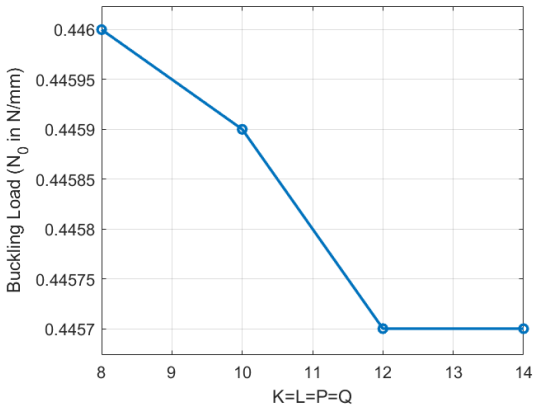

(b) Buckling Load convergence
Case: $M = N = 2$

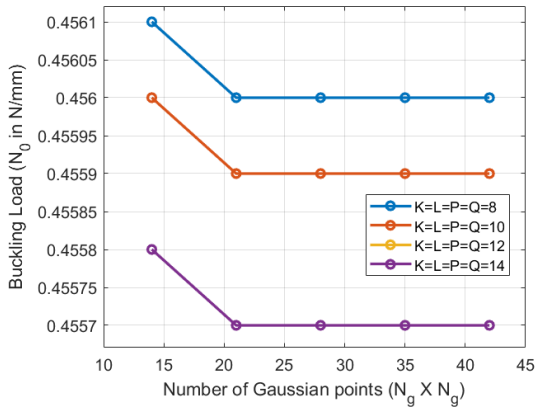

(c) Buckling load vs Gaussian Points
Case: $M = N = 3$

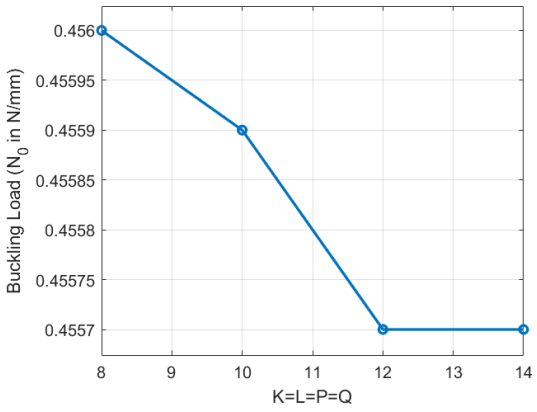

(d) Buckling Load convergence
Case: $M = N = 3$

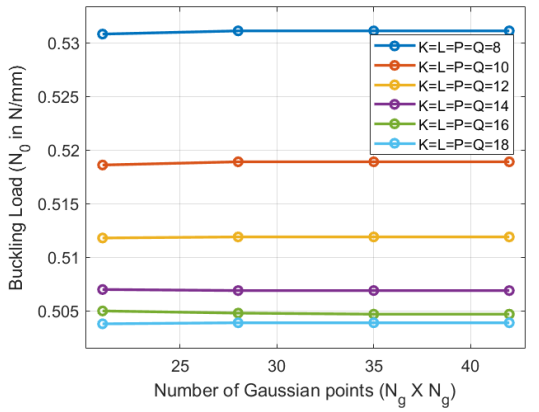

(e) Buckling load vs Gaussian Points
Case: $M = N = 5$

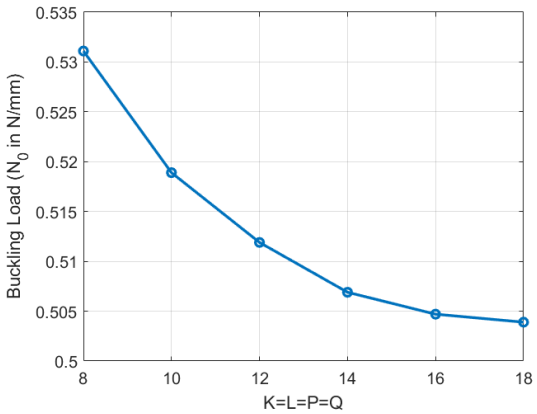

(f) Buckling Load convergence
Case: $M = N = 5$

Figure 5.13: Buckling Load approximation vs Polynomial terms(K, L, P, Q) required

Chapter 6

Results and Conclusion

6.1 Comparison of optimum buckling load

The optimized buckling load achieved using MFEM-framework and Semi-analytical method (Ritz method) are compared with benchmarked CS composite plate for each case in this section. Figure 6.1 shows Optimization convergence plot of buckling load using both method and final optimized results for all the study(Optimization of buckling load for CS, Univariate VS, Bivariate VS plate) conducted in the thesis are summarized in the Table 6.1.

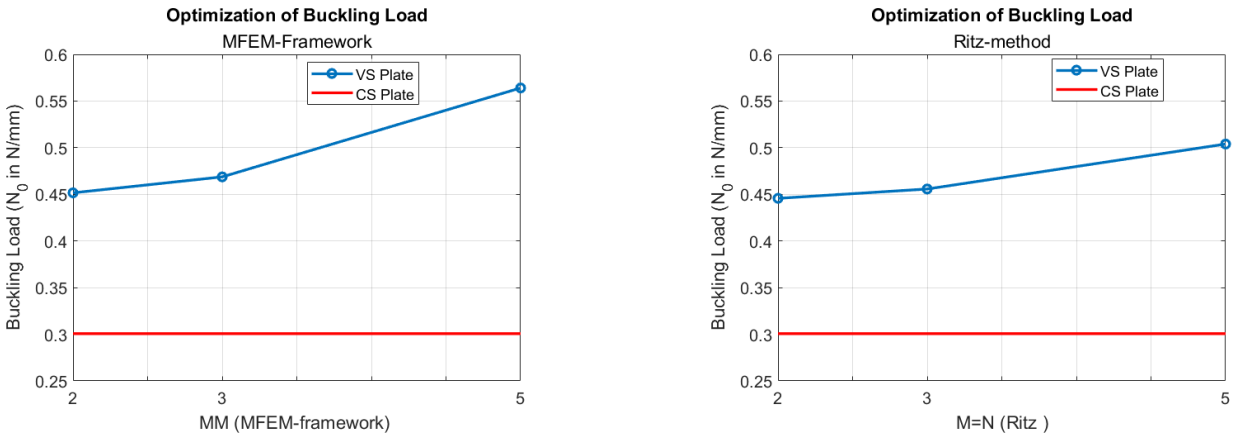

(a) Optimization using MFEM

(b) Optimization using Ritz

Figure 6.1: Buckling load optimization convergence for MFEM-framework and Ritz-method

Case	Buckling Load N_0 (N/mm)
CS Plate(Benchmark)	0.3007
Univariate VS Plate $\theta(x)$	0.3249
Univariate VS Plate $\theta(y)$	0.3968
Bivariate MFEM-framework	0.5640
Bivariate Ritz-method	0.5039

Table 6.1: Optimization results for MFEM and Ritz.

The optimization results from the two approaches MFEM and Ritz(semi-analytical method) shows that there is 87% and 67% improvement in buckling load for a bivariate VS composite plate respectively as compared to benchmarked CS composite plate under investigation.

Even though the fiber angle distribution for the optimized buckling load using MFEM-framework(MM: 5×5) and Semi-analytical method ($M = N = 5$) shows similar ($S - shape$) pattern for each ply, as shown in Section 4.4.1 and Section 5.3.1, the optimized buckling load achieved using MFEM is 11% higher than the optimized buckling load achieved using Semi-analytical. The reason for the discrepancy in the buckling load cannot not be explained easily by fiber angle distribution alone. Instead the distribution of bending stiffness D_{ij} throughout the plate may provide a better explanation.Therefore, the comparison of bending stiffness D_{ij}

are shown in Figure 6.2 to 6.5 for Optimized constant stiffness plate, Univariate Variable stiffness, and Bivariate VS stiffness(MFEM vs Ritz). There is noticeable difference in the distribution of the bending stiffness $D_{ij}(x, y)$ in each case and therefore in the buckling load. Which indicates that distribution of bending stiffness $D_{ij}(x, y)$ is the influential parameter for the buckling load.

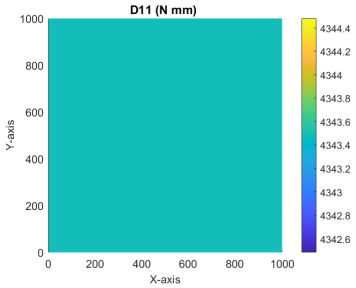

(a) Distribution of D_{11} for Optimized CS Plate

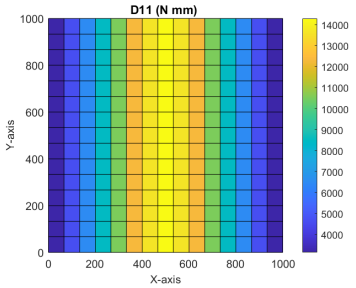

(b) Distribution of D_{11} : Optimized Univariate VS Plate $\theta(x)$

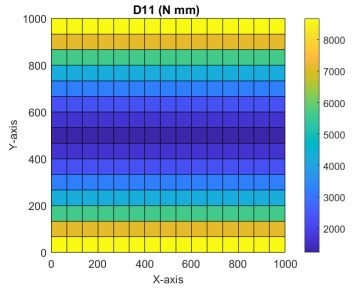

(c) Distribution of D_{11} : Optimized Univariate VS Plate $\theta(y)$

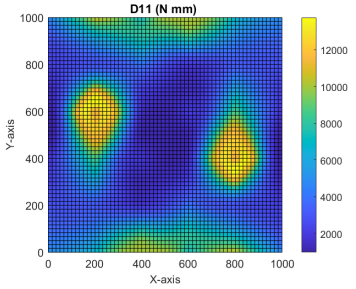

(d) Distribution of D_{11} : (MFEM) MM: 5×5

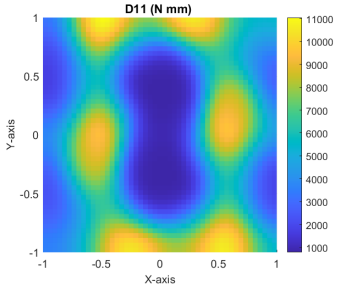

(e) Distribution of D_{11} : (Ritz) M=N=5

Figure 6.2: Comparison of Distribution of D_{11} for optimized CS, Univariate VS, Bivariate VS plate

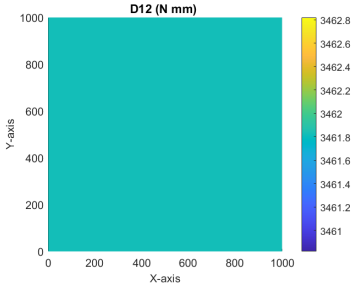

(a) Distribution of D_{12} for Optimized CS Plate

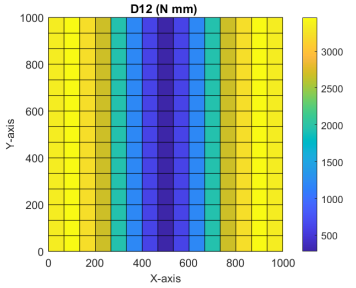

(b) Distribution of D_{12} : Optimized Univariate VS Plate $\theta(x)$

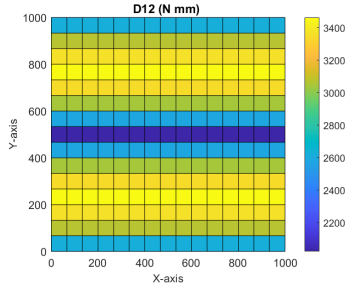

(c) Distribution of D_{12} : Optimized Univariate VS Plate $\theta(y)$

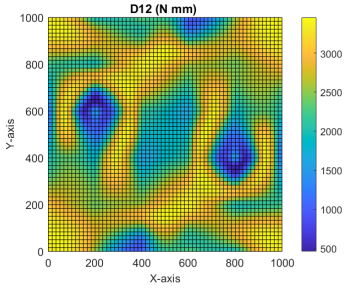

(d) Distribution of D_{12} : (MFEM) MM: 5×5

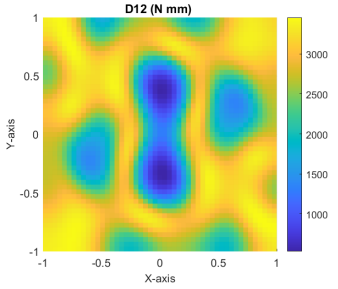

(e) Distribution of D_{12} : (Ritz) M=N=5

Figure 6.3: Comparison of Distribution of D_{12} for optimized CS, Univariate VS, Bivariate VS plate

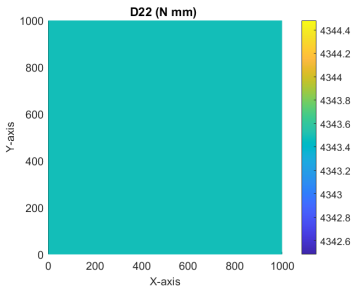

(a) Distribution of D_{22} for Optimized CS Plate

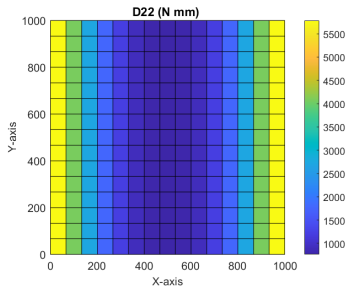

(b) Distribution of D_{22} : Optimized Univariate VS Plate $\theta(x)$

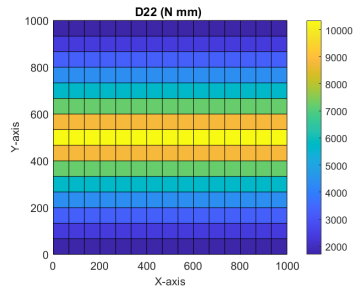

(c) Distribution of D_{22} : Optimized Univariate VS Plate $\theta(y)$

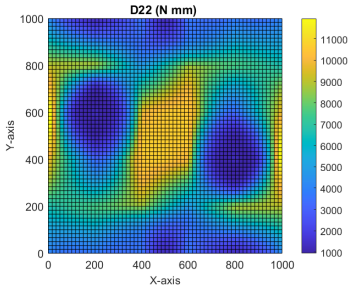

(d) Distribution of D_{22} : (MFEM) MM: 5×5

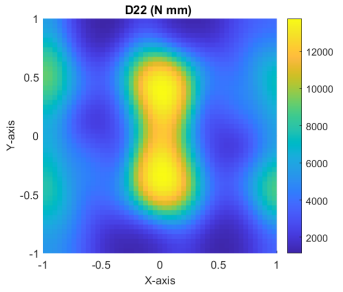

(e) Distribution of D_{22} : (Ritz) M=N=5

Figure 6.4: Comparison of Distribution of D_{22} for optimized CS, Univariate VS, Bivariate VS plate

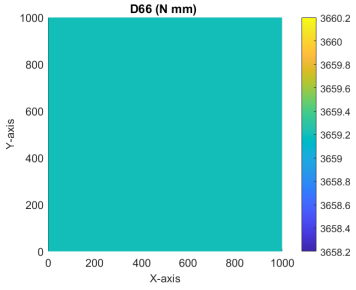

(a) Distribution of D_{66} for Optimized CS Plate

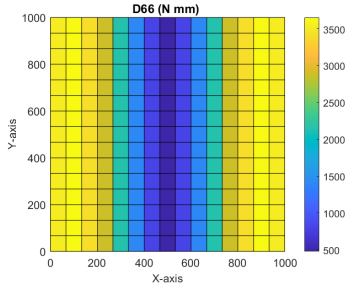

(b) Distribution of D_{66} : Optimized Univariate VS Plate $\theta(x)$

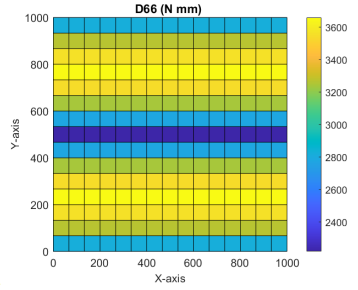

(c) Distribution of D_{66} : Optimized Univariate VS Plate $\theta(y)$

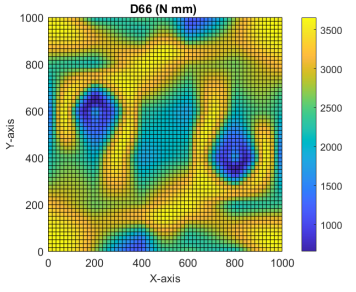

(d) Distribution of D_{66} : (MFEM) MM: 5×5

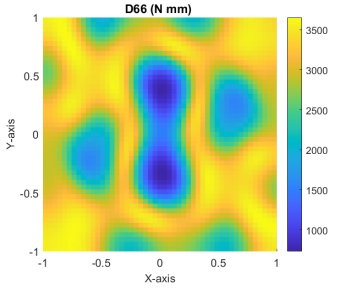

(e) Distribution of D_{66} : (Ritz) M=N=5

Figure 6.5: Comparison of Distribution of D_{66} for optimized CS, Univariate VS, Bivariate VS plate

6.2 Conclusions and Unique contribution

- From the optimized results shown in Table 6.1, it can be easily concluded that Variable stiffness composite plate shows better buckling performance than the constant stiffness composite plate by redistributing the load and stiffness in the domain of the plate.
- It also can be concluded from the optimized results achieved for Univariate VS Plate and Bivariate VS plate that bi-directional variability in fiber angle distribution(or ultimately stiffness) widen the design

space for the optimization result in higher buckling load as compared to Univariate VS Plate.

- It can be easily observed from the Figure 6.2 to 6.5 that the optimized distribution of D_{ij} achieved using MFEM-framwork has discrete jump element to element where as optimized distribution of D_{ij} achieved using semi-analytical method has higly smooth variation of the stiffness. Therefore it can be concluded that highly smooth resolution or variation of stiffness may not be required to achieve better buckling load capacity as it highly depends on localized sharp fiber angle variation or ultimately stiffness variation.
- Moreover, semi-analytical method can be used as a substitute to the FEM for the optimization by following the proposed methodology in this thesis.
- The main contribution to this thesis are; First, the development of a python module which can utilize the MFEM-framework explained in Chapter 4 for the optimization of the Variable stiffness plate for buckling load . Secondly, development of a methodology/framework which can unitize the semi-analytical method to optimize the buckling load.

Chapter 7

Future work

In this study, all the optimization were performed on a plate having aspect ratio ($length/width = 1$)with simply supported boundary condition as shown in Chapter 3 or Shown in Equation 5.2 and 5.3. This optimization study can be extended with the different boundary condition such as clamped or hinged edges of plate with different aspect ratios to understand the effect of proposed method on convergence and the buckling behaviour of the plate. For different boundary condition shape function for the Ritz-approximation(semi-analytical method) should be such that it satisfy the necessary boundary condition. Moreover, the study shown here can be expanded for a cylindrical shell where first flatten the shell as shown in Figure 7.1 and apply the MFEM-framework for the buckling load optimization using FEM and from the results of the study, approximate what function should be used (either double sin Fourier approximation or double cosine Fourier approximation) for the fiber angle distribution and apply the semi-analytical method [19] using the fiber angle distribution function for the buckling load optimization.

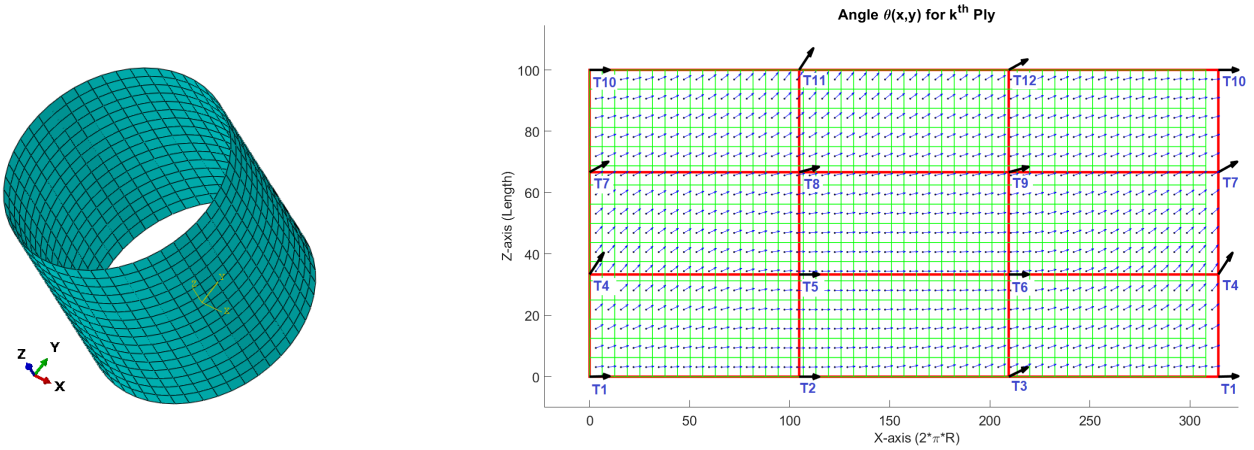

(a) Cylinder meshed with stress-mesh elements

(b) 3 X 3 Manufacturing mesh on a flatten Cylinder

Figure 7.1: MFEM-framework on a Cylinder

Note that boundary condition for the optimization variable should be periodic as shown in Figure 7.1b where angle at the left edge and right edge of the flatten cylinder are same.

Moreover, the study in thesis is only considered for the buckling load optimization,however, real structure have to also sustain the load without failing in tension, shear or compression. There for it should have enough in-plane stiffness to withstand general loading condition. Therefore the buckling load needs to be optimized with other constraints such as longitudinal(tensile) strength, shear strength etc.

It can be observed from the fiber angle distribution of the optimized panel that divergence of the fiber angle vectors are positive at the center of the plate and negative at the corner, which results in gaps and overlap of between the adjacent tow path. If gaps are large enough, it may results in the reduced buckling resistance of the panel due to reduced bending or axial stiffness at the location where there are gaps. Similarly, if overlaps are large enough, it may results in better buckling resistance and increased axial stiffness but it also increase the weight of the plate. To avoid gaps and overlap, fiber tow paths can be generated similar to the stripe pattern [12] as shown in Figure 7.2 where Figure 7.2a represents optimal fiber angle distribution of k^{th} ply and Figure 7.2b represents the center-lines of AFP tow paths such that it minimize the gaps and overlaps.

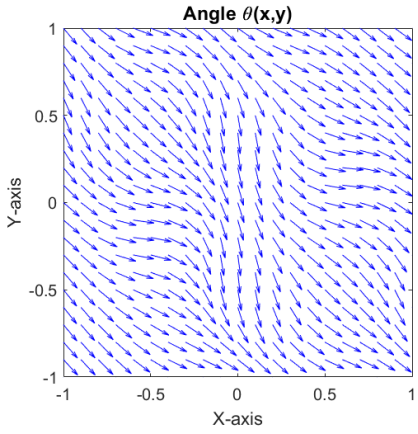

(a) Optimized Fiber Angle distribution of $k^{th} ply$

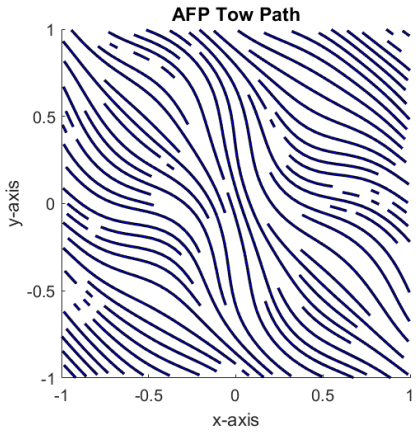

(b) Discontinuous AFP Path

Figure 7.2: AFP Path generation using Stripe Pattern

Since, each evaluations of the objective function is expensive, it is time consuming to optimize using Genetic-algorithm or BFGS method using true expensive objective function. There for it is convenient to develop a surrogate model which mimic the true objective function and perform different optimization study using the surrogate model which is less time consuming.

The optimization study can be extended to the multiple objective function optimization where variable stiffness panel can be optimized for the buckling simultaneously with the axial stiffness which minimize the axial strain.

Appendix A

Appendix A

A.1 Genetic Algorithm

Out of many optimization algorithm, Genetic algorithm [5] is used for the global optimization as it is superior in finding global minima than the other optimization algorithm such as gradient-decent(GD), which depends on the initial guess or starting point of the input variable and usually get stuck at the local minima. Despite of being superior at finding global minima, GA is poor in convergence as compared to gradient-decent and require to many function evaluation to reach to the global minima. GA works on the three basic principal, 'Selection', 'Mutation' and 'Crossover' and typically requires,

- Genetic representation of solution domain(which are input variables)
- Fitness function to evaluate the solution domain (which is output or objective function)

further, There are certain parameters needs to be set for the optimization which are discussed here briefly,

- Generation : Which decides the maximum number of generation to perform the iteration, which is one of the stopping criteria for GA. Each Generation contains fixed number of populations(or candidate solution) for which fitness function gets evaluated.
- Population :Which decides the number of trial solutions in each iteration or Generation.
- Mutation Probability: Which decide the probability of mutation of each gene(variable) in each individual solution to be replaced by a random value. This parameter is one of the reason why GA does not get stuck at a point and make it possible to explore the domain as much as possible.
- Crossover Probability: Which determines the probability of an existed solution to pass its genome to new trial solutions.
- Crossover type: Which determines the type of crossover to perform between two parent. There are many type of crossover possible such as One-point crossover,Two-point crossover, Three parent crossover and Uniform crossover.
- Parents Portion: Which is the percentage of the population in current generation filled by the members of the previous generation who were selected as a parents.
- Elit ratio: which decides the percentage of the best individual in the current generation is saved in the next generation as it is.

Here, main objective is to find highest linear buckling load (N_0) within the design space or variable bound. Mathematically, it can be written as,

$$\begin{aligned} &\min_{\theta} \; -N_0(\theta) \\ \theta \; &\in \; [-90^\circ, 90^\circ] \end{aligned} \tag{A.1}$$

Where θ is optimization variable.

A.2 BFGS Algorithm

The Genetic-algorithm is better in finding global optimum solution but it is poor in finding converged solution. Therefore The same laminate is optimized using Broyden, Fletcher, Goldfarb, and Shanno (BFGS) [14] method which is a popular class of quasi-Newton method and elite in finding an optimal solution which may be a local optimal solution but converged. In BFGS method, objective function (f) is approximated by a convex quadratic model m_k at current iterate step x_k as follows [14],

$$m_k(p) = f_k + \nabla f_k^T p + \frac{1}{2} p^T B_k p \tag{A.2}$$

Where B_k is an n x n symmetric positive definite matrix(approximated Hessian) instead of true Hessian matrix, updated at every iteration. When $p = 0$, the value and gradient of the approximated convex quadratic model match f_k and ∇f_k respectively. The minimizer p_k of the model can be written as [14],

$$p_k = -B_k^{-1} \nabla f_k \tag{A.3}$$

which is used as search direction and new iterate is written as,

$$x_{k+1} = x_k + \alpha_k p_k \tag{A.4}$$

Where α_k is a step length in the direction of search, which is chosen such as to satisfy the Wolfe condition which requires that α_k should be such that it gives sufficient decrease in the objective function (f) represented by following inequality which is referred as Armijo condition [14],

$$f(x_k + \alpha p_k) \leq f_k + c_1 \alpha \nabla f_k^T p_k \quad \text{Where, } (c_1 \ \in \ (0,1)) \tag{A.5}$$

To avoid small steps in the direction of search, curvature condition is introduced which requires α_k to satisfy [14],

$$\nabla f(x_k + \alpha_k p_k)^T p_k \geq c_2 \nabla f_k^T p_k \quad \text{Where, } (c_2 \ \in \ (c_1, 1)) \tag{A.6}$$

The gradient vector of the objective function ∇f in R^n can be written analytically as,

$$\nabla f(x) = [\frac{\partial f(x)}{\partial x_1}, \frac{\partial f(x)}{\partial x_2}, ..., \frac{\partial f(x)}{\partial x_n}]^T \tag{A.7}$$

If it is not possible to get the gradient vector analytically, it can be calculated numerically as,

$$\nabla f(x) = [\frac{\Delta f(x)}{\Delta x_1}, \frac{\Delta f(x)}{\Delta x_2}, ..., \frac{\Delta f(x)}{\Delta x_n}]^T \tag{A.8}$$

Where Δf represents change in the objective function, and Δx_n represents finite difference step (ϵ) of n^{th} variable or change in the n^{th} variable .

Bibliography

[1] Mostafa M. Abdalla, Shahriar Setoodeh, and Zafer Gürdal. Design of variable stiffness composite panels for maximum fundamental frequency using lamination parameters. *Composite Structures*, 81(2):283–291, 2007.

[2] J.E. Ashton and M.E. Waddoups. Analysis of anisotropic plates. *Journal of Composite Materials*, 3(1):148–165, 1969.

[3] Darun Barazanchy, Michael J. Van Tooren, and Ali Elham. *A new framework for optimization of variable stiffness plates.*

[4] Zdeněk P. Bažant and Luigi Cedolin. *Stability of structures: Elastic, inelastic, fracture and damage theories.* World Scientific Publishing Co., January 2010. Publisher Copyright: © 2010 by World Scientific Publishing Co. Pte. Ltd. All rights reserved.

[5] O. Bozorg-Haddad, M. Solgi, and H.A. Loáiciga. *Meta-heuristic and Evolutionary Algorithms for Engineering Optimization.* Wiley Series in Operations Research and Management Science. Wiley, 2017.

[6] W. Cheney and D. Kincaid. *Linear Algebra: Theory and Applications.* Jones & Bartlett Learning Inte. Jones & Bartlett Learning, 2012.

[7] ZAFER GUERDAL and REYNALDO OLMEDO. *Composite laminates with spatially varying fiber orientations - 'Variable stiffness panel concept'.*

[8] Z. Gürdal, B.F. Tatting, and C.K. Wu. Variable stiffness composite panels: Effects of stiffness variation on the in-plane and buckling response. *Composites Part A: Applied Science and Manufacturing*, 39(5):911–922, 2008.

[9] S.T. IJsselmuiden. Optimal design of variable stiffness composite structures using lamination parameters, 2011.

[10] A. Jeffrey. *Advanced Engineering Mathematics.* Elsevier Science, 2001.

[11] Dawn Jegley, Brian Tatting, and Zafer Gurdal. Nasa/cr-2003-212679 automated finite element analysis of elastically-tailored plates. 01 2004.

[12] Felix Knöppel, Keenan Crane, Ulrich Pinkall, and Peter Schröder. Stripe patterns on surfaces. *ACM Trans. Graph.*, 34, 2015.

[13] H. Koerber and P.P. Camanho. High strain rate characterisation of unidirectional carbon–epoxy im7-8552 in longitudinal compression. *Composites Part A: Applied Science and Manufacturing*, 42(5):462–470, 2011.

[14] Jorge Nocedal and Stephen J. Wright, editors. *Quasi-Newton Methods*, pages 192–221. Springer New York, New York, NY, 1999.

[15] REYNALDO OLMEDO and ZAFER GURDAL. *BUCKLING RESPONSE OF LAMINATES WITH SPATIALLY VARYING FIBER ORIENTATIONS.*

[16] J.N. Reddy. *Mechanics of Laminated Composite Plates and Shells: Theory and Analysis, Second Edition.* CRC Press, 2003.

[17] Shahriar Setoodeh, Mostafa M. Abdalla, Samuel T. IJsselmuiden, and Zafer Gürdal. Design of variable-stiffness composite panels for maximum buckling load. *Composite Structures*, 87(1):109–117, 2009.

[18] Michael Smith. *ABAQUS/Standard User's Manual, Version 6.9.* Dassault Systèmes Simulia Corp, United States, 2009.

[19] J. Tang. Semi-analytical solution to buckling of variable-stiffness composite panels (plates and shallow cylindrical shells), 2015.

[20] J.M. Whitney. *Structural Analysis of Laminated Anisotropic Plates.* Taylor & Francis, 1987.